UNIVERSITY OF CALIFORNIA SAN DIEGO

Optimal Scheduling and Control of Microgrid Power Flow

A dissertation submitted in partial satisfaction of the
requirements for the degree Doctor of Philosophy

in

Engineering Sciences (Mechanical Engineering)

by

Amir Valibeygi

Committee in charge:

Professor Raymond A. de Callafon, Chair
Professor Robert R. Bitmead
Professor Mauricio de Oliveira
Professor Massimo Franceschetti
Professor Jan Kleissl

2020

The Dissertation of Amir Valibeygi is approved and is acceptable in quality and form for publication on microfilm and electronically:

_____

_____

_____

_____

_____
Chair

University of California San Diego

2020

DEDICATION

To my beloved parents.

TABLE OF CONTENTS

LIST OF FIGURES

LIST OF TABLES

ACKNOWLEDGEMENTS

This dissertation concludes my PhD journey at UC San Diego. Reflecting back upon the twisty road behind, I feel indebted to a large number of individuals who helped, supported, and inspired me along the way.

First and foremost, I would like to express my sincere gratitude to my advisor Dr. Raymond de Callafon for his patience, support, and invaluable guidance throughout my PhD. Raymond has been an insightful teacher, assiduous problem solver, and a condoning friend. Working with him was particularly rewarding as he entrusted me with my adventures yet welcomed me with open arms whenever I needed help or guidance. My PhD journey would not be as successful and memorable were it not for Raymond's patience and continuous support.

I would like to further thank the rest of my doctoral committee members, Dr. Bitmead, Dr. Kleissl, Dr. Oliveira, and Dr. Franceschetti for their thoughts and comments that have improved the quality of this work. I am particularly thankful to Dr. Jan Kleissl for his rigorous review of parts of my work and his extremely valuable remarks. I am additionally grateful to Dr. Bitmead for his keen knowledge and insights that have always been a source of inspiration. I feel blessed that for more that four years, I have started my morning inspired by a glimpse of Bob busy solving a problem in his office down the hall.

My great appreciation also goes to my caring lab-mates who have been examples of helpfulness and support: Dr. Abdulelah Habib, Dr. Sai Akhil Reddy, Dr. Joe Jiang, Dr. Xin Zhao, Alicia Dautt-Silva, and Yangsheng Hu. Before colleagues in the lab, they are real friends in life and for that I am extremely thankful. I would like to especially thank Sai, Habib, and Joe for their support and helpfulness during the times I needed it the most.

I would like to further express my sincere appreciation to Dr. David Bliss from Charge Bliss and Mr. GB Singh from Solar Turbines Inc. for believing in me and

providing me with opportunities that have greatly expanded my technical and professional horizons. My appreciation also goes to Mark, Karl, and Rick from CAPS-FSU as well as our friends at NREL for their insight and helpfulness during our collaborations; it has been an amazing experience to work with every single one of you.

I am additionally thankful to my dear friends for their support and kindness throughout my PhD and beyond that: Parisa, Amirali, Niloofar, Sahand, Mohammad, Roya, Siavash, Sina, Mostafa, Sadegh, Masih, Adel, Hamid, Soheyl, Reza, Vahid, Hadi, Ali, Roozbeh, and Shirin; you have a special place in my heart.

Last and beyond all, I am truly thankful to my father, my mother, and my siblings Adib, Alireza, and Sana. My family have been my greatest supporters in life.

dissertation author was the primary investigator and author of this material.

Chapter 6, in full, is a reprint of the material as it appears in "Cooperative Energy Scheduling for Microgrids under Peak Demand Energy Plans", Amir Valibeygi, and Raymond A. de Callafon. In 2019 Conference on Decision and Control (CDC), IEEE, 2019. The dissertation author was the primary investigator and author of this paper.

VITA

2013	Bachelor of Science, Amirkabir University of Technology
2015	Master of Science, Simon Fraser University
2020	Doctor of Philosophy, University of California San Diego
2018-2020	Controls Design Engineer, Solar Turbines Inc.

PUBLICATIONS

Amir Valibeygi, Amirmasoud Toudeshki, and Krishna Vijayaraghavan. "Observer-based sensor fault estimation in nonlinear systems" Proceedings of the Institution of Mechanical Engineers, Part I: Journal of Systems and Control Engineering", 230.8 (2016): 759-777.

Krishna Vijayaraghavan and **Amir Valibeygi** "Adaptive nonlinear observer for state and unknown parameter estimation in noisy systems", International Journal of Control 89. 1 (2016): 38-54.

Amir Valibeygi, and Krishna Vijayaraghavan. "A comparative study of Extended Kalman Filter and an optimal nonlinear observer for state estimation", In 2017 American Control Conference (ACC), pp. 5211-5216. IEEE, 2017.

Yunfeng Jiang, Xin Zhao, **Amir Valibeygi**, and Raymond A. de Callafon. "Dynamic prediction of power storage and delivery by data-based fractional differential models of a lithium iron phosphate battery", Energies 9.8 (2016): 590

Amir Valibeygi, and Raymond A. de Callafon. "Adaptive regulation for disturbance rejection with uncertain parameters: Stability analysis", In 2017 American Control Conference (ACC), pp. 1493-1498. IEEE, 2017.

Amir Valibeygi, Raymond A. de Callafon, Mark Stanovich, Michael Sloderbeck, Karl Schoder, James Langston, Isaac Leonard, Sourindu Chatterjee, and Rick Meeker. "Microgrid control using remote controller hardware-in-the-loop over the Internet", In 2018 IEEE Power Energy Society Innovative Smart Grid Technologies Conference (ISGT), pp. 1-5. IEEE, 2018.

Amir Valibeygi, Abdulelah H. Habib, and Raymond A. de Callafon. "Robust power scheduling for microgrids with uncertainty in renewable energy generation", In 2019 IEEE Power & Energy Society Innovative Smart Grid Technologies Conference (ISGT),

pp. 1-5. IEEE, 2019.

Sai Akhil Reddy Konakalla, **Amir Valibeygi**, and Raymond A. de Callafon. "Microgrid Dynamic Modeling and Islanding Control With Synchrophasor Data", IEEE Transactions on Smart Grid 11.1 (2019): 905-915.

Amir Valibeygi, and Raymond A. de Callafon. "Cooperative Energy Scheduling for Microgrids under Peak Demand Energy Plans", In 2019 Conference on Decision and Control (CDC), IEEE, 2019.

Amir Valibeygi, and Raymond A. de Callafon. "Optimal Battery Dispatch and Real-Time State of Charge Tracking for Microgrid Applications", In 2020 American Control Conference (ACC), IEEE, 2020.

ABSTRACT OF THE DISSERTATION

Optimal Scheduling and Control of Microgrid Power Flow

by

Amir Valibeygi

Doctor of Philosophy in Engineering Sciences (Mechanical Engineering)

University of California San Diego, 2020

Professor Raymond A. de Callafon, Chair

The operation of renewable microgrids is undergoing rapid transformations due to increasing renewable resources penetration, making their energy management and control more crucial for economic and reliability goals. The increasing penetration of solar resources introduces a significant degree of intermittency and uncertainty. As a measure to increase reliability in the face of such uncertainty, future microgrids will require operational flexibility including ramping capacity and the ability to swiftly respond to grid conditions. Real-time feedback control is known for handling uncertainty and can play an instrumental role in real-time scheduling update along with other non-

intermittent reserves. Motivated by this changing prospect, this dissertation proposes multiple techniques for optimal microgrid control, energy management, and scheduling in the presence of intermittent renewable resources, reserve non-renewable resources, and energy storage systems. The presented approaches consider microgrid optimization problems from the viewpoint of a single microgrid as well as multiple cooperating microgrids under a variety of energy cost structures and operating limitations imposed by resource constraints and the grid. Additionally, we present an approach of addressing both short-term scheduling and real-time power control in a unified model predictive control framework where the microgrid controller operates at two separate time scales. Techniques are proposed to relax the non-convex resource scheduling problem and enable solving the MPC at update rates comparable with renewable generation and demand variability time scales. To facilitate testing of different microgrid controllers with fast update rates, a remote hardware-in-the-loop microgrid testing setup is designed and utilized for testing the controllers proposed in this work. The proposed control and scheduling approaches are developed using data and models from real-world microgrids and some of the techniques are implemented in an actual microgrid in California with solar energy generation and energy storage.

Chapter 1

Introduction

1.1   Renewable Microgrids

A microgrid as defined by IEEE [1] is "a group of interconnected loads and distributed energy resources with clearly defined electrical boundaries that acts as a single controllable entity with respect to the grid and can connect and disconnect from the grid to enable it to operate in both grid-connected or island modes." Microgrids are arguably among the most thriving components of energy infrastructure in many regions around the world and continue to grow in size and capability in the foreseeable future. Whether connected to the main electricity grid or running independently, a microgrid should maintain safe, reliable, and in most cases economical operation. Operations of microgrids and power grids have been substantially transformed in recent years, mainly due to increasing penetration of renewables, and changing demand patterns [2]. Energy management of microgrids in a way that makes its operation economically feasible has been receiving broad interest over the past decade due to the rise of microgrid deployments in industrial and commercial applications. The significance of such studies has particularly increased due to the growing flexibility of existing energy sources, as well as energy storage technologies for microgrid applications [3].

Increasing renewable penetration poses challenges on the power grid due to

the intermittency and uncertainty of most renewable resources, most notably solar and wind [4]. As a pivotal transition, it has been acknowledged over the past decade that net demand, that is the total grid load minus renewable generation is highly uneven throughout a day. This condition has been escalated over the past few years with increasing solar generation since solar energy exists merely during the day and vanishes during night time [5]. This phenomena is known as "duck curve" and has raised concerns about maintaining the balance of the grid in the years to come. To make up for the unmet demand in the absence of solar resources during the night, conventional generation resources should ramp up their generation. On the other hand, the grid frequently has excess renewable energy, without adequate customer demand to use it. This phenomena known as oversupply has become common over the past years and has lead to curtailment of renewable Distributed Energy Resources (DERs). While curtailment has become necessary to maintain the balance between generation and consumption, it is contrary to environmental and economic goals as it reduces renewable energy generation. Renewable DERs not only demonstrate fluctuation and volatility, but are also often hard to predict particularly over longer time horizons. Temporary cloud cover, for example, could reduce the output of a solar plant to a fraction of its normal power output.

Instances of energy and environmental policy initiatives contributing to rising renewable penetration in California include the goal of reaching 50% of retail electricity from renewable power by 2030, greenhouse gas emissions reduction goal to 1990 levels, policies to increase distributed generation, and an executive order for 1.5 million zero emission vehicles by 2025 [6]. These policies will in turn facilitate the shift in power generation from traditional centralized plants to intermittent distributed renewable plants which are connected to the grid via low-inertia inverters, highlighting the need for rigorous frequency response to ensure reliability of future grids. In the renewable integration study by California Independent System Operator (CAISO) [7], it is shown that the 2020 target
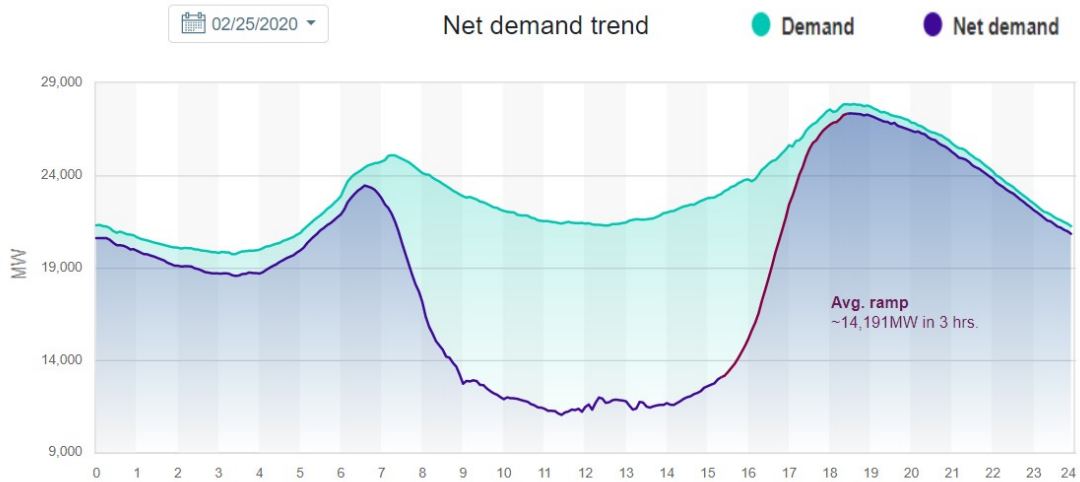
Figure 1.1. Illustration of California net demand profile (demand minus renewables) over one day, also known as the duck curve - Meeting the afternoon net demand ramp by non-renewable resource dispatch is a challenge recognized by grid operators.

of 33% renewable penetration could lead to 60% renewable generation in times of high renewable generation and low load and such condition could lead to loss of reliability in the grid. For instance, loss of a large conventional generator under these conditions could impose frequency drops that cannot be recovered by renewable assets as renewable inverters are not required to include automated frequency response capabilities. Such conditions would make the system highly vulnerable to generation loss and prone to blackouts.

Fig. 1.2 shows an overview of different timescales concerned in operations of the power grid. As renewable inverters are becoming commonplace in microgrids, considering faster timescales is becoming increasingly necessary to ensure smooth and reliable operation. While traditionally most frequency and voltage regulation operations have been done in seconds timescales (for example Automatic Generation Control - AGC), sub-second regulation and control has become necessary due to the mentioned transformations of low inertia renewable resources.
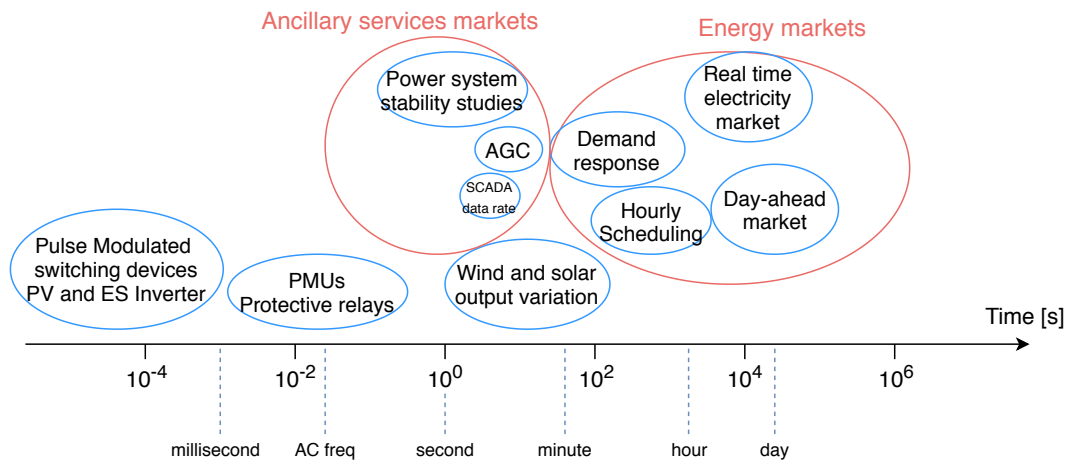
Figure 1.2. An overview of time scales involved in different power system operations and variabilities

A study by the National Renewable Energy Lab (NREL) [8] investigating options for advancing system flexibility for high penetration renewable integration, identifies fast scheduling, strategic renewable curtailment, new ancillary services, and energy storage as viable options for enhancing flexibility. It proposes extending current ancillary services markets to include faster real-time dispatch intervals and upward and downward ramps to account for variability (known ramps) and uncertainty (unforeseen ramps). CAISO has additionally defined flexible resources characterized by their operating capabilities as requirements for meeting the changing grid patterns. The identified features include the ability to sustain upward or downward ramp, change ramp directions quickly, store energy, react quickly and meet expected operating levels, start with short notice from a zero or low-electricity operating level, start and stop multiple times per day, and accurately forecast operating capability.

Energy storage is recognized as a possible solution to some of the prevailing challenges resulting from high renewable penetration [9]. By allowing the energy produced at one time to be used at a later time, it could add flexibility to the power system

operation and alleviate variability and uncertainty. Storage can provide firm capacity, energy shifting, and ancillary services. Additionally, the ability of energy storage systems to respond to power demands in short time scales, from minutes to fractions of seconds, is an enabling factor for maintaining grid resiliency, frequency regulation, and transient stability. Large energy storage deployments could be used to store excess solar generation during the day and make it available during evening ramps, reducing curtailment and reducing evening ramp slopes. Energy storage can additionally be utilized by microgrid owners to optimally schedule their demand and reduce energy costs associated with power exchange with the main grid. Multiple chapters of this dissertation will discuss strategies and techniques for energy storage scheduling to benefit the customers as well as the overall grid.

Another major transition brought about by surging renewable penetration is the distributed nature of most renewable assets where DERs generating as few as kilowatts of energy up to hundreds of Megawatts are spread across the transmission and distribution grids. Such distributed nature implicates the need for more systematic power and frequency control in order to maintain the balance of the grid.

The above mentioned transformations together with advances in power systems sensing, communication, and actuation technologies demand novel control, optimization, and power management schemes that are economically more efficient yet ensure energy safety and security for grids and microgrids of the future. This dissertation is an attempt to address just a few of these prevailing problems in microgrid optimal power management and power control.

1.2   Problem Formulation

Motivated by the mentioned challenges of renewable microgrids, this dissertation is an attempt to address the problems of microgrid power flow scheduling and control. In

5

particular, we will approach the following problems:

1. Design and implementation of a hardware-in-the-loop controller test setup for testing and evaluating real-time power feedback control algorithms in a networked communication setting. This problem is covered in chapter 2.

2. Design and implementation of an economic scheduling and power feedback controller for a solar microgrid with high renewable generation uncertainty. This problem is studied in chapters 3 and 4. In these chapters, robust economic scheduling techniques are devised for a microgrid with PV energy generation and energy storage system to reduce microgrid energy costs by optimal utilization of the energy storage system.

3. Co-design of slow optimal scheduling and fast power control at separate time scales in a model predictive control framework. This problem is discussed in chapter 5 where a hierarchical model predictive controller is designed.

4. Development of a cooperative economic scheduling algorithm for multiple microgrids to reduce their energy costs. This problem is studied in chapter 6, where a new paradigm in shared energy storage utilization among multiple microgrids is envisioned and the stability properties of their cooperation is investigated.

Fig. 1.3 indicates the range of time scales considered and Fig. 1.4 presents the overall power scheduling and control structure devised in this work. In this structure, economic scheduling is solved to determine optimal power profile at slow time scales whereas real-time power control is performed at a faster update rate aiming to adjust the setpoitns of different DERs.
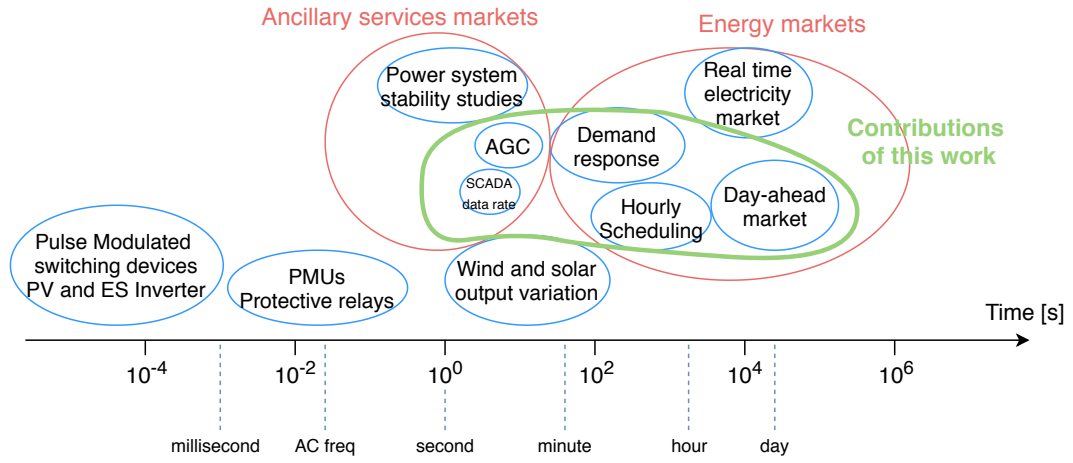
Figure 1.3. Scope of timescales considered in this work.
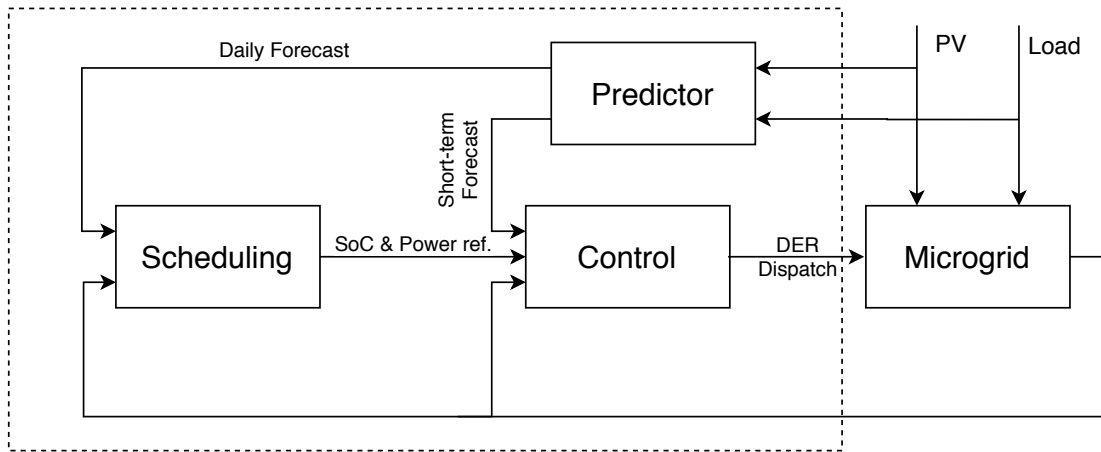
Figure 1.4. Schematic of the structure of control and scheduling techniques proposed in this work.

1.3   Highlights of this dissertation

Chapter 2 proposes a remote microgrid controller testing setup where communication between the controller and the testbench happens over the Internet. With the advancement of cloud computing technologies, the idea of implementing microgrid controllers as cloud-based services is gaining interesting interest. Additionally, network-based microgrid control provides the possibility of testing different microgrid controllers against a single Hardware-in-the-Loop (HIL) testbench. In this regard, performance and resiliency of different controllers can be tested in closed-loop with a remote HIL setup over a communication network (Internet). The testbench utilizes a Real-Time Digital Simulator (RTDS) to model an existing hospital microgrid with PV and energy storage. It communicates in real-time with the controller over the Internet. The controller leverages Phasor Measurement Units (PMUs) for measuring power flow and adjusting inverter power references in real-time. The control objectives are power and State-of-Charge (SoC) control, subject to inverter power amplitude and rate limits and communication constraints. The controller incorporates units of power control, SoC control, and adaptive reference scheduling to achieve seamless microgrid operation. Real-time, over the internet, hardware-in-the-loop tests between the controller and the simulator are realized and indicate stability and performance of the microgrid control system.

Chapter 3 presents a combined approach of robust economic scheduling and real-time power feedback control for an integrated solar PhotoVoltaic (PV) system and Energy Storage (ES) system to achieve the objective of reducing energy costs at a commercial facility. The scheduling is based on the computation of a nominal robust dispatch schedule for the ESS that exploits allowable energy storage capabilities to simultaneously reduce energy Time-of-Use (TOU) and power demand charges. To handle the unpredictable variability in PV generation and load demand in real-time, the dispatch schedule is given

as a reference to a power feedback controller (PFC) that monitors the power flow at the point of common coupling and applies necessary adjustments to meet the target demand reduction. The approach is implemented on a commercially operated microgrid in California. The microgrid achieved both energy and peak demand charge reduction over a one-month billing cycle.

In chapter 4, a robust power scheduling algorithm is proposed for a grid-connected microgrid with PV and energy storage to schedule power flow subject to uncertainty in solar energy generation. To avoid over-conservatism in power scheduling while guaranteeing robustness against uncertainties, time-varying "soft" constraints on the State of Charge (SoC) of the battery are proposed. These soft constraints allow SoC limit violation at steps far from the current step but aim to minimize such violations in a controlled manner. The approach entails a model predictive scheduling strategy over a receding time horizon and ensures that the resulting solution eventually conforms to the hard SoC limits of the system at every step. The optimization problem for each step is formulated as a quadratic programming problem that is solved iteratively to find the soft constraints that are closest to the actual constraints and still yield a feasible solution. Optimization results demonstrate the effectiveness of the approach.

Chapter 5 discusses problems associated with large PV microgrids scheduling and control. Large PV plants constitute a growing portion of distributed renewable generation in the US power grid. Managing the operation of such microgrids and in particular their interaction with the main electricity grid is a challenging task as it involves controlling large intermittent PV resources. The addition of auxiliary DERs and energy storage technologies to such PV microgrids is a promising solution that provide additional flexibility in utilizing PV resources. In this chapter, a hierarchical predictive controller is designed that controls the operation of a PV microgrid with energy storage and auxiliary diesel generation. The controller aims to increase utilization of the available PV resources,

reduce the variability of power flow between the microgrid and the main grid, while at the same time controlling power flow fluctuations at the point of connection. The controller is designed to utilize updating load and PV predictions on a receding time horizon and uses the flexibility of energy storage and diesel resources to compensate for prediction errors. A study of multiple operational scenarios demonstrates successful operation of the proposed controller.

Chapter 6 presents a cooperative energy scheduling method for a group of microgrids with energy storage that allows joint energy optimization to achieve cost savings that the microgrids could not achieve individually. The goal is to investigate cost implications of such cooperation on the participating microgrids. The considered microgrids may be commercial entities in a distribution network under utility electricity rate plans comprising both Time of Use (ToU) and peak demand charge. Defining a stable operation as a situation where all microgrids would be willing to participate in the cooperation, it is shown that under such rate plans and in particular due to the peak demand charge, a cost distribution that is seemingly fair does not necessarily result in a stable cooperation. These results are derived using concepts from cooperative games. It is therefore sought to devise a stable cost distribution algorithm that, while maximizing some measure of fairness among the participating microgrids, ensures they all benefit from their participation.

Chapter 2

Microgrid Feedback Control and HIL Testing over the Internet

2.1   Introduction

Distributed Generation (DG) is reaching unprecedented levels of penetration in the global power industry. This has been realized as more economic and efficient Distributed Energy Resources (DER) have become available [10]. A microgrid is a group of local DERs, storage units, and loads that are able to operate in both connected and isolated modes from the main electricity grid [11]. In the connected mode, microgrids are connected to the main grid at the Point of Common Coupling (PCC) and may provide part, or all of the power demand of their local facility; hence reducing power required from the main grid. Further, excess power generation may be stored or sold to the main grid.

In grid-connected mode of operation, the microgrid can regulate the amount of active and reactive power exchange with the main grid. Numerous planning, energy management, and control strategies have been devised to manage the flow of power between microgrid and the main grid, in order to maximize economic efficiency and maintain reliability and availability [12, 13, 14, 15].

2.1.1 Phasor Measurement Unit (PMU)

Microgrid operations and controls can be significantly improved by utilizing Phasor Measurement Units (PMUs). PMUs can be utilized at different points within the grid or microgrid to provide synchronized and frequent measurements of voltage and current phasors (synchrophasors) and therefore compute power and frequency [16], [17]. With the increased availability of PMUs for use in power system applications, high feedback rate control, state estimation, and event detection can be introduced into power systems. Although PMUs provide an unprecedented level of fidelity in electric power system measurements for use in control, they also pose communication and computational challenges due to the massive amount of data they generate. Control strategies can be implemented by feedback loops that use such PMU measurements. Furthermore, any undesired behavior in the microgrid including faults, power fluctuations at the PCC due to the varying demand, etc., could be sensed and sent to a central controller that takes appropriate control actions accordingly to ensure quality, reliability, and economic operation [18].

2.1.2 Remote HIL testbench

With the advancement of cloud computing technologies, the idea of implementing microgrid controllers as cloud-based services is gaining increasing interest. Network-based controllers have been widely studied in the recent literature due to the increasing presence of cyber-physical systems in various industries [19, 20, 21]. Additionally, network-based microgrid control provides the possibility of testing different microgrid controllers against a single Hardware-in-the-Loop (HIL) testbench. In this regard, performance and resiliency of different controllers can be tested in closed-loop with a remote HIL setup over a communication network (Internet).

In this chapter, one of the first instances of microgrid remote power flow control

is implemented and tested on a HIL setup. In particular, microgrid power control is implemented to manage power flow at the PCC of a grid-connected microgrid. In the first stage of the work, a real-time simulation of a microgrid equipped with inverter-interfaced PV generation and battery storage was developed for developing a microgrid power management and control algorithm. A Controller Hardware-In-the-Loop (CHIL) setup is established wherein a RTDS-based microgrid simulator (CAPS, FSU) and controller (SyGMA Lab, UCSD) communicate over the Internet. The controller performs computations in real-time and sends control commands to the inverter that is part of the microgrid model. The long-distance communication testbed has enabled two research entities with different expertise and resources, separated by over 2000 miles, to successfully collaborate throughout the development and testing process. This real-time control platform over the Internet has extensive potential applications for various experiments and validation tests in the power industry [22].

The objective of the control system is to track the power reference for PCC and simultaneously maintain the State-of-Charge (SoC) of the battery within an acceptable range while conforming to system (e.g., inverter and communications delay) limitations. This two-fold objective is achieved by utilizing a centralized cascaded control system. The controller incorporates a fast inner loop that aims at power control and a slower event-triggered outer loop for SoC control. A reference calculation module is implemented in the controller that estimates the demand profile (disturbance) and sets the power reference based on the estimation.
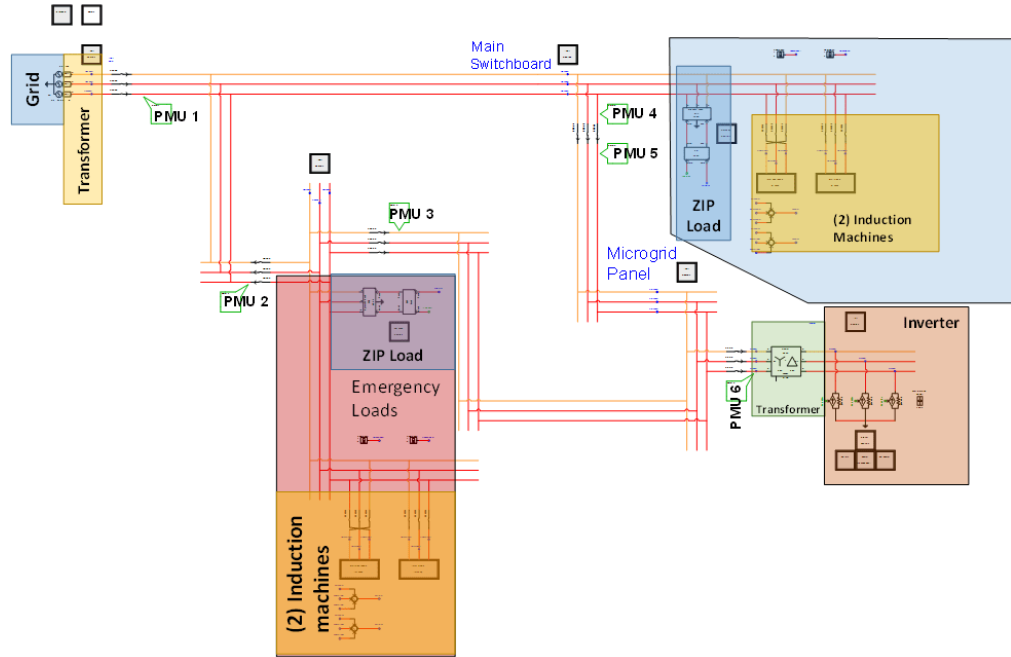
Figure 2.1. Overview of RTDS microgrid model, emergency and non-emergency loads, PMUs, and transformers

2.2 Verbose System Model and Control Strategy

2.2.1 Microgrid modeling and simulation

A microgrid model was developed in this project to capture salient characteristics of an existing hospital microgrid in Northern California and perform real-time simulation with RTDS Technologies hardware and software [23]. This model and simulation is primarily used for de-risking and development of controls for planned hardware additions to the hospital electrical system including PV and batteries. A high-level illustration of microgrid model in the RTDS design environment, along with annotations, is shown in Figure 2.1. The microgrid model has loads which can be categorized as non-emergency and emergency. The emergency loads draw much less power than the non-emergency loads and can therefore be powered solely by the planned hardware installation. The emergency and non-emergency loads each consist of a constant impedance-current-power

(ZIP) load and two induction machines. The grid interconnection is modeled using an infinite source and transformer equivalent impedance. The modeled planned additions to the microgrid include 6 PMUs, a PV array, an inverter, and a battery. The inverter and battery storage are rated at 250 kW/250 kVar and 250 kW/1 MWh, respectively.

TCP/IP Modbus and C37.118 data communication is implemented in the real-time simulation. The model includes 6 PMUs that send C37.118 messages providing measurements throughout the microgrid. The simulated inverter provides a Modbus TCP/IP interface, which is the communication channel for controlling real and reactive power and information including battery SoC and PV power generation.

2.2.2   Microgrid dynamic model estimation

The dynamics of the central microgrid controller is developed based on only an approximate model of the detailed microgrid dynamics captured in the RTDS model. The approximate model is found through system identification tests, which were performed to model the relationship between the power flows at the inverter and PCC [24, 25]. To achieve this, step tests are conducted with the inputs being active and reactive power at the inverter and the outputs active and reactive power flow measured at the PCC by PMU 1. A two-input-two-output discrete-time model $\hat{G}$ between the inverter and the PCC is identified through a step-based realization algorithm [26].

$$\hat{G}(q) = \begin{bmatrix} \hat{G}_{11}(q) & \hat{G}_{12}(q) \\ \hat{G}_{21}(q) & \hat{G}_{22}(q) \end{bmatrix} \qquad (2.1)$$

The identified model is used in the next section to design controllers and to estimate microgrid's power demand.
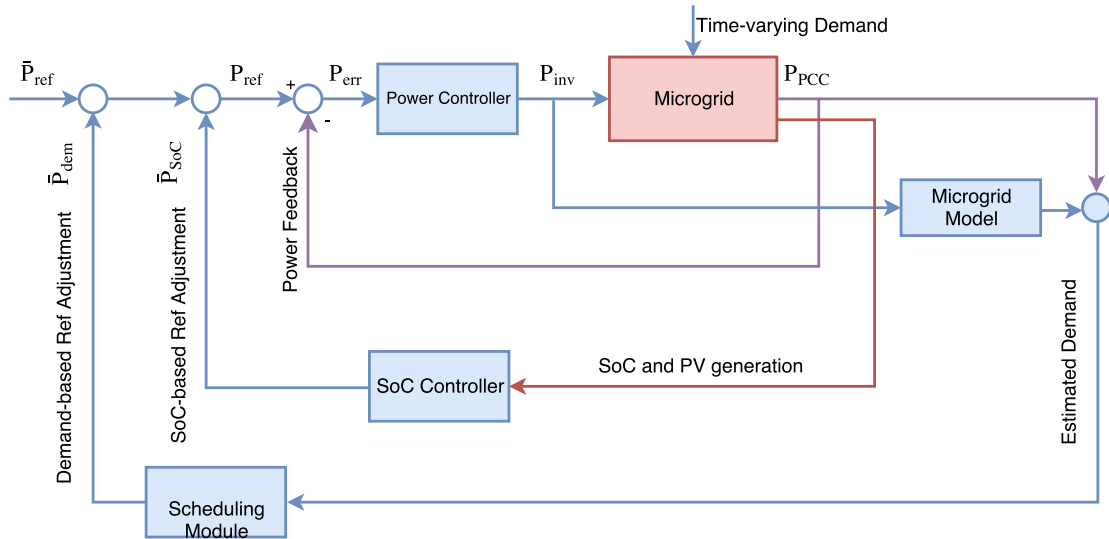
Figure 2.2. Cascaded controller block diagram consisting fast power control loop, slow SoC control loop, and reference adjustment module

2.2.3 Control strategy and implementation

The microgrid supervisory control system is a central controller that gathers PMU data as well as battery and PV generation data as input. The collected information is processed and appropriate control commands (inverter active and reactive power reference) are computed and sent back as demand signals to the inverter via the Internet.

The goal of the proposed control system is to track a reference for active and reactive power at PCC, as long as SoC of the battery is within its acceptable range. The reference could be set either adaptively by computing a rate-limited tracking of demand trend estimate or set manually by an operator. Due to the limited inverter power, the adaptive reference allows the implementation of power peak shaving at different demand levels. On the other hand, the controller should also be able to follow a user-defined reference when requested allowing the suppression of short time, small magnitude demand variations. In the case that SoC drifts outside its acceptable range, the outer loop is triggered to refine the reference and recover the SoC until it reaches an acceptable level.

16

The controller comprises three main units of power control, SoC control, and power scheduling which are described in more details below.

2.3 Control algorithms

2.3.1 Power control

Controlling power flow at the PCC is a primary objective of the microgrid central control system. Power control loop is the core control unit in the control system and is also the fastest loop. The input of this control unit is the inverter power error (adjusted by SoC control loop and reference calculation unit).

$$P_{err} = P_{ref} - P_{PCC}$$
$$P_{ref} = \bar{P}_{ref} + \bar{P}_{dem} + \bar{P}_{SoC} \tag{2.2}$$

where $\bar{P}_{dem}$ and $\bar{P}_{SoC}$ are refinements due to demand following and SoC control respectively. The controller incorporates proportional, integral, and derivative control actions.

$$P_{inv}(k) = K_P(P_{err}(k) - P_{PB})$$
$$+ K_I x_I(k) + K_D(x_D(k) - P_{DB}) \tag{2.3}$$

where x_I and x_D are integrator and derivative states in the controller and P_{PB} and P_{DB} are bias terms to avoid proportional and derivative jumps and ensure bump-less transfer. The integrator state in the controller is updated as

$$x_I(k) = T_s P_{err}(k) + x_I(k-1)$$

and the output of the controller $P_{inv}(k)$ is the inverter's power references and is amplitude-and rate-limited to ensure it conforms with the inverter's limitations. As a result of this output limitation, integrator windup effect may occur in the integrator state. To avoid this, the computed control command $P_{inv}(k)$ is compared with amplitude and rate limits of the inverter and if the limits are violated, maximum possible power is commanded instead of the computed value and using (2.3), the integrator state is updated by the following correction.

$$x_I(k) = [P_{inv,max}(k) - K_P(P_{err}(k) - P_{PB})$$
$$- K_D(x_D(k) - P_{DB})]/K_I \qquad (2.4)$$

2.3.2 SoC control

While power control is the main objective of the control system, this task should be accomplished with the consideration of SoC level of the battery. Battery SoC should ideally be kept close to a nominal value; however, slow dynamics of SoC variation as well as the communication constraints motivate us to take an event-triggered approach to the SoC control loop. Therefore, this loop will remain inactive in the vicinity of the nominal SoC value (dead zone) where full control authority is dedicated to power control loop. If SoC drifts too far from its reference value, SoC compensation takes action to recover SoC and adjusting the power reference until it is brought back inside the dead zone. This reference correction would be helpful especially when average PV generation

drops at night time or during cloudy days.

$$\bar{P}_{SoC} = \begin{cases} f(SoC, P_{PV}) & \text{for } 20 \leq SoC < 30 \\ 0 & \text{for } 30 \leq SoC \leq 80 \\ f(SoC, P_{PV}) & \text{for } 80 < SoC \leq 90 \end{cases}$$

This control loop involves proportional as well as integral control actions similar to (2.3). Due to slow dynamics of the loop, integration windup limits are set to avoid large integrator accumulation and achieve steady-state error correction.
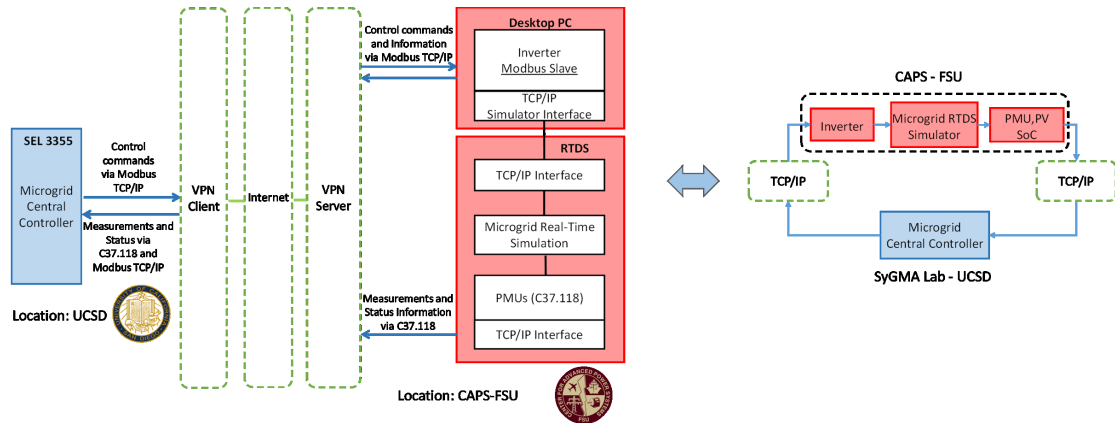
Figure 2.3. CHIL Setup with microgrid controller at UC San Diego and microgrid simulator at FSU communicating in real time over the Internet

2.3.3 Demand estimation and power scheduling

As depicted in fig. 2.2, this unit is in charge of providing power reference value based on either manual power reference or adaptive demand following and smoothening requirement depending on the operator's decision. The first strategy fits facilities with more frequent short-term load variations and constant long-term average while the latter suits those with low frequency power variations and variable average demand. In the latter case, in order to adapt the controller to the time-varying average demand, the

19

demand is first estimated and then a rate-limited filtering of it is used as the adaptive power reference. An estimation of instantaneous load demand at the PCC is computed by adding measured power at the PCC and inverter power filtered by the system model.

$$\hat{P}_{dem}(k) = P_{PCC}(k) +$$
$$\hat{G}_{11}(q)P_{inv}(k-1) + \hat{G}_{12}(q)Q_{inv}(k-1) \tag{2.5}$$

where $\hat{P}_{dem}(k)$ is the estimated microgrid demand, $P_{PCC}(k)$ is the measured power flow by the PMU at PCC, $\hat{G}_{11}(q)$ and $\hat{G}_{12}(q)$ are the identified system models from (2.1), and P_{inv} and Q_{inv} are the inverter's control inputs. Next, a rate-limited version of this estimation is used as the adaptive power reference. If the rate limit parameter is R, we define the rate r for the demand signal $\hat{P}_{dem}$ as

$$r(k) = \frac{\hat{P}_{dem}(k) - \bar{P}_{dem}(k-1)}{T_s} \tag{2.6}$$

and the output rate limitation is performed as

$$\bar{P}_{dem}(k) = \begin{cases} T_s R + \bar{P}_{dem}(k-1) & \text{for } r > R \\ \hat{P}_{dem}(k) & \text{for } -R \leq r \leq R \\ -T_s R + \bar{P}_{dem}(k-1) & \text{for } r < -R \end{cases}$$

This enables the microgrid to automatically change its reference and achieve power control at different load levels. The output of this unit will then be adjusted by the output of the SoC control unit and later compared with the output of the system. Similar expression holds for reactive power at the PCC.

Due to the electric microgrid network between the generation units and the PCC, some active-reactive power coupling exists between power injected by the DG (inverter)

20

and the measurement at the PCC. Therefore, in order to design independent control loops for controlling active and reactive power at the PCC, power decoupling is performed in the controller.

2.4 Implementation

The real-time simulation and control facilities used for this project are located on opposite sides of the United States. The RTDS is located at the Center for Advanced Power Systems (CAPS), Florida State University. The digital controller is located at the Synchro-phasor Grid Monitoring and Automation (SyGMA) lab, San Diego Supercomputer Center, UC San Diego. A CHIL setup is created wherein the simulator and controller communicate over a virtual private network (VPN) as illustrated in Figure 2.3. Data from RTDS is communicated to the controller via TCP/IP at the rate of 10 Hz. The communicated data items are shown in Table 2.1. PMU communication adheres to the IEEE C37.118 standard, which is the common IEEE standard for PMUs in power systems [27] and inverter communication follows the Modbus TCP/IP protocol.

Table 2.1. Communicated data in the Controller HIL test setup

Data	From	To	Comm. Protocol
Active and reactive power at 6 points	PMUs 1-6	Controller	IEEE C37.118
Voltage, current, and frequency at 6 points	PMUs 1-6	Controller	IEEE C37.118
Battery SoC	Inverter	Controller	Modbus
PV Generation	Inverter	Controller	Modbus
Inverter active and reactive power reference	Controller	Inverter	Modbus
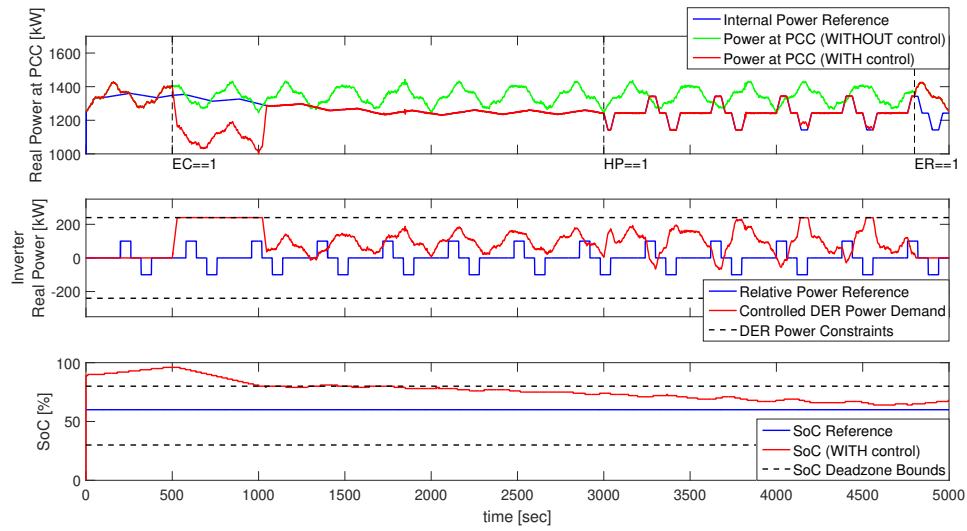
Figure 2.4. Active Power control at PCC (top), Inverter Input (middle), and SoC variation (bottom)
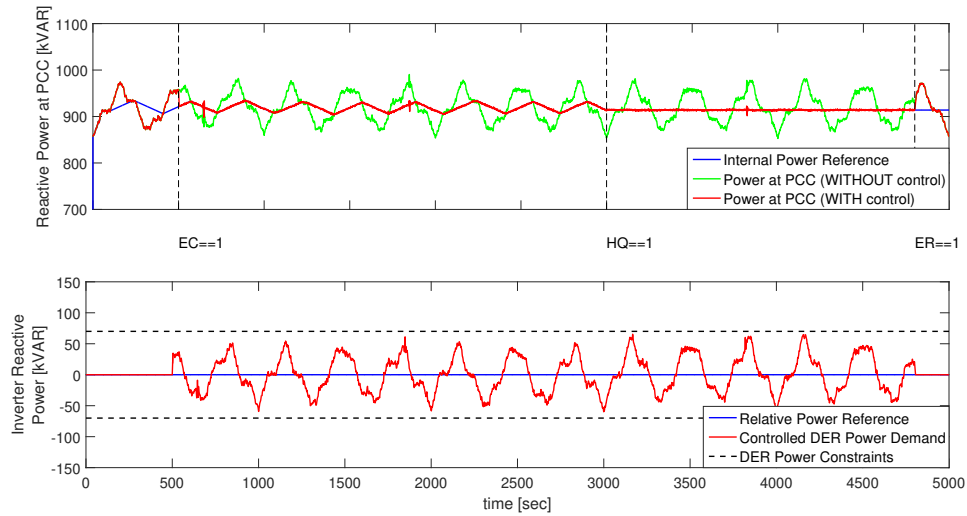
Figure 2.5. Reactive Power control (top), and Inverter Input (bottom)
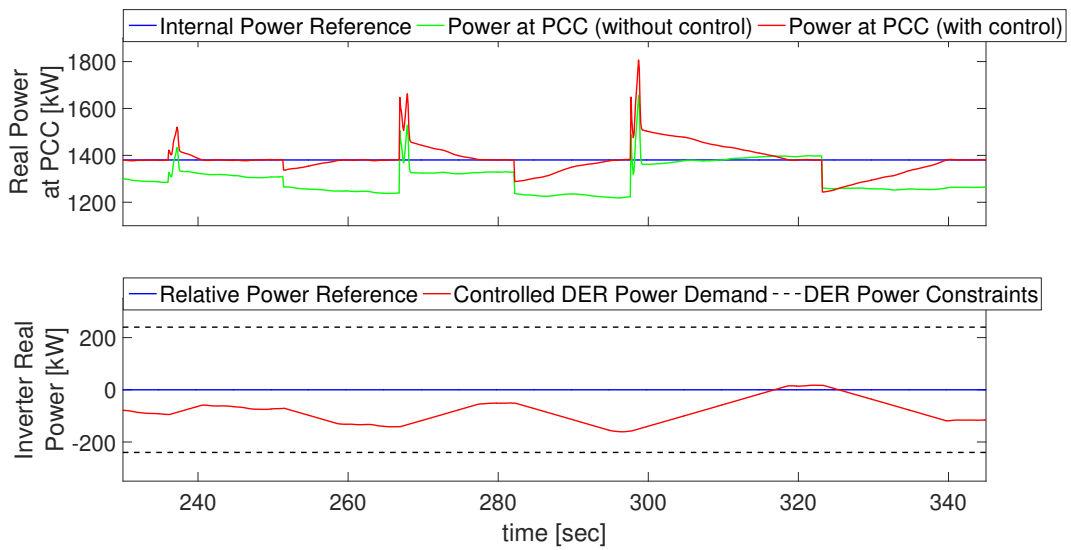
Figure 2.6. Load Switch Test with Slow Inverter
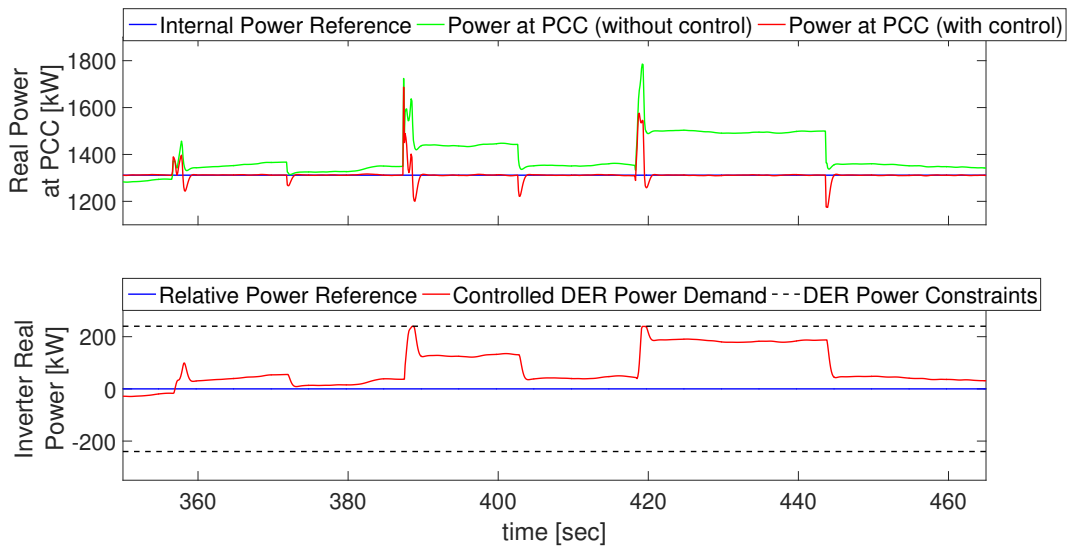
Figure 2.7. Load Switch Test with Fast Inverter

2.5   Results

Microgrid control and scheduling results are summarized in this section. The two simulated scenarios aim to examine different features of the controller for illustration purposes.

2.5.1   Demand following test

The first test examines power control and tracking at PCC under different PCC power requirements during the total test duration of 5000 seconds. The controller is off during the first 500 seconds, operates in the adaptive reference mode from 500 s to 3000 s, in the manual reference mode from 3000 s to 4800 s, and is commanded to switch off at 4800 s. Additionally, as observed in the SoC plot, the starting SoC of the battery is set outside the dead zone band for test purposes. The controller is activated at 500 s from when it is commanded to operate in the adaptive reference mode. However, by this time, since the SoC has already grown largely out of limits and passed its absolute limits, the only priority of the control system becomes SoC recovery until it reaches the safe zone. This is done by operating the inverter in the full power mode and continues until SoC reaches safe zone at around 1000 s. Afterwards, the controller switches to the normal adaptive reference mode until time 3000 s and the power measured at PCC is able to follow the reference. The reference computed by the adaptive reference computation module is shown by blue in the top figure. Inverter's control input during this period is shown by red in the middle figure and falls within the inverter's power limits. At time 3000 s, the controller is switched from adaptive to non-adaptive reference mode, where the controller is able to follow a trapezoidal reference set by the user. As observed in Figures 2.4 (middle) and 2.5 (bottom), the inverter's control input is barely reaching its limits after time 1000 s, which means the reference variations are within the inverter's

24

power control capability. The controller is finally switched off at 4800 s.

2.5.2   Load switching test

This test is designed to emulate more transient microgrid events. In particular, we have studied abrupt load switching events and the effect of inverter's ramp rate limitation and the communication delay on the controller's ability to suppress those events. The test scenario comprises the microgrid with its usual time-varying load demand while an additional 50 kW motor is suddenly switched in. The switch-in event causes PCC power to experience a sudden jump, however, the controller should be able to recover the previous PCC power level in a timely manner. After successful recovery, the 50 kW motor is switched off and a 100 kW motor is switched at this time. A similar scenario then happens for a 150 kW motor. The tests are performed for two different values of inverter ramp rates. Figure 2.6 shows slow ramp rate power control with a maximum ramp rate of 8 kW/s while Figure 2.7 shows controlled power for a fast inverter with ramp rate of 80 kW/s. In both cases, a controller delay of one time step and a communication delay of one time step exist. The fast inverter obviously outperforms the slow one despite the existing delays in both cases. This is apparent in both PCC power plots (top) and inverter power plots (bottom). In case of the faster ramps (Fig. 2.7), the inverter not only corrects the steady state power level but also partly diminishes the effects of fast power transients that occur during the load switching (apparent in the instantaneous spikes after each event in Fig. 2.7). This indicates that with the 10 Hz communication frequency and despite delays, the controller is still capable of capturing and controlling highly transient power fluctuations provided that the inverter is fast enough.

2.6 Summary of discussed problem

A centralized power scheduling and control system is developed for a microgrid that is simulated in real-time and communicates with the controller over the Internet at a rate of 10 Hz. The controller is able to compute a power reference for the microgrid, adjust power to that reference, and control SoC of the storage unit within the microgrid simultaneously. It is shown that despite the inherent delays in the system, the controller is able to react to both steady state and transient events in a timely manner while maintaining battery State of Charge within its desirable bounds.

Acknowledgements

Chapter 2, in full, is a reprint of the material as it appears in [28] "Microgrid control using remote controller hardware-in-the-loop over the Internet", Amir Valibeygi, Raymond A. de Callafon, Mark Stanovich, Michael Sloderbeck, Karl Schoder, James Langston, Isaac Leonard, Sourindu Chatterjee, and Rick Meeker. In 2018 IEEE Power & Energy Society Innovative Smart Grid Technologies Conference (ISGT), pp. 1-5. IEEE, 2018. The dissertation author was the primary investigator and author of this paper.

Chapter 3

Economic Scheduling and Real-Time Power Control for Time of Use and Demand Charge Reduction

3.1 Introduction

Integration of a solar PhotoVoltaic (PV) system with an Energy Storage System (ESS) in a microgrid provides opportunities for reducing facility energy costs. These economic benefits can be realized through the application of real-time control and optimization of energy storage and power flow, taking into account time-of-use (TOU) rates and peak demand charges. There is a growing interest in optimizing PV-ESS utilization in various microgrid applications [29, 30]. The energy cost reduction and local electric reliability benefits that can be achieved are very dependent on the strategy and methods implemented for control of power exchange and management of battery state of charge (SoC).

A number of solutions have been proposed for the day-ahead microgrid scheduling problem in the presence of uncertainties [30, 31]. In our study, the main two sources of uncertainty are load and PV. If such uncertainties are ignored, the resulting optimal schedule may turn out to be impractical due to constraint violations resulting from unanticipated variations in PV or load. A robust optimal scheduling approach is needed

that can tolerate uncertainty.

Demand charge is an electricity charge proportional to the customer's highest average 15-min demand during an entire monthly billing cycle. In applications involving demand charge, predictive schemes are among the most popular approaches as they allow an updated solution to the problem as new predictions become available at each step and therefore maintain high levels of optimality while ensuring constraints satisfaction [32, 33]. Demand charges constitute a major part of commercial and industrial facilities electricity charges in California, in some cases accounting for up to 50% of charges for such users [3]. Consequently, any PV-ESS system and algorithm for Demand Charge Management (DCM) should be able to accomplish peak demand reduction consistently over the entire month in order for it to be effective. This is often a daunting challenge given considerable uncertainty and variability in both PV generation and energy consumption.

The work of [34] evaluates the impact of two basic ESS utilization strategies over one month of system operation and investigates the peak reduction achieved in each case. Although they can achieve some degree of peak reduction, they do not demonstrate an optimal ESS utilization. Predictive approaches for demand charge reduction could potentially result in more optimal storage utilization. In [35], a predictive approach is used for daily minimization of peak demand and the robustness and peak reduction capabilities of the algorithm are studied. The optimization is run on a 24-hr basis at every hour beginning at midnight. As this work targets peak demand reduction over one day at a time, it does not ensure a month-long effective peak reduction as required for DCM. Clearly, a single unaccounted demand surge period can potentially destroy the month-long effort of the peak reduction algorithm. Due to the hard (financial) constraints in peak demand reduction, deterministic prediction-based approaches are susceptible to ineffectiveness due to prediction errors in conjunction with hard peak constraints. Under-

prediction of load could lead to battery failure (zero charge) while over-prediction results in over-conservative storage dispatch. It is shown in [36] that even small forecasting errors in dispatch algorithms with sophisticated forecasting could make these DCM algorithms perform worse than basic on-off approaches. Focusing entirely on DCM and disregarding TOU charges will also lead to sub-optimal solutions for the PV-ESS utilization. Therefore, the integrated PV-ESS system should be dispatched to reduce both TOU and peak demand charges to provide maximum savings.

In this work we present a strategy for simultaneous TOU and peak demand charge reduction over one full billing cycle of microgrid operation in the presence of variability in both PV generation and load demand. The approach is based on the computation of a nominal robust dispatch schedule for the ESS that exploits ESS capabilities to simultaneously reduce TOU and demand charges while considering possible uncertainties in PV generation and load demand. The nominal dispatch is computed by solving an optimization that minimizes the cost under normal PV/load conditions while also performing acceptably during periods of extreme PV/load by design of its constraints. This step also involves calculation of a target peak reduction level that is deemed achievable considering uncertainties within a month. To handle the unpredictable variability in PV generation and load demand in real-time, the optimal dispatch schedule is given as a reference to a power feedback controller (PFC). The PFC monitors the actual power flow at the PCC of the microgrid to ensure that power flow never exceeds the target peak demand by additional modulation of the ESS power dispatch around the computed nominal dispatch schedule. We apply the method to operate a commercial microgrid in California and present results for one month of successful operation. The reduction in peak demand translates into utility cost reduction during the billing cycle.

3.2   System overview

Microgrid Components. We consider a medical facility in Northern California that contains solar PV generation with a capacity of 250 kW integrated with 1 MWh of energy storage in a DC-coupled configuration as shown in Fig. 3.1. The DC/AC inverter of the integrated PV-ESS system has a maximum power capacity of 250 kW. The average load of the microgrid is about 530 kW while its minimum load is around 400 kW. Therefore, the microgrid would not be expected to export power to the utility grid.

Load and Solar Profiles. The solar generation and load profiles of the microgrid exhibit a significant amount of variability as shown in Fig. 3.2. Solar generation for 31 summer days is highly variable from day to day and shows the region's typical fog and low clouds pattern that are often observed during summer mornings. Overcast conditions are less common in the afternoon hours. The timing of burn-off of these low clouds is generally hard to predict day-ahead. A great degree of day-to-day variability is also observed in the load pattern of the microgrid. The variability is evident not only in the peak and off-peak power demand, but also in the time shift in the load patterns on different days. Some of these variations, such as the elevated early morning loads on six days appear to be independent of typical attributing factors such as weather and day of week, making load prediction very difficult.

In particular, the most crucial aspect of each day's load profile for our scheduling purpose is the amount and duration of each day's peak demand. This is due to the fact that this peak demand should be anticipated by the ESS to reduce demand charges of the microgrid. While most days show a broad peak around 650 kW to 700 kW, there are elevated peaks on two days. The possible co-occurrence of a load peak with overcast low-solar conditions creates a worst-case scenario that poses the greatest challenge for monthly peak reduction.
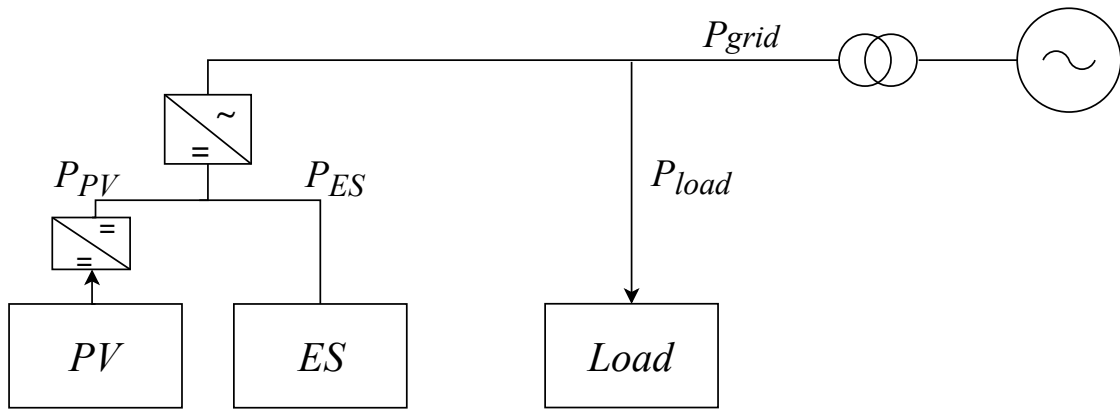
Figure 3.1. Schematic of the PV-ESS integrated system for a microgrid application.
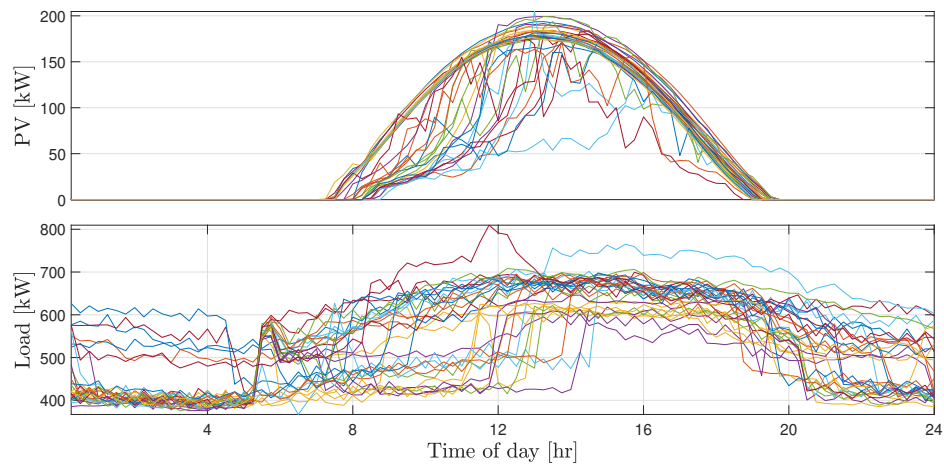
Figure 3.2. Daily PV power generation (top) and load demand (bottom) for 31 days during a full billing cycle (August 16 through September 15, 2018.
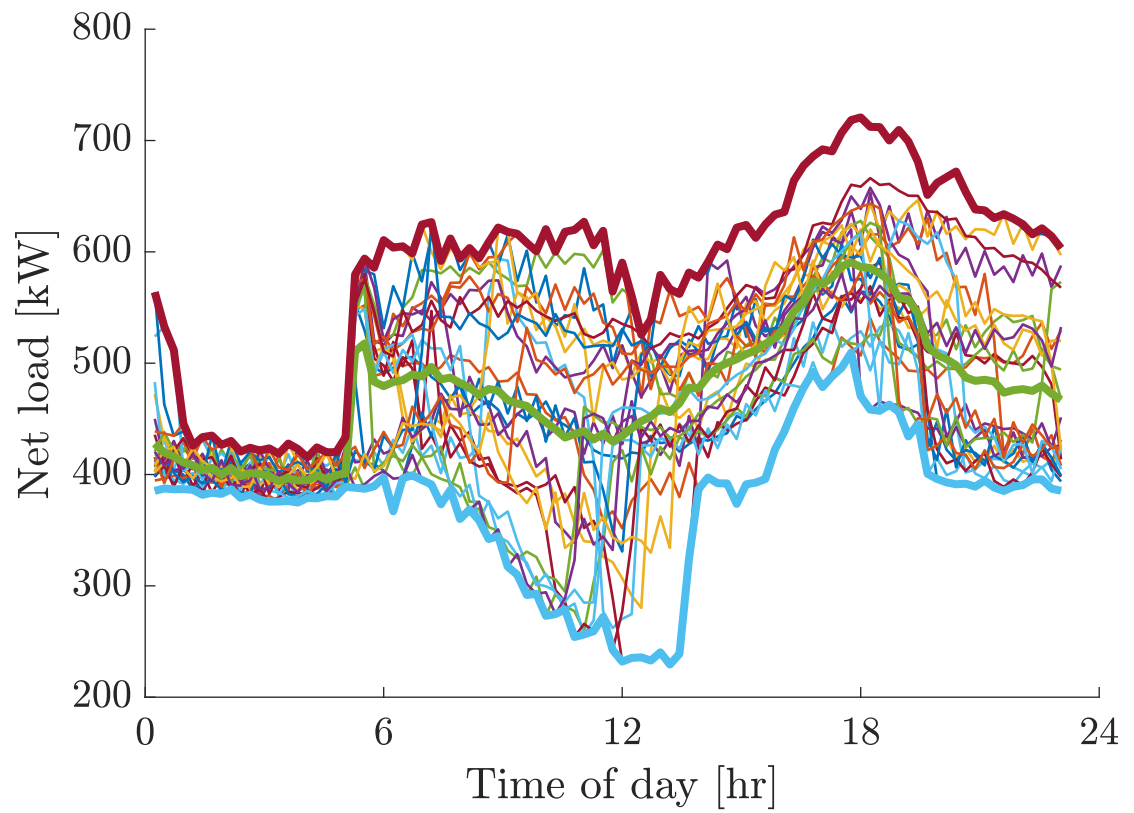
Figure 3.3. Daily net load and its uncertainty bounds for 31 days during a full billing cycle

Cost structure. Customer utility tariffs at the microgrid location include both energy time-of-use charges **TOU** and peak power demand charges **DC**. The cost is defined as

$$\mathbf{J}(P_{\text{load}}, P_{\text{PV}}, C) = \text{TOU} + \text{DC},$$

with

$$\mathbf{TOU} = \sum_{t=1}^{T} P_{\text{grid}}(t) \gamma_{\text{TOU}}(t)$$

$$\mathbf{DC} = \gamma_{\text{DC}}^{NC} \max_{t \in \text{all}} P_{\text{grid}} + \gamma_{\text{DC}}^{peak} \max_{t \in \text{peak}} P_{\text{grid}} + \gamma_{\text{DC}}^{semi} \max_{t \in \text{semi}} P_{\text{grid}}$$

Table 3.1 shows the structure of the cost coefficients γ. The non-coincident demand charge is 17.57 \$/kW for the overall peak demand of the month; an additional 18.64 \$/kW is assessed for peak demand during the peak hours of the month.

Table 3.1. Time-of-use and demand charge utility rates

Period	Time	γ_{DC}	[\$/kW]	γ_{TOU} [\$/kWh]
Peak	12pm-6pm		γ_{DC}^{peak}=18.64	0.1524
Semi-peak	8:30am-12pm 6pm-9:30pm	γ_{DC}^{NC}= 17.57	γ_{DC}^{semi}= 5.18	0.1119
Off-peak	9:30pm-8:30am		-	0.0851

3.3 Economic scheduling

3.3.1 Optimization

Standard cost minimization problem. We first formulate the standard cost minimization problem for one day of microgrid operation assuming foresight of load and

PV

$$\min_{P_{\text{inv}}} \mathbf{J}(P_{\text{load}}, P_{\text{PV}}, C). \tag{3.1}$$

The optimization is subjected to the constraints

$$
\begin{aligned}
&P_{\text{grid}}(t) + P_{\text{PV}}(t) + P_{\text{ES}}(t) = P_{\text{load}}(t) \\
&-P_{\text{inv}}^{max} \leq P_{\text{inv}}(t) \leq P_{\text{inv}}^{max} \\
&C_{\min} \leq C(t) \leq C_{\max} \\
&C(1) = C(N),
\end{aligned}
\tag{3.2}
$$

where $P_{\text{inv}} = P_{\text{ES}} + P_{\text{PV}}$ and $C(t)$ is the charge of the battery, which is updated as

$$
C(t) = \begin{cases}
C(t-1) + \eta P_{\text{ES}} \Delta_T & \text{charging} \\
C(t-1) - P_{\text{ES}} \Delta_T / \eta & \text{discharging}
\end{cases}
\tag{3.3}
$$

where η accounts for charge and discharge efficiency of the battery. In order to solve this problem, we define the variables $P_{ES,C}$ and $P_{ES,D}$ as the battery system's charging and discharging power respectively. Since only charge or discharge can happen at a time, we also define auxiliary binary variables $\delta_{ES,D}^t$ and $\delta_{ES,C}^t$ and convert the above state of charge constraints into

$$
\begin{aligned}
&0 \leq P_{\text{PV}}(t) + P_{\text{ES,D}}(t) \leq \delta_{ES,D}(t) P_{\text{inv}}^{max} \\
&-\delta_{ES,C}(t) P_{\text{inv}}^{max} \leq P_{\text{PV}} - P_{\text{ES,C}} \leq \delta_{ES,C}(t) P_{\text{inv}}^{max} \\
&\delta_{ES,D}(t) + \delta_{ES,C}(t) \leq 1 \\
&\delta_{ES,D}(t), \delta_{ES,C}(t) \in \{0, 1\} \\
&C(t) = C(t-1) + \eta P_{\text{ES,C}}(t) \Delta_T - P_{\text{ES,D}}(t) \Delta_T / \eta
\end{aligned}
\tag{3.4}
$$

This constitutes a mixed integer linear program that computes optimal daily energy storage schedule defined as $C^*(t), t = 1, 2, \ldots, T$ by scheduling inverter power dispatch $P_{\text{inv}}(t)$. Solving this program gives the reduced peak demand ($P^*_{\text{grid}} = \max P_{\text{grid}}$). The above optimization assumes full knowledge of the load demand $P_{\text{load}}(t)$ and the PV power $P_{\text{PV}}(t)$ which is an unrealistic assumption. Under the ideal case that the actual load and PV equal their predicted values, following the ESS schedule $C^*(t)$ from Eq. 3.2 also achieves the peak demand reduction predicted by this optimization. However, if PV and load differ from the values used for the optimization, following the ESS schedule results in a different and potentially higher peak demand. In the following, we formulate a modified version of this problem to ensure that the peak reduction is robust over one month despite the uncertainty in $P_{load}(t)$ and $P_{PV}(t)$.

Robust peak demand reduction. Individual day-to-day demand charge minimization independent of other days' peak demand is futile from a cost perspective. Any strategy chosen for demand charge reduction must consider the span of the entire month in order for it to be effective.

In particular, we define *extreme days* as days with low PV generation and high load demand. Net load is defined as the load - PV for each time of the day. To characterize extreme days, first the net load is computed for each data point and then the 2% and 98% quantiles are computed as extreme scenarios for each time step along the day. If the resulting solution from the previous optimization is chosen as the ESS schedule during an extreme day, it tends to incur substantial demand charge as it tries to follow the energy storage schedule of a day with normal load and therefore does nothing to reduce the particularly high net peaks for that specific day. If, on the other hand, the algorithm tried to match the peak target achieved under normal PV/load by deviating from its planned charge schedule, its overly aggressive target tends to deplete the battery to zero charge and the high demand peaks following battery depletion could incur substantial demand

charge for the month. This could possibly be prevented by computing a less aggressive peak reduction target that is achievable even in the event that extreme PV/load scenarios occur. In case of unforeseen variations, a controller will manage dispatch of the storage to maintain the peak of all days under the target value. As such, when extreme cases happen, the battery dispatch schedule is allowed to deviate from the nominal schedule in an attempt to keep peak demand below its target. This strategy involves A) computing a new robust scheduling profile and B) real-time power control to shave off unanticipated peaks by deviating from the nominal scheduling profile.

3.3.2   Robust scheduling

The robust scheduling algorithm aims at computing a robust charge scheduling profile as well as peak target that are achievable even under extreme PV/load scenarios. The algorithm involves solving the standard problem (3.1) with expected load/PV scenarios but additionally enforce that the resulting peak demand P^* can be satisfied under upper and lower extreme scenarios.

Although The resulting dispatch schedule is sub-optimal under nominal load/PV conditions, demand charge reduction remains feasible even under extreme load/PV conditions. While the above algorithm can mitigate net load peaks, it is not robust to uncertainty. The actual storage dispatch profile should be allowed to deviate from the nominal profile computed using the above algorithm in order to reach the peak reduction target set for the entire month. This amounts to temporarily sacrificing TOU savings during critical intervals to satisfy the peak reduction targets. In the following, we will introduce a controller that allows deviation from the nominal profile to achieve peak reduction under extreme load/PV conditions.

3.3.3 Power feedback control

The computed schedule for the charge profile $C(t)$ from the modified (robust) optimization algorithm is used as a reference signal to the power feedback control (PFC). The PFC monitors both the real-time power flow $P_{\text{grid}}(t)$ as indicated in Fig. 3.1, and the measured charge level $C(t)$ reported by the ESS. The PFC algorithm is a basic Proportional-Integral controller given by

$$P_{\text{inv}}(t) = K_p(P_{\text{ref}}(t) - P_{\text{grid}}(t)) + K_i \sum_{\tau=0}^{t-1} P_{\text{inv}}(\tau), \tag{3.5}$$

where the power reference signal $P_{\text{ref}}(t)$ is computed from the observed ESS charge $C(t)$ and subject to the imposed demand limit $\bar{P}$ as

$$P_{ref}(t) = \min\{P_{uc}(t-1) - K_{SoC}(\bar{C}(t) - C(t)), \bar{P}\} \tag{3.6}$$

where $K_{SoC} > 0$ and $P_{uc}(t-1) = P_{grid}(t-1) + P_{inv}(t-1)$ is the previous value of the *uncontrolled* grid power flow at the PCC. t is the time step and τ is an index over each step of the current demand charge interval. Choosing the time increment $\Delta T = 1$ sec will additionally result in power flow smoothing. Eq. (3.6) ensures that $P_{ref}(t)$ is adjusted in comparison to $P_{uc}(t-1)$ in case $\bar{C}(t) \neq C(t)$ to allow for additional (dis)charging of the ESS to track the computed schedule for the charge profile $\bar{C}(t)$. However, $P_{ref}(t)$ is always guaranteed to be less than $\bar{P}$ to enforce peak demand limitations. The PI control parameters K_p and K_i in (3.5) and the proportional SoC adjustment parameter K_{SoC} in (3.6) are tuned to accommodate for the dynamics and delay in the ESS inverter response and battery storage size respectively.

3.4 Testing and hardware implementation

A Controller Hardware-in-the-Loop (CHIL) simulation was developed to assist with the development, testing, and evaluation of the optimal scheduling and real-time power control algorithms and code throughout the project, as also described in [28]. The modeled system included the on-site electric power hardware including the inverter, PV, ESS, and loads. A digital real-time simulator (DRTS) was used for the power system simulation, and other peripheral computers provided computer network interfaces (e.g., Modbus). The CHIL setup provided a realistic environment to benchmark and de-risk power control performance before installation and operation within the actual system. The economic scheduling and real-time power feedback control have been implemented on a SEL-3355 industrial computer that acts as the supervisory microgrid controller. Synchronized high-resolution power flow data is collected at 60 Hz using IEEE certified Phasor Measurement Unit's (PMU's) monitoring 3-phase current and voltage at the PCC of the microgrid, as also described in [28]. Following the CHIL testing, the verified controller was set up to connect to the actual hardware (inverter) and actual real-time operation was performed on site.

3.5 Results and discussion

Fig. 3.4 and Table 3.3 indicate the peak demand of the facility with and without the dispatch algorithm over the billing period starting on August 16 through September 15, 2018. Fig. 3.5 provides the resulting ESS charge for all days of the month. Without PV and ESS, the peak load of the microgrid over this 31-day period would have remained below 710 kW except for days 27 and 28 of the period. The peaks in the building load on day 27 and 28 were respectively 56 kW and 101 kW higher than the peak of the rest of the month, which occurred on day 26. This would have amounted to about 14% or

$1,775 increase in non-coincident demand charge. The addition of PV alone without any control would have diminished the peak on days 27 and 28 to 720 kW resulting in a $[809 - 720]/809 = 10.9$ % or $1,564 savings in demand charge. But even with PV, days 27 and 28 still increase the monthly peak demand by 54 kW. Therefore, levelling the peak of these two days and following a simple nominal profile for the rest of the month, could possibly provide substantial savings. Fig. 3.4 shows that this has been achieved as the monthly peak demand is reduced by 62 kW to 658 kW by reducing peak demand of those two extreme days below the peak of rest of the month, which now occurred on day 15. Different components of the utility bill under different scenarios are summarized in Table 3.2.

Table 3.2. Breakdown of different components of the utility bill over one month.

Cost Component	No PV	PV	PV & ES
TOU	45207	40271	39910
DC^{NC}	14224	12664	11576
DC^{peak}	14679	12900	11212
DC^{semi}	3525	3254	3255
Total	77636	69089	65954

The algorithm could have targeted even more substantial peak reduction over the month. Simplistically, considering the 250 kW power limit of the inverter, one may expect that the target peak could be around 250 kW less than the original load peak (without PV and ES). This is unrealistic as the ESS cannot sustain the duration of time needed to reduce the peak. For example, consider the original (load) and reduced demand (P_{grid}) on day 27 in Fig. 3.6. Significantly higher than normal load was present starting around noon and continued until midnight. To achieve the peak demand target and stay under the dashed black line during that day, the algorithm forces the ESS to deviate from the nominal charge profile and discharge at a higher power. The discharging continues until around 2100 h when the load has decreased sufficiently that discharging is no longer required to reduce the peak load. The strategy leaves the ESS at SoC that is only slightly

above its minimum allowable SoC of 10%. If a more ambitious peak reduction had been targeted for the month, although it could have achieved a larger peak reduction for all days up to day 27, the unusually high demand on day 27 would have ruined the savings. If the peak target had been set any lower on day 27, the battery's limited energy capacity to provide the required power over that extended period would have resulted in complete battery discharge during the afternoon. That would have resulted in zero savings when the evening peak occurred on the 27th and therefore the entire month's peak reduction effort would have been wasted. This example clearly makes the case for the strategy proposed in this work; i.e. utilizing ESS to partially achieve both TOU and demand charge savings during days with close to normal load/PV conditions while prioritizing peak demand reduction over TOU for days with extreme load/PV conditions.

Table 3.3. Load data for the billing cycle showing peak load, peak load if only PV existed and peak load under the current algorithm.

Date	Max load [kW]	Max load with PV [kW]	Max load w/ PV and ES [kW]
Aug 16 (Day 1)	682	628	641
Aug 17 (Day 2)	697	611	610
Aug 18 (Day 3)	621	564	584
Aug 19 (Day 4)	602	551	583
Aug 20 (Day 5)	676	579	594
Aug 21 (Day 6)	681	653	648
Aug 22 (Day 7)	688	643	646
Aug 23 (Day 8)	694	641	644
Aug 24 (Day 9)	664	627	620
Aug 25 (Day 10)	624	593	619
Aug 26 (Day 11)	618	590	600
Aug 27 (Day 12)	692	615	643
Aug 28 (Day 13)	692	630	638
Aug 29 (Day 14)	699	646	651
Aug 30 (Day 15)	687	638	658
Aug 31 (Day 16)	695	620	623
Sep 1 (Day 17)	610	550	550
Sep 2 (Day 18)	612	571	602
Sep 3 (Day 19)	621	580	610
Sep 4 (Day 20)	701	610	594
Sep 5 (Day 21)	677	588	609
Sep 6 (Day 22)	696	623	642
Sep 7 (Day 23)	698	657	645
Sep 8 (Day 24)	633	626	620
Sep 9 (Day 25)	646	627	629
Sep 10 (Day 26)	708	666	653
Sep 11 (Day 27)	764	720	652
Sep 12 (Day 28)	809	705	649
Sep 13 (Day 29)	697	643	638
Sep 14 (Day 30)	681	620	615
Sep 15 (Day 31)	627	580	570
Max	809	720	658
Reduction	–	10.9%	18.6%
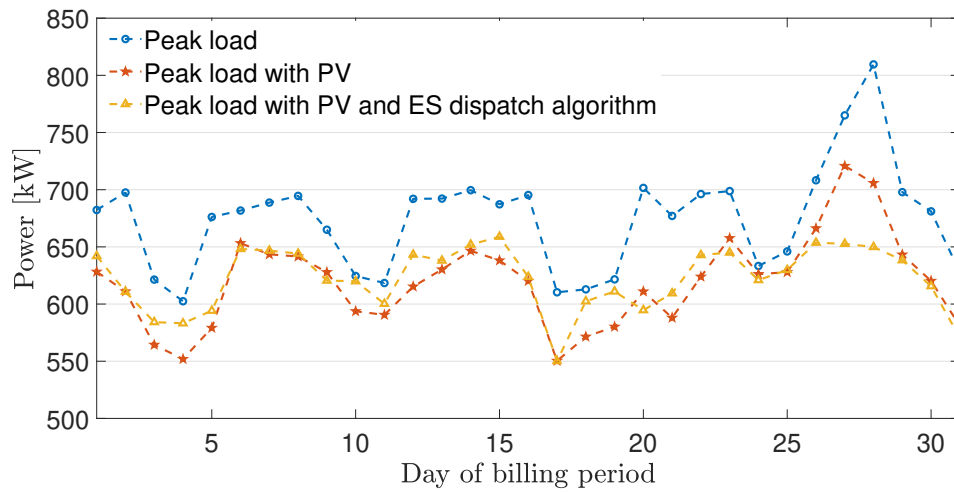
Figure 3.4. Daily peak load of the microgrid without PV or ESS; with PV, but no ESS; with PV, ESS and optimal scheduling over a full 31 day billing cycle
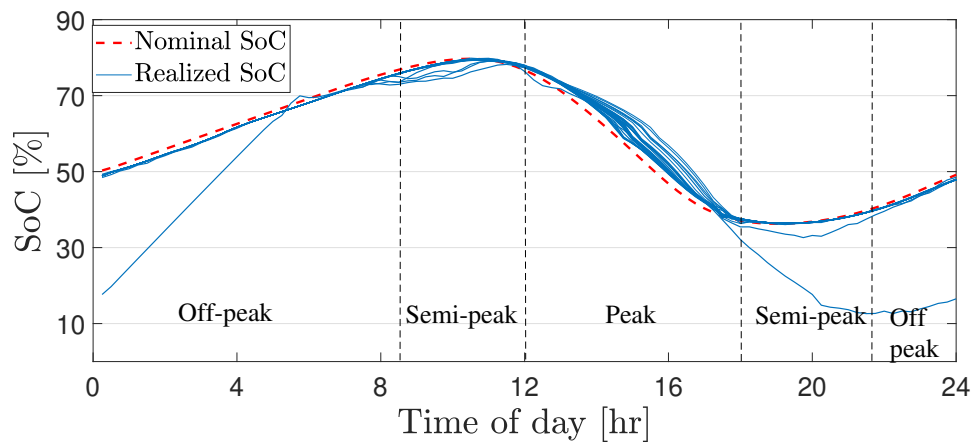
Figure 3.5. Daily ESS SoC profile for 31 days of a full billing cycle. While for all days except one, the charge profile is close to the nominal profile, the profile deviated from the nominal profile during a day with high load (Sep. 11th, Day 27 of the period) to minimize peak demand and maximize demand charge savings. This deviation is performed by the power feedback controller.
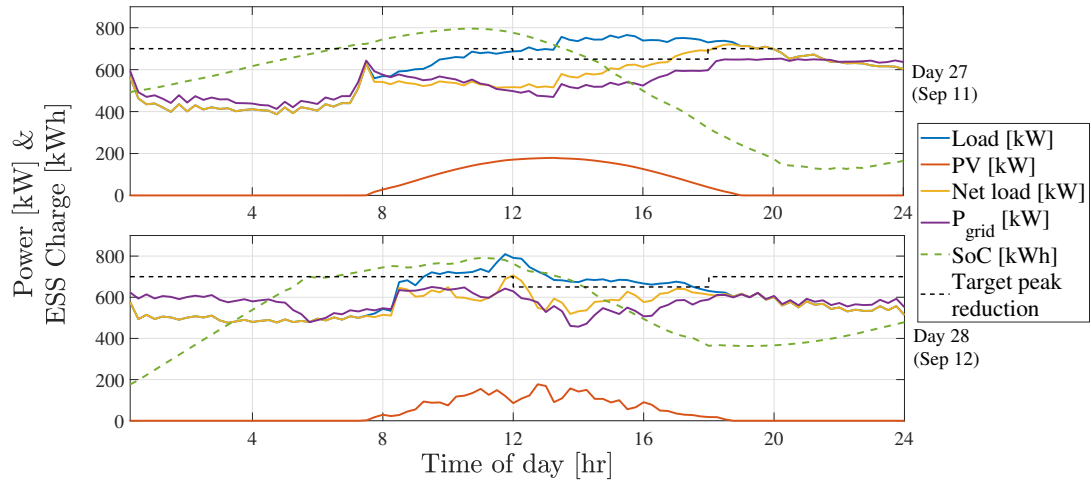
Figure 3.6. Microgrid load, PV, and controlled power flow from the main grid during the two days (27 at the top and 28 at the bottom) with unanticipated high load. Note the satisfaction of peak demand targets for both days and the deviation of the SoC profile $C(t)$ during the first day to maximize the peak reduction.

3.6 Summary of discussed problem

This paper presents a systematic methodology for simultaneous Time of Use (TOU) and peak demand charge reduction over a billing cycle for a microgrid with a solar PhotoVoltaic (PV) system and battery Energy Storage System (ESS). The approach is formulated by first modifying the daily optimal scheduling problem to ensure robust scheduling and peak reduction despite uncertainties existing over an extended period. Next, by combining the robust scheduling with a real-time power feedback controller (PFC) to modulate the ESS power dispatch, the system is driven to reach the target peak demand consistently. The optimal schedule is computed via a convex optimization while the PFC algorithm ensures peak demand reduction in the presence of unpredictable variability in PV generation and load in real-time. The scheduling and control system developed and tested for this application is currently performing reliably, reducing energy costs for a sustained period of time in a commercially operated microgrid at a California

hospital.

Acknowledgements

Chapter 4

Robust Power Scheduling Under Uncertainty in Renewable Energy Generation

4.1   Introduction

With the rapid growth of renewable Distributed Energy Resources (DERs) in power systems and due to their inherent uncertainties, economic energy management and planning is of great importance for microgrids of different scales. A Microgrid is defined as a group of interconnected DERs, loads, and storage units that act as a unified entity in the electricity market and is able to operate in both connected and islanded modes from the main electricity grid. In the connected mode, microgrids are connected to the main grid at the Point of Common Coupling (PCC) and any power exchange between the microgrid and the main grid is measured at this point. DERs within the microgrid may provide part or all of the microgrid's energy demand; hence reducing the energy drawn from the main grid. Electricity providers use different pricing schemes to encourage certain consumption behaviors among consumers and make power grids more efficient and reliable. Microgrids may use such energy price data to optimally schedule their loads, storage units, and dispatchable DERs [37].

The existence of storage provides additional flexibility to benefit from such

pricing schemes. Optimal microgrid scheduling should take into account microgrid operational costs and seek to compute optimal storage/DER dispatch schedule [38, 39, 40]. This optimal power value should be computed based on load requirements, hardware constraints, storage capacity, and with the consideration of intermittent and uncertain nature of renewables. Load and renewable generation uncertainty are two major sources of uncertainty in microgrids that could highly impact its economic performance [30]. Various approaches have been proposed to address uncertainties in the predicted load [41, 42]. Renewable uncertainties generally impose a greater impact if a significant portion of microgrid energy is provided by renewable DERs. Various robust and stochastic microgrid scheduling methods have been studied to address renewable uncertainty challenges.

A widely popular approach to handle uncertainty is to formulate the problem as an stochastic programming problem by considering different scenarios for the uncertain parameters and their probabilities [43]. The goal of the problem will then be minimizing cost of current decisions plus the expected value of cost of future decisions. In an alternative approach, uncertain generation can be handled by robust optimization formulations where all possible scenarios within the uncertainty set are accounted for and constraint satisfaction is guaranteed regardless of the realization of the random variables within a certain set [44, 32]. If a feasible solution exists for this problem, it tends to be more conservative yet less computationally intensive compared to the stochastic formulation. In a different approach, the problem can be studied within the framework of Chance Constrained Programming (CCP). Assuming known distribution for the uncertain variables, CCP can be used to compute a minimizing solution that meets inequality constraints with a certain probability [45, 46]. Although less conservative for most realizations of the random variable, this approach may lead to constraint violation if knowledge of distribution is inaccurate or if extreme realizations of the random variables occur.

In the context of day-ahead microgrid scheduling, the intended scheduling interval is relatively large. In addition, forecast of uncertain renewable generation will be updated and more accurate forecasts will become available as time progresses. These are two motivations behind taking a model predictive approach to the scheduling problem. If such approach is taken, one need not determine a unique scheduling at the beginning of the 24-hr interval that is robust against all possible uncertainties. Instead, some possible realizations may be allowed to violate the conditions at steps far into the future. Future updates of the model predictive solution will guarantee that no actual condition violation will happen. This framework will however allow for more optimal (less conservative) solutions to the problem. Diferent works have taken a model predictive approach to the scheduling problem [47, 48]. Reference [43] compares the performance of stochastic and deterministic MPC in economic scheduling of microgrids. Also, [49] provides a model predictive economic scheduling solution and discusses the impact of forecast error.

In this work, microgrid optimal scheduling problem is considered for a grid-connected microgrid with solar generation and energy storage. Approximate solar forecast and its uncertainty bounds are assumed to be known for the day-ahead microgrid operation and are updated at 15-min intervals. To reduce conservatism in the presence of inherent uncertainties of PV generation, the problem is formulated within a model predictive framework and hard constraints are replaced with their relaxed versions at each step of MPC. At each step with the newly updated predictions, a quadratic programming problem is solved to yield an economic solution.

Notation. Set of time intervals over 24 hours is denoted as $\mathcal{T} = \{1, 2, ..., T\}$. $s(t)$ is a random variable representing solar generation during interval t, while $\bar{s}(t, \tau), s_u(t, \tau), s_l(t, \tau)$ are solar generation forecast, its upper bound, and its lower bound during interval t for predictions made at step τ. In a similar way, $c(t)$ is a random variable showing the charge level of the battery during interval t and $\bar{c}(t, \tau), c_u(t, \tau), c_l(t, \tau)$ are

charge level forecast, its upper bound, and its lower bound during interval t for MPC step τ. In the remainder of the paper, τ indices for MPC steps are dropped for simplicity when it does not lead to confusion. $d(t), e(t)$, and $r(t)$ show load demand, energy to/from the inverter, and energy flow at PCC during interval t. Energy variables (s, d, e, r) are assumed uniform over the intervals and represent total energy over the 15-min interval.

4.2   System description and problem formulation

We study a grid-connected microgrid consisting solar energy generation, battery energy storage and several loads. Strict load requirements of the microgrid enforce that complete demand must be met at each time. The storage unit can be exploited to implement power shifting by using the stored energy at times of high market price and therefore reduce energy input from the main grid at those times. The economic scheduling problem is expected to propose a microgrid power flow solution at the point of common coupling that while reducing a certain cost function, meets microgird's operational constraints and guarantees robustness against PV prediction uncertainties. This work aims to develop a model-predictive robust optimization scheme based on 24-hr prediction of solar energy, load demand, and price. The 24-hr horizon is divided into $\Delta_T = 15$ min intervals and the optimization algorithm for the remaining intervals of the 24-hr period is run at the beginning of each MPC step. However, only the results for the impending interval will be implemented. We first formulate the benchmark scheduling problem without uncertainties.

4.2.1   Benchmark problem

The microgrid is assumed to have a certain energy demand for each of the considered intervals $t \in \mathcal{T}$. The sum of energy from the main grid and energy from

47

DER/storage during each interval should meet this load demand

$$d(t) = e(t) + r(t) \tag{4.1}$$

Additionally, variation in the charge level of the battery can be expressed as

$$c(t+1) = c(t) + s(t) - e(t) \tag{4.2}$$

It should be noted that as indicated in this equation, a unique decision variable $e(t)$ (inverter energy to/from microgrid) should be applicable regardless of the actual realization of PV generation. This means that uncertainty in PV generation should only translate into uncertainty in the state of charge of the battery.

Constraints. The microgrid optimal scheduling problem should be solved with the consideration of operational constraints of the system. A few of the most essential constraints are formulated in this section. The inverter can only provide power to the microgrid subject to its operational limits

$$P_{min}.\Delta_T \leq e(t) \leq P_{max}.\Delta_T \tag{4.3}$$

where $P_{min/max}$ is min/max inverter power. The state of charge of the battery should stay within its upper and lower limits

$$C_{min} < \bar{c}(t, \tau) < C_{max} \tag{4.4}$$

The scheduling should further enforce that the final charge level of the battery at the end

of the 24-hr interval is equal to its initial charge.

$$\bar{c}(t=T,\tau) = C_0 \tag{4.5}$$

Taking into account the last two constraints, the set of feasible battery charge levels can be denoted as

$$\mathscr{C} = \{c(t,\tau) \mid C_{min} < c(t,\tau) < C_{max} \; \forall t \geq \tau;$$
$$c(t=T,\tau) = C_0\} \tag{4.6}$$

Cost function. The optimal scheduling problem is expected to minimize a cost function comprising cost of electricity and other operational costs of the microgrid. Cost of energy provided by the renewable source is assumed to be negligible. The total cost associated with microgrid operation is formulated below. The first term accounts for energy charge during the 24-hr period and the second term shows demand charge incurred during the time interval with maximum energy consumption. The last cost term is a penalty on battery charge/discharge to reduce energy loss due to battery round-trip efficiency.

$$f = \sum_{t=1}^{T} v(t)r(t) + kr_{max} + \alpha \sum_{t=1}^{T} e(t)^2 \tag{4.7}$$

where $v(t)$ is electricity unit price at time t, r_{max} is energy flow at PCC during the interval with maximum energy consumption, and k and α are weighting coefficients.

4.2.2 Renewable forecast uncertainty

Numerous solar forecasting methods have been explored in the literature. In this work, we assume knowledge of expected value of solar generation during interval t at

MPC step τ, $E\{s(t)\}_\tau = \bar{s}(t, \tau)$ as well as its upper and lower bounds $s_u(t, \tau), s_l(t, \tau)$ is available for all $t \geq \tau$. These bounds should guarantee with a high degree of confidence that the realized amount of solar generation will be within their range. This solar forecast data is updated with the most recent data at each step. Clearly, more accurate predictions and smaller uncertainty bounds are available if forecast interval t is closer to current step τ. For each MPC step τ, we define the sequence $S_u : \{s_u(\tau), s_u(2), ..., s_u(T)\}$ as a solar scenario consisting of upper forecast points for all times $\tau \leq t \leq T$. This scenario represents an unlikely realization of $s(t)$ over the remainder of the 24-hr period which takes the upper solar forecast value at each time. In a similar way we define S_l and $\bar{S}$ as the lower and average solar scenarios. In order to be able to implement the unique decision variable $e(t)$ for all possible solar scenarios, the uncertainty in solar generation should only translate into uncertainty in the state of charge of the battery. With the motivation to obtain a single scheduling plan that accommodates various solar generation scenarios $(\bar{S}, S_u, S_l)$, we intend to extend the aforementioned problem into a robust scheduling problem.

4.3 Uncertainty handling and robust scheduling

4.3.1 Existing Approaches

A rudimentary approach would be to enforce the above hard constraint (4.4) on charge level of all possible solar generation scenarios.

$$C_{min} < c_u(t, \tau) < C_{max}$$

$$C_{min} < c_l(t, \tau) < C_{max} \tag{4.8}$$

Such constraint over the 24-hr period could make the solutions highly conservative or even infeasible [44]. To reduce the conservatism knowing that the solution will be

updated at later steps, a chance constrained formulation would require

$$P(C_{min} < c_u(t, \tau) < C_{max}, C_{min} < c_l(t, \tau) < C_{max}] \geq \beta$$

where $P(.)$ is probability of the constraint satisfaction. This constraint is a rational relaxation of the previous constraint. It can therefore yield feasible/more optimal solutions for the next MPC step and update its solution at every step. It however requires knowledge of distribution of the uncertainty and demands higher computational complexity than the previous approach. A different approach would be to implement an additional cost term in the cost function associated with SoC limit violation in the place of SoC constraints for upper and lower SoC scenarios [41].

$$
\begin{aligned}
f_{aug} = {} & \sum_{t=1}^{T} max\{0, c_u(t) - C_{max}\} \\
& + \sum_{t=1}^{T} max\{0, C_{min} - c_l(t)\}
\end{aligned}
\tag{4.9}
$$

Although this additional cost term could act as a soft constraint on SoC limit violation, it has no structure to differentiate between intervals with and without uncertainty.

4.3.2 Proposed method

We propose a framework to generalize the regular SoC constraints (4.6) in a structured way that makes it applicable to uncertain solar scenarios. The idea is to enforce the hard constraint (4.6) only on the expected value of solar forecast and a relaxed version of it on other possible solar generation scenarios (S_u, S_l). The result is that instead of limiting all possible charge level realizations to fall within upper and lower limits, we allow them to linearly grow out of bounds during uncertain intervals, but control their growth by a parameter representing tightness of the constraint. The rationale behind this scheme is that the uncertainty in accumulative solar generation is

additive over time and therefore storage scheduling over time should allow more relaxed constraints in the future in order for the solution to remain feasible. We define parameter η to characterize such relaxed constraints on SoC of battery under upper and lower PV scenarios. Figure 4.1-top shows the proposed constraint on the battery charge level across different uncertainty scenarios at the beginning of the 24-hr interval. Also, Figure 4.1-bottom shows the updated constraints at time τ for the remainder of the 24-hr interval. These constraints can be formulated as

$$C_l(t, \tau) < c_u(t, \tau) < C_u(t, \tau)$$
$$C_l(t, \tau) < c_l(t, \tau) < C_u(t, \tau) \tag{4.10}$$

$$C_{l[u]}(t, \tau) = \begin{cases} C_{min[max]} & t < t_a \\ C_{min[max]} - [+](t - \tau).\eta & t_a < t < t_b \\ C_{min[max]} - [+](t_b - \tau).\eta & t_b < t \end{cases}$$

t_a and t_b are the time stamps of start and end of uncertainty in solar prediction. For $\eta = 0$, this condition is equivalent to the strict conditions in (4.4). Applying the hard constraint ($\eta = 0$) may yield no feasible solution over the entire 24-hr interval which means the problem was not solvable if hard SoC constraints were to be enforced on all possible scenarios at all times. For larger values of η, condition (4.10) means relaxation of conditions (4.4) as time progresses. Condition (4.10) could be tested iteratively with different values of η to obtain the smallest η (η^*) for which a solution exists. Solutions will then exist for all $\eta > \eta^*$. The bigger the choice of η, the less conservative and less robust the solution will be. The benefit of the alternative soft SoC constraint, as opposed to hard SoC requirement (4.4), is the reduced conservatism on the optimal solution

freedom while keeping different scenarios under control. However, by running this algorithm at regular 15-min periods with updated forecast, we ensure that the resulting schedule will strictly meet hard SoC requirements (4.4).
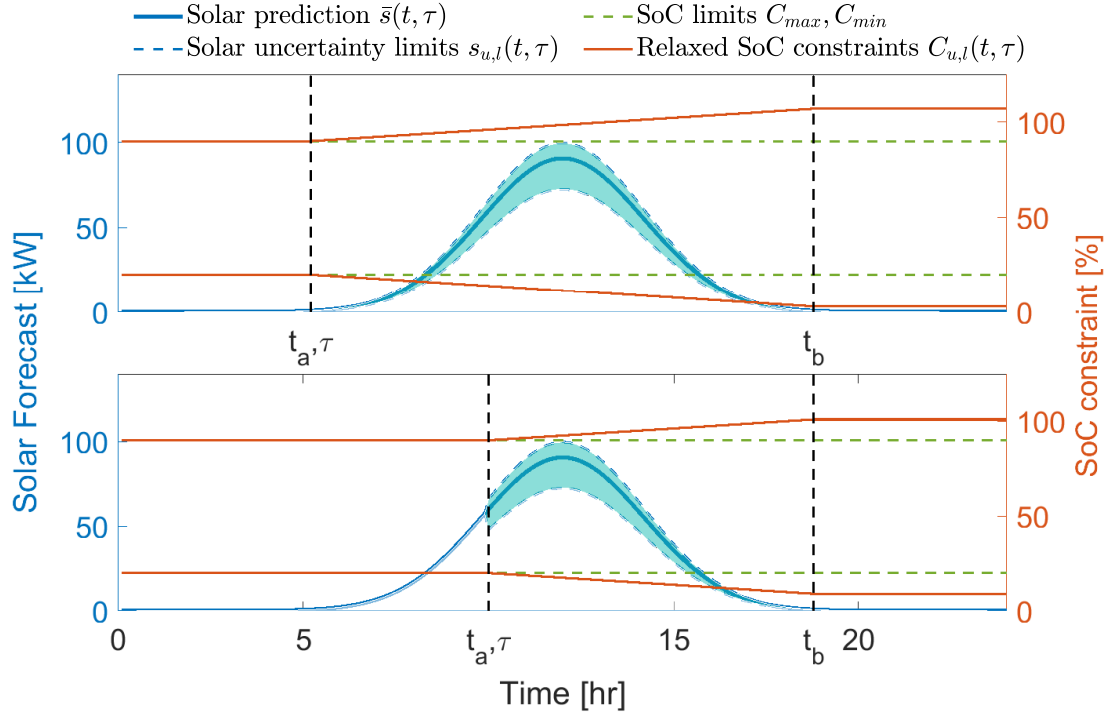
Figure 4.1. Top. Uncertainty plot at the beginning of the 24-hr interval. Expected solar generation and its upper and lower uncertainty bounds are shown in blue. Hard SoC limits (green) are replaced by soft constraints (orange) to reach feasible solutions and reduce conservatism when there is uncertainty in solar prediction. **Bottom.** Uncertainty plot at time $\tau = 10\ hr$ of the 24-hr interval. Updated solar forecast and its upper and lower uncertainty bounds for the remainder of the 24-hr interval $(t \geq \tau)$ are shown in blue.

Robustness analysis. At each step of MPC, we want to make sure that the output $e(t)$ computed for the next step with soft SoC constraints does not lead to SoC limit violation. To achieve this, one can shift the soft constraint one step to the right so that the impending step always follows the hard limits while steps after that follow soft limits. Another less conservative approach would be to limit next step's optimal solution

according to the following

$$c(\tau) + s_u(\tau) - C_{max} \leq e(\tau) \leq c(\tau) + s_l(\tau) - C_{mn} \qquad (4.11)$$

Based on the previous discussion, we can formalize Algorithm 1 for microgrid robust optimal scheduling.

Algorithm 1. Microgrid Robust Optimal Scheduling

1: Start at the beginning of the 24-hr interval $\tau = 1$
2: Obtain price and load demand data for the next 24-hr
3: **while** $\tau \leq T$ **do**
4:     Update solar forecast and its bounds for $t = \tau : T$
5:     Initialize parameter $\eta = \eta_0$
6:     **repeat**
7:         Solve the quadratic programming problem with
          cost function (7) and subject to constraints
          $(1 - 5, 11, 12)$ using any available solver
8:         Update η using bisection to find smaller values
          of η that gives a feasible solution
9:     **until** $|\eta_{current} - \eta_{last}| < \varepsilon$
10:     $\eta^* = \eta$
11:     Obtain Optimal scheduling solution with $\eta = \eta^*$ for
          $t = \tau : T$ but implement only $e(t = \tau)$
12:     Wait until the beginning of the next scheduling
          period and arrival of updated forecast data
13: **End while**

4.4   Results

We study the microgrid of a medical facility that is planning integration into the main grid. Solar generation forecast at the beginning of the 24-hr horizon and its uncertainty bounds for the considered facility are illustrated in Figure 4.1.Load demand and price data are also illustrated in Figure 4.2. Also, microgrid specifications are listed in table 1.
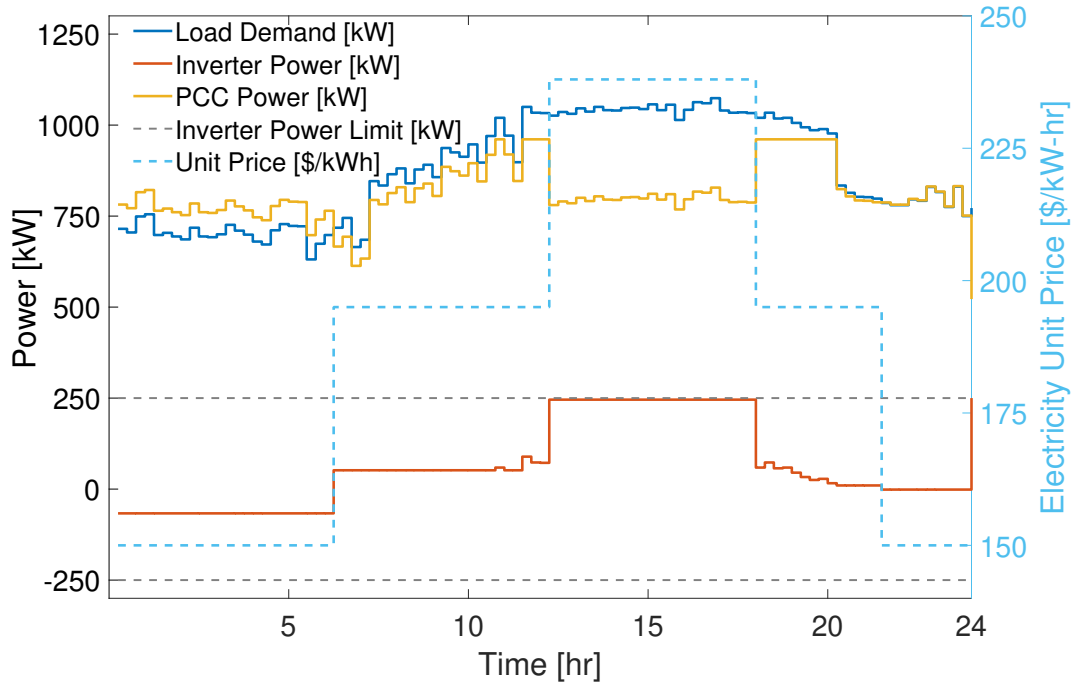
Figure 4.2. Optimization results for scheduling performed at time $\tau = 1$.
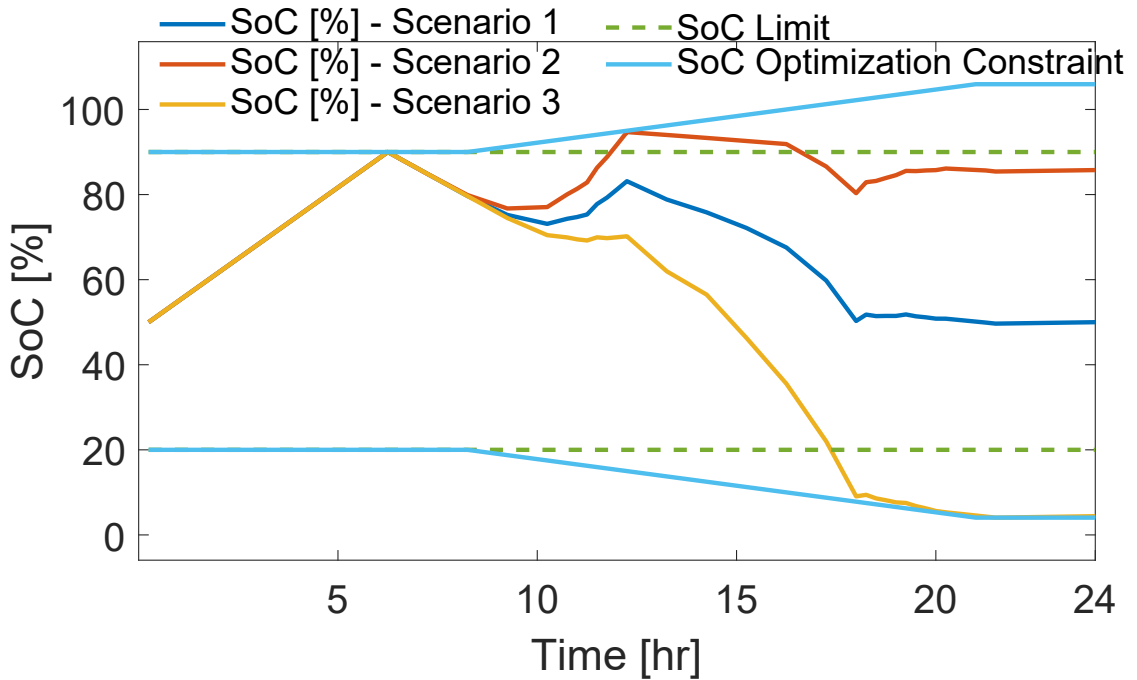
Figure 4.3. SoC variation within relaxed constraints for MPC step 1 (time step $\tau = 1$) with expected $\bar{S}$, upper S_u, and lower S_l solar generation scenarios
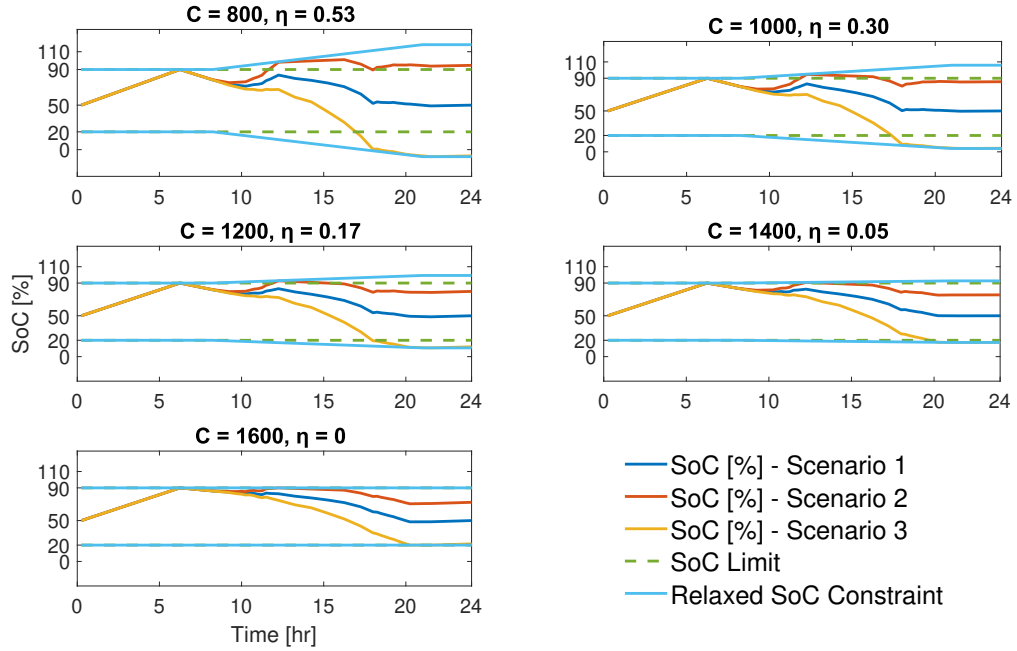
Figure 4.4. Effect of storage size on scheduling with uncertainty. With increasing storage size, η^* decreases meaning that relaxed constraints come closer to hard SoC constraints.

We seek to compute an economic schedule for inverter power that can be implemented regardless of the realization of solar profile within the estimated boundaries. An attempt to solve the problem with the given solar bounds and hard constraints of equation (4.4) on all solar scenarios reveals that no feasible solution exists. Even if such solution existed, it would be highly conservative due to the requirement that all possible scenarios should stay within bounds even for time intervals far from the current interval for which accurate predictions do not exist. Since we assume no knowledge of uncertainty distribution except its upper and lower bounds, CCP is not a good solution fit for our problem.

Next we investigate microgrid scheduling problem over 15-min intervals using the proposed algorithm. Algorithm 1 is implemented on a system with parameters $C = 1$ MWh, $C_0 = 500$ kWh, $SoC_{min} = 20\%$, $SoC_{max} = 90\%$, $P_{min,max} = -(+)250$ kW, $\eta_0 = 1$, and $\varepsilon = 0.01$. Gurobi commercial solver is used for solving the quadratic programming

problem at each step. The resulting power profile as well as battery charge levels are presented. Figures 4.2 and 4.3 show the result of scheduling at time $\tau = 1$. Maximum power flow at PCC over the entire 24-hr interval is remarkably reduced by flattening PCC power profile. The inverter power profile has also low volatility in this case which makes it robust against unmodelled prediction errors. Evolution of battery charge level within the soft SoC constraints under three scenarios of solar generation is indicated in Figure 4.3.
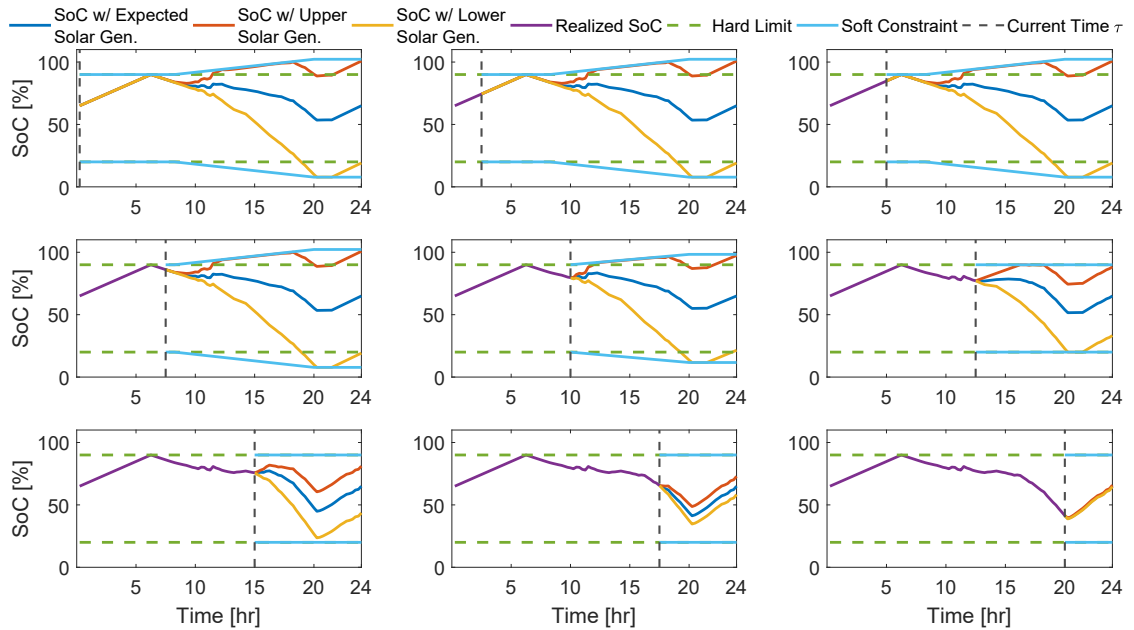
Figure 4.5. Evolution of battery SoC over the 24-hr interval shown at 9 steps during the day. The dashed line shows the current step of optimization and the purple line shows the actual realization of battery charge level for past times. While the results of optimization at earlier steps show apparent SoC limit violation at times far from the current step, no actual SoC violation occurs as time proceeds as the optimization is updated at every MPC step.

To investigate the effect of storage size while solar uncertainty exists, Figure 4.4 shows economic scheduling results at the start of the 24-hr horizon. For microgrids with different storage sizes, the minimum viable η (η^*) for solution feasibility is obtained for each case. For smaller storage sizes (800, 1000, 1200, 1400), η^* is greater than zero

meaning that no feasible solution would exist had the soft constraints not replaced the hard ones. For storage of size 1600, the problem is solvable with $\eta = 0$ or equivalently hard SoC constraints.

To illustrate the evolution of microgrid charge level over the 24-hr interval, Figure 4.5 shows the evolution of battery charge level as the result of scheduling over the 24-hr interval. It is seen that as time proceeds and updated solar predictions become available, soft SoC constraints become tighter and no violation of hard SoC limits is observed at the end of the 24-hr interval.

4.5   Summary of discussed problem

A robust microgrid scheduling algorithm is proposed to optimize power exchange between microgrid and the main grid with uncertain solar prediction. To implement the algorithm, it suffices to have upper and lower bounds on solar generation to describe such uncertainty. By relaxing the original constraint on the charge level of the battery, optimal solutions are sought in a larger space of possible battery charge levels. The problem is formulated as a quadratic program and is solved at 15-min steps over a 24-hr interval and updated prediction data is used for each step. The model predictive formulation of the problem ensures that the apparent hard constraint violation does not lead to charge level requirement violation. The results indicate scheduling profiles that are in agreement with the defined cost function and follow the expected requirements under different uncertainty scenarios. Also, the effect of storage size on handling the uncertainty is investigated.

Acknowledgements

Energy Society Innovative Smart Grid Technologies Conference (ISGT), pp. 1-5. IEEE, 2019. The dissertation author was the primary investigator and author of this paper.

Chapter 5

Predictive Hierarchical Control of Power Flow in Large-Scale PV Microgrids with Energy Storage

5.1 Introduction

Utility scale solar generation has been attracting increasing interest in light of various factors [51]. Besides its environmental benefits, it offers the main grid a single large resource, helping to maintain its balance. This is appealing to the utilities as it allows for dealing with a single aggregated entity, thereby facilitating high PV penetration. Emergence of PV-based microgrids where a small residential community or commercial entity consumes power generated by large PV resources while also being connected to the main grid is a thriving application of large-scale PV. As PV penetration throughout the grid rises, the intermittency and variability of PV and the ensuing challenge of maintaining balance between generation and demand throughout the day has become a central problem that needs to be addressed systematically. Such intermittency is observed both on a daily time scale as solar ramps down at nights and up again the next morning and also on shorter scales with PV variations due to temporary cloud cover. Due to such intermittency and uncertainty, real-time adjustment of resource dispatch as more accurate forecast information becomes available has become necessary. Moving

towards scheduling generation over shorter time steps constitutes a paradigm shift from more traditional economic dispatch frameworks where variations were slower and lower uncertainty did not necessitate fast updating generation schedule [52]. Further details and analysis on the risks posed by PV intermittency can be found in [5].

From the perspective of the main electricity grid, the variation rate of power provided by a solar plant should not exceed the ability of the grid to safely handle such variations. For this reason and due to the limited ramp rate of most non-renewable generation reserves, power agreements between grid operators and solar microgrids may impose ramp rate limits on power flow between the microgrid and the main grid. On the other hand, solar microgrids may be needed to meet ramping capacity requirements, enabling them to swiftly ramp up their output as grid conditions demand. It is expected that with the current trend of increasing solar penetration, these rate limits would be more strictly enforced and additionally, upper and lower power level limits would also be restricted in the future. California Independent System Operator has identified requirements for meeting changing grid patterns including the ability to react quickly, sustain upward or downward ramps, store energy, and meet expected operating levels.

With intermittent solar generation, grid operators start to incorporate other forms of often non-renewable energy generation or energy storage to maintain the balance of the grid. PV curtailment is a measure taken to meet rate limits and maintain balance but is contrary to environmental and economic goals of renewable penetration. Diesel generation is another reserve resource to help maintain balance and meet demand under PV intermittency, yet is environmentally and economically unfavorable. The emergence of large-scale Energy Storage (ES) systems has proved promising in making up for PV intermittency [53]. Such systems can help compensate PV intermittency and meet rate limitations with little PV curtailment or limited emergency diesel dispatch within the microgrid, thereby bringing both economic and environmental benefits.

Coordinated control of renewable and non-renewable DERs together with ES systems is a major topic of interest due to its far-reaching implications for economic and reliable microgrid operation. Model Predictive Control (MPC) is a commonly used paradigm for optimization of such microgrids often on a daily optimization horizon. As such, power flow model of the microgrid together with predictions of future load and PV are utilized to solve an optimization problem that computes optimal DER dispatches over the span of one day. The first instance of the optimal solution is implemented and the solution is updated at each new time update as new predictions become available. Some major contributions can be found in [33, 54, 55, 56]. Stochastic MPC for management of microgrids with load and renewable uncertainties has been studied in [43]. Other works have proposed hierarchical MPC structures for power management of hybrid microgrids where one MPC layer runs at a slow time scale trying to optimize DER dispatches and the other at a faster time scale, trying to reduce the deviation of power from the reference provided by the slow layer between each two updates of the slower layer [57, 58, 59]. Most of these works formulate an optimization problem on the basis of predicted renewable generation and load demand and propose a model predictive approach that recomputes optimal DER setpoints at each update. Such existing MPC approaches often operate with a fast layer update rate in the order of minutes. The work of [60] implements a single-layer distributed MPC architecture at two different time-steps of 5 mins and 1 hour and compares its computational efficiency with centralized MPC approaches for problems involving a large number of generator resources. The proposed controller performs real-time adjustment of generation schedules as more forecast information becomes available. Such updates rates are computationally manageable and can provide more accurate adjustments, but are still unable to react to high frequency fluctuations in seconds time scales. The computational burden of implementing MPC at seconds time scales is a major hindrance to the adoption of such approaches.

Building on the vast literature on optimal and model predictive control of microgrids, this work is motivated by the prospect of two impending paradigms in control of PV microgrids with energy storage, i.e. ramp rate control and fast power control. Given a PV microgrid with auxiliary distributed energy resources and energy storage systems, this paper proposes a systematic method to first compute best achievable power flow profile with the main grid that maximizes utilization of the PV resources while observing the variability and ramp limits of power flow throughout the day, and then implements the computed power flow profile by real-time dispatch of DERs and despite the variations of PV and load from their predicted values. Since loads and PV resources represent variations at time scales in the order of seconds, successful control of power in the presence of such disturbances requires comparable update rates for the controller. On the other hand, the controller should look into a horizon lasting until the end of the day in order to make optimal dispatch decisions by considering expected load and PV. Solving optimal dispatch problems on such long horizon would be highly inefficient if at all possible with update rates in the order of seconds. It is therefore decided to formulate and solve the problem at two different time scales. For this purpose, We propose a hierarchical MPC structure with two different update rates where the outer loop performs daily energy optimization and computes SoC and PCC power references for the inner loop on the basis of predicted load and PV, at an update rate of 15 minutes. The inner loop, on the other hand, aims to achieve these references by coordinated dispatch of the available DERs at seconds time scale and additionally makes decisions for on-demand use of emergency diesel generator. Model predictive control has proved to be a suitable candidate for such resource management problems due to its ability to handle multiple DERs with various constraints and dynamic characteristics, as well as to utilize predictions of intermittent renewable generation and load to enhance control performance.

5.2 Power flow modeling and optimization

We consider a microgrid with renewable and non-renewable DERs including solar generation (PV), backup diesel generator (DG), a number of energy storage (ES) systems from the set $\mathscr{E} = \{1, ..., N_{ES}\}$ and local loads, connected to the main grid. The following equations describe energy balance of the microgrid as well as charge variation of the ES systems considering their charge/discharge efficiencies.

$$
\begin{aligned}
P_{Load}^t &= P_{PCC}^t + P_{PV}^t + \sum_{ES_i \in \mathscr{E}} \left(P_{ES_i,D}^t - P_{ES_i,C}^t \right) + P_{DG}^t \\
E_{ES_i}^{t+1} &= E_{ES_i}^t + (P_{ES_i,C}^t \eta_i - P_{ES_i,D}^t / \eta_i) \Delta T, \quad \forall ES_i \in \mathscr{E}
\end{aligned}
\tag{5.1}
$$

where P_{Load}^t is the microgrid's power demand, P_{PCC}^t indicates the power flow between the microgrid and the main grid, P_{PV}^t is the power from solar resources, and P_{DG}^t is emergency diesel generator power, all at step t. Additionally, $P_{ES_i,D}^t$, $P_{ES_i,C}^t$ indicate storage i's average discharging and charging power during step t, respectively. η_i is charge/discharge efficiency of ES i. $E_{ES_i}^t$ is the charge level of ES i at step t and its state of charge can be computed as $SoC_{ES_i}^t = E_{ES_i}^t / C_{ES_i}$ where C_{ES_i} is the energy capacity of ES i. Limitations on power output of the ES systems are described as

$$
\begin{aligned}
0 &\leq P_{ES_i,D}^t \leq \delta_{ES_i,D}^t P_{ES_i}^{max} \\
0 &\leq P_{ES_i,C}^t \leq \delta_{ES_i,C}^t P_{ES_i}^{max} \\
\delta_{ES_i,D}^t &+ \delta_{ES_i,C}^t \leq 1 \\
ES_i &\in \mathscr{E}, \delta_{ES_i,D}^t, \delta_{ES_i,C}^t \in \{0,1\}
\end{aligned}
\tag{5.2}
$$

where $\delta_{ES_i,D}^t$ and $\delta_{ES_i,C}^t$ are binary variables used to ensure only either charge or discharge can happen at a time. Charge level of the ES systems should remain within upper and

lower bounds to respect capacity limits and avoid deep discharges.

$$SoC_{ES_i}^{min}C_{ES_i} \leq E_{ES_i}^t \leq SoC_{ES_i}^{max}C_{ES_i}, \quad \forall ES_i \in \mathscr{E} \tag{5.3}$$

Additionally, limitations on power output of PV and diesel generator (if the DG is on), can be described as

$$0 \leq P_{PV}^t \leq P_{PV}^{max}$$

$$P_{DG}^{min} \leq P_{DG}^t \leq P_{DG}^{max} \tag{5.4}$$

These equations constitute the basis for power and energy flow models governing the microgrid and will be used at two control levels. The overall objective of the control system is to regulate the microgrid's power flow with the main grid P_{PCC}. In particular, the control system aims to a. compute daily PCC power profile characterized by high PV utilization and low variability throughout the day despite load and solar uncertainties and b. implement the computed power flow schedule and reduce disturbances by fast control of the available DERs. Considering the different time scales and control requirements for each of the above objectives, they are divided between two separate layers of control, i.e. daily energy scheduling (slow updates) and fast power control (fast updates). The scheduling layer will be in charge of forward-looking energy optimization and considers a horizon up to the end of the day while the inner layer considers a short horizon in the future, typically a few seconds.

5.2.1 Daily Power Scheduling

Generally from a daily scheduling standpoint, a renewable-based microgrid connected to the utility grid aims to increase utilization of its renewable resources resulting in minimizing its power import (or maximizing its export for that matter) with the main grid. On the other hand, it is intended to reduce the variability of power flow

at PCC throughout the day, helping to maintain stability and security of the main grid and allow sufficient time for non-renewable reserves to take over the demand when renewable DERs are not sufficient. This scheduling level aims to leverage ES dispatch and, if needed, PV curtailment to reduce PCC power flow variability and increase PV utilization. However, the scheduling at this layer assumes no diesel generator dispatch as diesel dispatch is reserved as an emergency measure only for compensation of large deviations of predicted load and PV from actual values, to be decided by the lower level controller in real-time, as will be discussed in the next section. As can be noticed, with limited storage capacity, the two objectives of increasing PV utilization and decreasing PCC power variability are conflicting; hence, a trade-off between them may be favorable. Accordingly, the cost of the optimization is defined as a weighted sum of total PCC power flow over 24 hours and variance of PCC power flow during this period.

$$\mathbf{J}^H = k_1^H \sum_{k=t}^{T^H-1} P_{PCC}^k + k_2^H \sum_{k=t}^{T^H-1} (P_{PCC}^k - \bar{P}_{PCC})^2 \tag{5.5}$$

The first term in the cost functions serves to minimize power import from the main grid (maximize PV utilization) while the second term aims at minimizing the variance of power flow. The ratio of parameters k_1^h and k_2^h defines relative weight of the objectives and can be tuned to obtain the desired trade-off between PV utilization and PCC power variability. This optimization should minimize the above cost by scheduling existing DERs subject to their availabilities and constraints. As we desire no DG dispatch at this level, the following additional constraint is enforced.

$$P_{DG}^t = 0 \tag{5.6}$$

Future load and maximum available PV are assumed to be predicted up to the scheduling horizon that is the end of the day. Basic prediction schemes for this purpose will be presented in section 5.3.

$$\hat{\mathbf{P}}_{Load}^{t} \triangleq (P_{Load}^{t|t}, P_{Load}^{t+1|t}, ..., P_{Load}^{T^H-1|t})$$
$$\hat{\mathbf{P}}_{PV}^{max,t} \triangleq (P_{PV}^{max,t|t}, P_{PV}^{max,t+1|t}, ..., P_{PV}^{max,T^H-1|t})$$

(5.7)

Additionally, constraints on the allowable rate of change and amount of variation of PCC power throughout the day are imposed as

$$R_{PCC}^{min} \leq \frac{P_{PCC}^{t+1} - P_{PCC}^{t}}{\Delta T} \leq R_{PCC}^{max}$$
$$P_{PCC}^{min} \leq P_{PCC}^{t} \leq P_{PCC}^{max}$$

(5.8)

Constraints on ES charge level at the beginning and end of the day are defined as

$$SoC_{ES_i}^{t=0} = SoC_{ES_i}^{t=T}$$

(5.9)

The resulting optimization for daily power scheduling can be formulated as

High-level Optimization:

$$\min_{P_{ES_i,D,C}, P_{PV}} \quad J^H(P_{Load}, P_{ES_i,D,C}, P_{PV})$$

$$\text{subject to} \quad (5.1 - 5.4), (5.6 - 5.9)$$

5.2.2 Fast Power Control

To achieve the desired PCC power flow computed by the scheduling layer, reduce fluctuations of power flow at PCC resulting from load and PV variations, and enable fast response to power setpoints another control layer is devised that operates at a higher

update rate and provides fast power dispatch setpoints to each DER. To meet the PCC and SoC setpoints prescribed by the scheduling layer, this layer refines DER setpoints (including diesel generator) to make up for load and PV prediction errors. The update rate of this layer is chosen in order of seconds, comparable with renewable output variation time scales and is generally in the range $0.5s - 4s$. While disturbance reduction controllers have traditionally been implemented as PI or PID, the hybrid and constrained nature of the inputs as well as interoperability with the high-level optimization indicate motivations for adopting a finite-horizon predictive controller for this layer. The controller would take its high-level references (PCC power and SoC) from the power scheduling layer and solves a new optimization at each step to compute optimal DER dispatches. To address load and PV deviations from their predicted values, the optimization at this layer obtains a trade-off between slight deviation from SoC reference computed by the high-level optimization, deviation from reference PCC profile, and non-renewable DER (DG) dispatch. Different from the daily optimization, the cost of this problem is defined as a weighted sum of the above three costs.

$$
\begin{aligned}
J^L = \quad & k_1^L \sum_{k=t}^{t+H^L-1} (P_{DG}^k)^2 + k_2^L \sum_{k=t}^{t+H^L-1} (P_{PCC}^k - P_{PCC,ref}^k)^2 \\
& + k_3^L \sum_{ES_i \in \mathscr{E}} \sum_{k=t}^{t+H^L-1} (SoC_{ES_i}^k - SoC_{ES_i,ref}^k)^2
\end{aligned}
\tag{5.10}
$$

Given the relatively fast update rate of this loop, ramp rate limits of the dispatched DERs should be considered as they could become limiting factors in computing optimal DER dispatches. Hence, in addition to the energy balance (5.1) and power constraints (5.2, 5.3,

5.4) mentioned before, the following constraints apply to the optimization at this level.

$$
\begin{aligned}
\left| \frac{P_{ES_i,D}^{t+1} - P_{ES_i,D}^{t}}{\Delta T} \right| &\leq R_{ES_i,D} \\[2mm]
\left| \frac{P_{ES_i,C}^{t+1} - P_{ES_i,C}^{t}}{\Delta T} \right| &\leq R_{ES_i,C} \\[2mm]
\left| \frac{P_{PV}^{t+1} - P_{PV}^{t}}{\Delta T} \right| &\leq R_{PV} \\[2mm]
\left| \frac{P_{DG}^{t+1} - P_{DG}^{t}}{\Delta T} \right| &\leq R_{DG}
\end{aligned}
\tag{5.11}
$$

The above constraints limit the rate of variation of each DER's power output. Another operational constraint is the minimum on-time and off-time of the diesel generator. Once the diesel turns on, it should stay on for at least a minimum duration of time to avoid frequent startup and shutdown behavior. The same is also true when the DG turns off, it should remain in that state for a minimum period. These conditions can be formulated by defining a binary variable δ_{DG}^{t} indicating on-off state of the diesel generator

$$
\begin{aligned}
\delta_{DG}^{t+1} - \delta_{DG}^{t} &\leq \delta_{DG}^{\tau} \quad \forall \tau \in \{t+1,...,t+T_{DG,on}^{min}\} \qquad \text{minimum on time} \\[2mm]
\delta_{DG}^{t-1} - \delta_{DG}^{t} &\leq 1 - \delta_{DG}^{\tau} \quad \forall \tau \in \{t+1,...,t+T_{DG,off}^{min}\} \quad \text{minimum off time}
\end{aligned}
\tag{5.12}
$$

Similar to the high-level optimization, the optimal solution to this problem requires knowledge of load and solar energy generation for the short-term optimization horizon (few seconds). The resulting short-term, fast updating optimization can be

formulated as

Low-level Optimization:

$$\min_{P_{ES_i,D,C},P_{PV},P_{DG}} \quad J^L(P_{Load},P_{ES_i,D,C},P_{PV},P_{DG})$$

subject to $\qquad\qquad\qquad (5.1-5.4),(5.11),(5.12)$

It should be noted that although the two optimizations are concerned with the same overall energy flow model, they seek different objectives, each pertaining to its respective time scale and respective constraints. Altogether, the overall operation of these two loops leads to realization of overall control objectives of the system.

5.3 Load and PV Prediction

Following the requirement for load and PV prediction in obtaining solutions to the above optimization problems, Auto-Regressive Integrated Moving Average (ARIMA) models are used in this section. ARIMA models refer to a general class of models used for forecasting non-stationary time-series data [61]. A regular ARIMA model is represented as $ARIMA(p,d,q)$ where p is order of the autoregressive part, d is the number of differences needed for stationarity, and q is order of the moving average part of the model.

short-term prediction

Short term prediction is referred to load and PV predictions in time scales in the order of seconds. For short-term prediction, past PV and load data with 1-second sampling rate is used to train different ARIMA models for each of PV and load. Model orders are decided by examining ACF and PACF plots of load and PV data and in this work, are chosen to be $(p_{PV}^{short} = 8, d_{PV}^{short} = 1, q_{PV}^{short} = 0)$ for PV forecasts and

$(p_{Load}^{short} = 15, d_{Load}^{short} = 1, q_{Load}^{short} = 0)$ for load forecasts. The models are employed at every time step to make predictions over a horizon of length H^L using last $(p^{short}$ measurements of actual PV/load values. Models are updated by retraining with new data every 10 minutes.

Daily prediction

Daily PV and load prediction play central roles in optimal microgrid scheduling and DER dispatch throughout the day. Daily load prediction is obtained using ARIMA model structures described above, using historical load data up to the current time to train the models and then use the models to make predictions up to the end of the day. For this purpose, load data with 15-min sample rate is used to train two different models, one for normal weekdays and another for weekends and days with lower demand pattern. This is needed due to the difference observed in the pattern for these two groups of days. Forecasts are then updated every 15 minutes using the latest available load data.

Daily solar prediction, on the other hand, is performed using another technique. As recent sky conditions is responsible for PV generation over a day, making predictions for next day's PV using previous days' PV data tends to be less irrelevant. Instead, using dedicated solar forecasting methods or web-based forecasting services for the considered region is preferred. A detailed review of applicable solar forecasting techniques can be found in [62, 63] . In this work, for daily PV prediction, data from a solar forecasting technique is used together with the PV system characterization based one historical data. In this way, at the beginning of each day and at recurring steps along the day, solar energy generation is predicted to obtain $\hat{P}_{PV}^{max}(t|k)$ for $k = 0 : N - 1$ and $t = k : N - 1$ with $N = 96$ (prediction up to the end of the day).

5.4   MPC Formulation and Online Solution

The MPC controller is implemented by posing the two optimizations introduced in section II as two finite horizon optimal control problems that are solved at two separate times cales and are constructed in a cascaded fashion as shown in Fig. 5.1. The outer layer operates at a slower rate and is henceforth referred to as High-Level Predictive Controller (HLPC) while the inner fast layer is referred as Low-Level Predictive Controller (LLPC). The outputs of the HLPC are provided as references to the LLPC. These references include PCC reference power profile and SoC of the ES systems. The optimal solution to each problem is repeatedly computed at its respective sampling instant using the current state of the system as the initial state and only the first part of the computed control is applied.
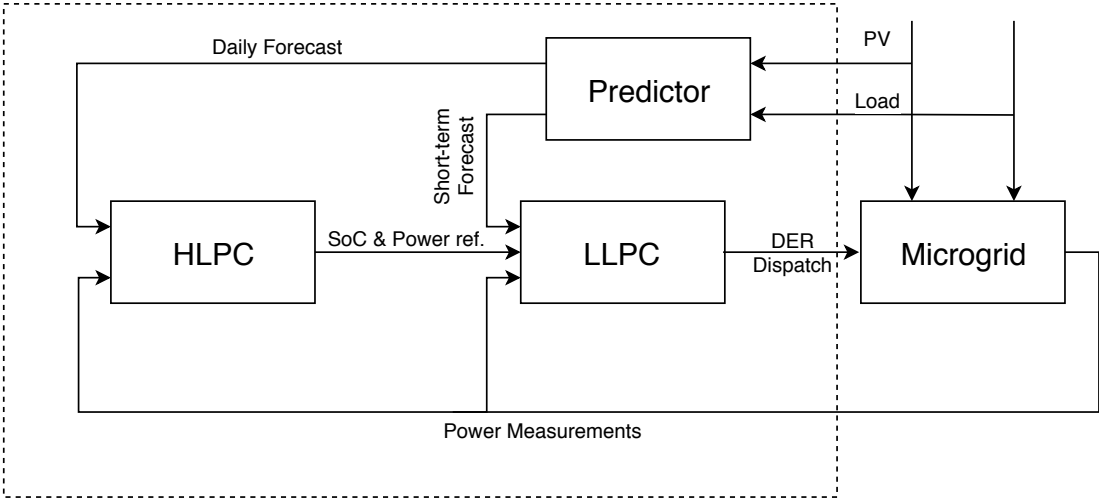
Figure 5.1. Schematic of the two-layer MPC control structure and the predictor. HLPC is the slowly-updating high-level layer computing optimal dispatch with a horizon lasting up to the end of day and LLPC is the fast updating layer reducing fluctuations and refining DER dispatches based on deviations from predicted load and PV

5.4.1 High Level Predictive Controller (HLPC) - Slow layer

The slow layer comprises daily power scheduling and concerns more forward-looking power optimization up to the end of the day. The objective of this layer is computing a PCC power set-point that meets certain requirements as outlined in section 5.2.1 and its corresponding SoC profile for the ES systems. These power and SoC set-points are then passed as references to the inner loop. The problem is posed as a model predictive control problem with a finite horizon starting at the current time step and lasting up to the end of day, with step size $\Delta T^H (= 15$ mins). Hence the length of the horizon decreases by one with each time update. New predictions are made at each new update based on which new optimal solution is computed for the optimization horizon. Only the first input of the resulting input sequence is implemented and the solution is recomputed at the new time update. The HLPC problem is represented in state-space as

$$\min_{\mathbf{u}_t, \mathbf{u}_{t+1},\ldots,\mathbf{u}_{T^H-1}} \quad \sum_{k=t}^{T^H-1} J(\mathbf{x}_k, \mathbf{u}_k, \mathbf{w}_k)$$

$$\text{subject to} \quad \mathbf{x}_{k+1} = A\mathbf{x}_k + B\mathbf{u}_k + E\mathbf{w}_k$$

$$(\mathbf{x}_k, \mathbf{u}_k) \in \mathscr{X} \times \mathscr{U}$$

where

$$J = k_1^H P_{PCC}^t + k_2^H (P_{PCC}^t - \bar{P}_{PCC})^2$$

$$T^H = 96$$

$$\Delta T^H = 15 \ min$$

$$\mathbf{x}_t = \begin{bmatrix} E^t_{ES_1} \\ E^t_{ES_2} \end{bmatrix}, \ \mathbf{u}_t = \begin{bmatrix} P^t_{ES_1,D} \\ P^t_{ES_1,C} \\ P^t_{ES_2,D} \\ P^t_{ES_2,C} \\ \delta^t_{ES_1,D} \\ \delta^t_{ES_1,C} \\ \delta^t_{ES_2,D} \\ \delta^t_{ES_2,C} \\ P^t_{DG} \\ P^t_{PV} \end{bmatrix}, \ \mathbf{w}_t = \begin{bmatrix} P^t_{Load} \\ P^{max,t}_{PV} \end{bmatrix}$$

$$A = \begin{bmatrix} 1 & 0 \\ 0 & 1 \end{bmatrix}, \ E = \begin{bmatrix} 0 & 0 \\ 0 & 0 \end{bmatrix}$$

$$B = \begin{bmatrix} -\Delta T^H/\eta_1 & \eta_1 \Delta T^H & 0 & 0 & 0 & 0 & 0 & 0 & 0 & 0 \\ 0 & 0 & -\Delta T^H/\eta_2 & \eta_2 \Delta T^H & 0 & 0 & 0 & 0 & 0 & 0 \end{bmatrix}$$

and the constraints are

$$0 \leq u_1^t \leq P_{ES_1}^{max} u_5^t, \ \ 0 \leq u_2^t \leq P_{ES_1}^{max} u_6^t$$

$$0 \leq u_3^t \leq P_{ES_2}^{max} u_7^t, \ \ 0 \leq u_4^t \leq P_{ES_2}^{max} u_8^t$$

$$u_5^t + u_6^t \leq 1, \ \ u_7^t + u_8^t \leq 1$$

$$u_5^t, u_6^t, u_7^t, u_8^t \in \{0,1\}, \ \ u_9^t = 0$$

$$0 \leq u_{10}^t \leq \hat{P}_{PV}^{max}(t|k)$$

$$\begin{bmatrix} SoC_{ES_1}^{min} C_1 \\ SoC_{ES_2}^{min} C_2 \end{bmatrix} \leq \mathbf{x}^t \leq \begin{bmatrix} SoC_{ES_1}^{max} C_1 \\ SoC_{ES_2}^{max} C_2 \end{bmatrix}$$

$$\hat{P}_{PCC}(t|k) = \hat{P}_{Load}(t|k) - P_{PV}^t - P_{ES_1,D}^t + P_{ES_1,C}^t - P_{ES_2,D}^t + P_{ES_2,C}^t - P_{DG}^t$$

$$= \hat{w}_1(t|k) - u_{10}^t - u_1^t + u_2^t - u_3^t + u_4^t - u_9^t$$

$$R_{PCC}^{min} \leq \frac{\hat{P}_{PCC}(t+1|k) - \hat{P}_{PCC}(t|k)}{\Delta T} \leq R_{PCC}^{max}$$

$$P_{PCC}^{min} \leq \hat{P}_{PCC}(t|k) \leq P_{PCC}^{max} \qquad t \in \{k, k+1, ..., N-1\}$$

$$\mathbf{x}^{t=0} = \mathbf{x}_0$$

The Output of this layer is provided as reference to the lower level until this reference is updated at the next time update of this loop.

$$y = \begin{bmatrix} E_{ES_1}^t \\ E_{ES_2}^t \\ P_{PCC}^t \end{bmatrix}$$

5.4.2   Low Level Predictive Controller (LLPC) - Fast layer

In contrast to the upper layer, the length of the moving horizon (H^L) is constant in this layer and the horizon only shifts one step at each new sampling time. This layer aims

to achieve the dual objective of following the SoC and PCC power references computed by the scheduling layer, and is granted the additional control freedom of DG dispatch, however the amount of this dispatch is penalized in the cost function. Additionally, the constraints (5.4) and (5.12) should be enforced which together with the cost function (5.10) make the optimization a mixed integer quadratic program. Solving such MPC problem at each time step with sampling time of 1 sec is computationally expensive and might even become impossible if smaller update times is required. Therefore in this section we devise a technique of turning this problem into a regular quadratic program by exploiting the minimum on-off property of the diesel generator.

Assuming the LLPC layer is being solved at step t with a horizon of the next H^L steps and with the DG being off at the beginning of the horizon, condition (5.12) on minimum on-time imply that switching from off to on can happen at most at only of the next H^L steps assuming the minimum off-time condition is already satisfied by time t [1]. As such switching may happens at each of the next H_L steps, we can decompose this MIQP into H_L different quadratic programs each of which account for switching from off to on at one of the next H_L steps. These QPs are all solved at step t and the one with the least cost turns out to be the optimal solution to the original MIQP. This technique allows us to solve a limited number of regular quadratic programs instead of a MIQP which could be computationally much more efficient if the size of the horizon H_L is not too large. Indexing these QPs by h where $1 \leq h \leq H^L$, the LLPC loop can be formulated as

$$\min_{\mathbf{u}_0, \mathbf{u}_1, \ldots, \mathbf{u}_n} \quad \sum_{k=t}^{t+H^L-1} J_h(\mathbf{x}_k, \mathbf{u}_k, \mathbf{w}_k)$$

$$\text{subject to} \quad \mathbf{x}_{k+1} = A\mathbf{x}_k + B\mathbf{u}_k + E\mathbf{w}_k$$

$$(\mathbf{x}_k, \mathbf{u}_k) \in \mathscr{X} \times \mathscr{U}$$

[1] This statement is valid under the assumption that $H^L < T^t_{DG,off/on}$ which is highly realistic since H_L is in order of seconds while minimum on- and off-time are in order of minutes.

with $\mathbf{u}_t$, $\mathbf{x}_t$, $\mathbf{w}_t$, A, B, and E the same as above and

$$J_h = k_1^L P_{DG}^t + k_2^L (P_{PCC}^t - P_{PCC,ref}^t)^2$$

$$+ k_3^L \sum_{ES_i \in \mathscr{E}} (SoC_{ES_i}^t - SoC_{ES_i,ref}^t)^2$$

$$H^L = 10$$

$$\Delta T^L = 1 \ sec$$

and

$$\hat{P}_{PCC}(t|k) = \hat{P}_{Load}(t|k) - P_{PV}^t - P_{ES_1,D}^t + P_{ES_1,C}^t$$

$$- P_{ES_2,D}^t + P_{ES_2,C}^t - P_{DG}^t$$

$$= \hat{w}_1(t|k) - u_{10}^t - u_1^t + u_2^t - u_3^t + u_4^t - u_9^t$$

and the constraints

$$0 \leq u_1^t \leq P_{ES_1}^{max} u_5^t, \ \ 0 \leq u_2^t \leq P_{ES_1}^{max} u_6^t$$

$$0 \leq u_3^t \leq P_{ES_2}^{max} u_7^t, \ \ 0 \leq u_4^t \leq P_{ES_2}^{max} u_8^t$$

$$u_5^t, u_6^t, u_7^t, u_8^t \in \{0,1\}$$

$$u_9^t = u_9^0 \ \ t \leq h, \ \ 0 \leq u_9^t \leq P_{DG}^{max} \ \ t > h$$

$$0 \leq u_{10}^t \leq \hat{P}_{PV}^{max}(t|k)$$

$$-R_{ES_1,D} \leq \frac{u_1^{t+1} - u_1^t}{\Delta T^L} \leq R_{ES_1,D}$$

$$-R_{ES_1,C} \leq \frac{u_2^{t+1} - u_2^t}{\Delta T^L} \leq R_{ES_1,C}$$

$$-R_{ES_2,D} \leq \frac{u_3^{t+1} - u_3^t}{\Delta T^L} \leq R_{ES_2,D}$$

$$-R_{ES_2,C} \leq \frac{u_4^{t+1} - u_4^t}{\Delta T^L} \leq R_{ES_2,C}$$

$$-R_{PV} \leq \frac{u_{10}^{t+1} - u_{10}^t}{\Delta T^L} \leq R_{PV}$$

$$-R_{DG} \leq \frac{u_9^{t+1} - u_9^t}{\Delta T^L} \leq R_{DG}$$

$$\begin{bmatrix} SoC_{ES_1}^{min} C_1 \\ SoC_{ES_2}^{min} C_2 \end{bmatrix} \leq \mathbf{x}^t \leq \begin{bmatrix} SoC_{ES_1}^{max} C_1 \\ SoC_{ES_2}^{max} C_2 \end{bmatrix}$$

5.5   Results and discussion

To quantify PV power utilization and PCC power variability, we define

$$\text{PV Utilization} = \frac{\int_{t=0}^{24 \ hr} P_{PV}^t}{\int_{t=0}^{24 \ hr} P_{PV}^{max,t}} \times 100$$

$$\text{PCC Variability} = \frac{\max P_{PCC}^t - \min P_{PCC}^t}{\max P_{PCC}^t} \times 100 \tag{5.13}$$

Table 5.1. Microgrid Specifications

DER	Specification		
Energy Storage 1	Energy Capacity	C_1	5000 kWh
	Power limit	$P_{ES_1}^{max}$	5000 kW
	Ramp limit	R_3	500 kW/s
	Minimum SoC	SoC_{min}	10 %
	Maximum SoC	SoC_{max}	90 %
	Efficiency	η_1	0.95
Energy Storage 2	Energy Capacity	C_2	5000 kWh
	Power limit	$P_{ES_2}^{max}$	5000 kW
	Ramp limit	R_3	500 kW/s
	Minimum SoC	SoC_{min}	10 %
	Maximum SoC	SoC_{max}	90 %
	Efficiency	η_2	0.9
PV	Peak power	PV_{max}^t	8000 kW
	Ramp limit	R_9	500 kW/s
Diesel Generator	Min power limit	P_{DG}^{min}	1000 kWh
	Max power limit	P_{DG}^{max}	2000 kWh
	Min on time	$T_{DG,on}^{min}$	15 mins
	Min off time	$T_{DG,off}^{min}$	15 mins
	Ramp limit	R_{10}	30 kW/s

where the former shows total utilized PV energy over total available PV energy computed over one day and the latter is used as a measure of power flow variability over one day. Fig. 5.2 indicates possible values of PV utilization and PCC variability achievable by varying the ratio k_1^h/k_2^h and for different initial SoCs. The results are obtained at the beginning of day with the assumption of perfect PV and load prediction and with microgrid specifications of Table 5.1. It is clearly seen that the ratio of these two parameters specifies the compromise between PV utilization and PCC variability. Also, it is evident that the choice of higher initial SoC can result in higher PV utilization with equal variability (equivalently lower variability with equal PV utilization).
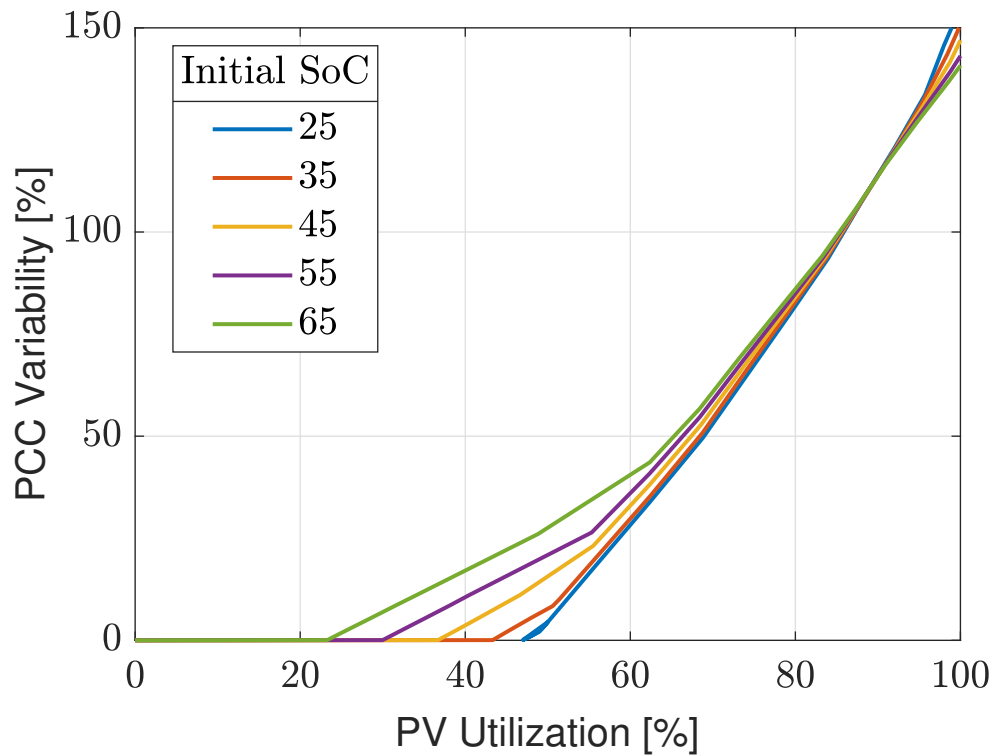
Figure 5.2. Lowest possible PCC power variability for different PV utilizations shown for five different initial SoCs. Microgrid specifications are shown in Table 5.1.

The hierarchical MPC controller and predictor are implemented in real-time on

an Intel Core i7-7500U computer in MATLAB. The fast control loop is executed at 1 Hz though higher update rates are also tested and proved manageable with the described setup. Next, four different test scenarios are simulated to indicate the performance of the cascaded MPC controller throughout the day. These scenarios aim to capture marginal cases of prediction errors and PCC power variability according to Table 5.2.

Table 5.2. Simulation Scenarios

	Load Overprediction	Load Underprediction
High PCC variability	Scenario 1	Scenario 2
Low PCC variability	Scenario 3	Scenario 4

Scenarios 1 and 2 enforce high PV utilization at the expense of high PCC power variation. Scenarios 3 and 4, on the other hand, enforce low PCC power variability over one day at the expense of lower PV utilization. PCC variability is controlled by changing the ratio k_1^h/k_2^h in the high level controller parameters. Scenarios 1 and 3 employ conservative load and PV predictions, as opposed to scenarios 2 and 4. However, in all scenarios, predictions are refined as time proceeds and as forecasts are updated.

Table 5.3. Controller design parameters for different simulation scenarios

	Scenario 1 and 2	Scenario 3 and 4
k_1^h	1×10^3	1×10^3
k_2^h	2×10^{-1}	6×10^{-1}
k_1^l	1×10^{-2}	1×10^{-2}
k_2^l	5×10^{-2}	5×10^{-2}
k_3^l	1×10^2	1×10^2
$\mathbf{x}_0$	$[1500 \ 1500]^T$	$[1500 \ 1500]^T$

HLPC and LLPC design parameters for each of the scenarios are shown in table 5.3. Four full days of control operation is shown in Figs. 5.3-5.6, each pertaining to one of the four scenarios. The top plot in each scenario shows load and PV predictions updated at each hour. Using the daily predictions and control parameters of table 5.3, the HLPC problem is solved and optimal PCC power and ES SoCs references (output vector

Figure 5.3. Scenario 1: High PCC power variability and load overprediction
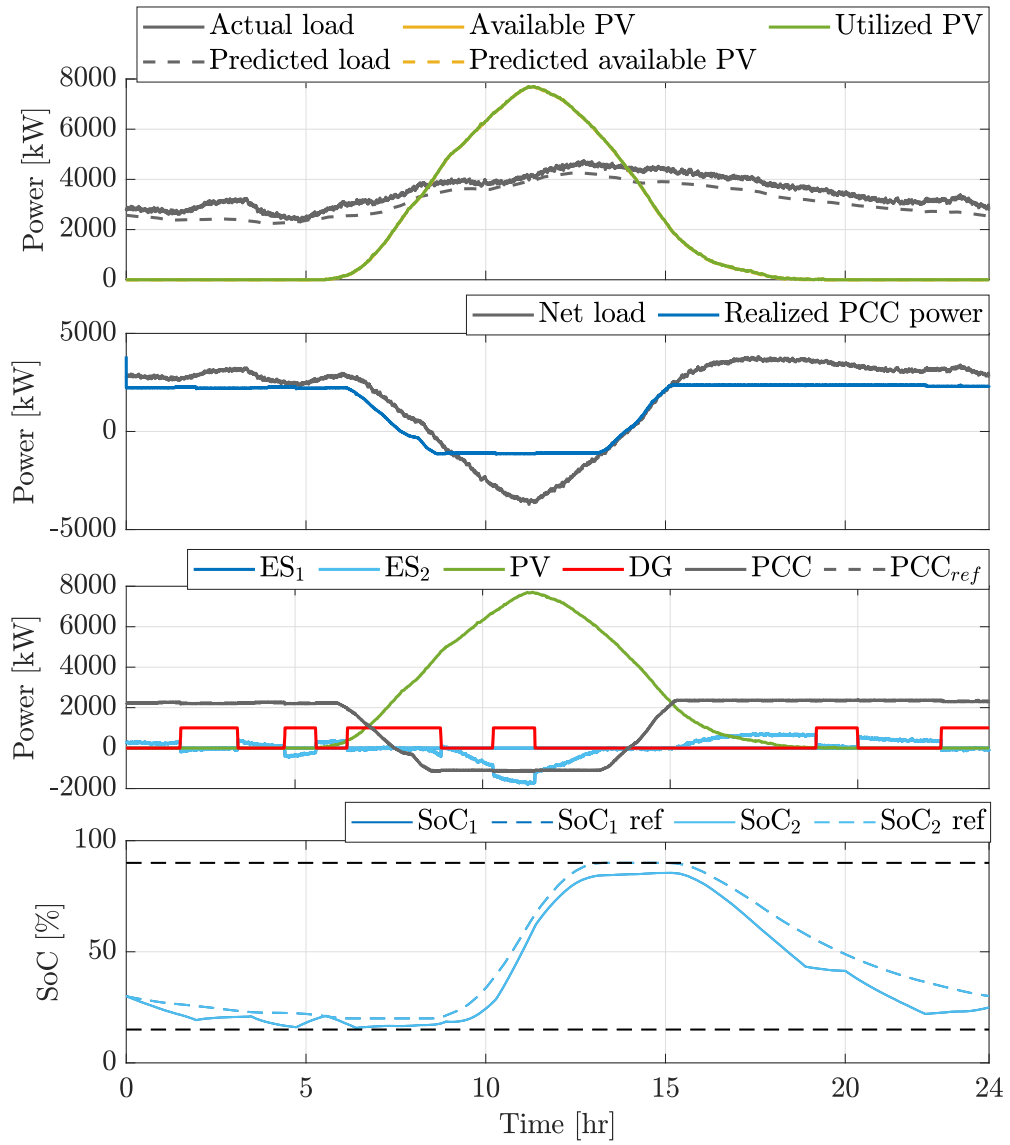
Figure 5.4. Scenario 2: High PCC power variability and load underprediction
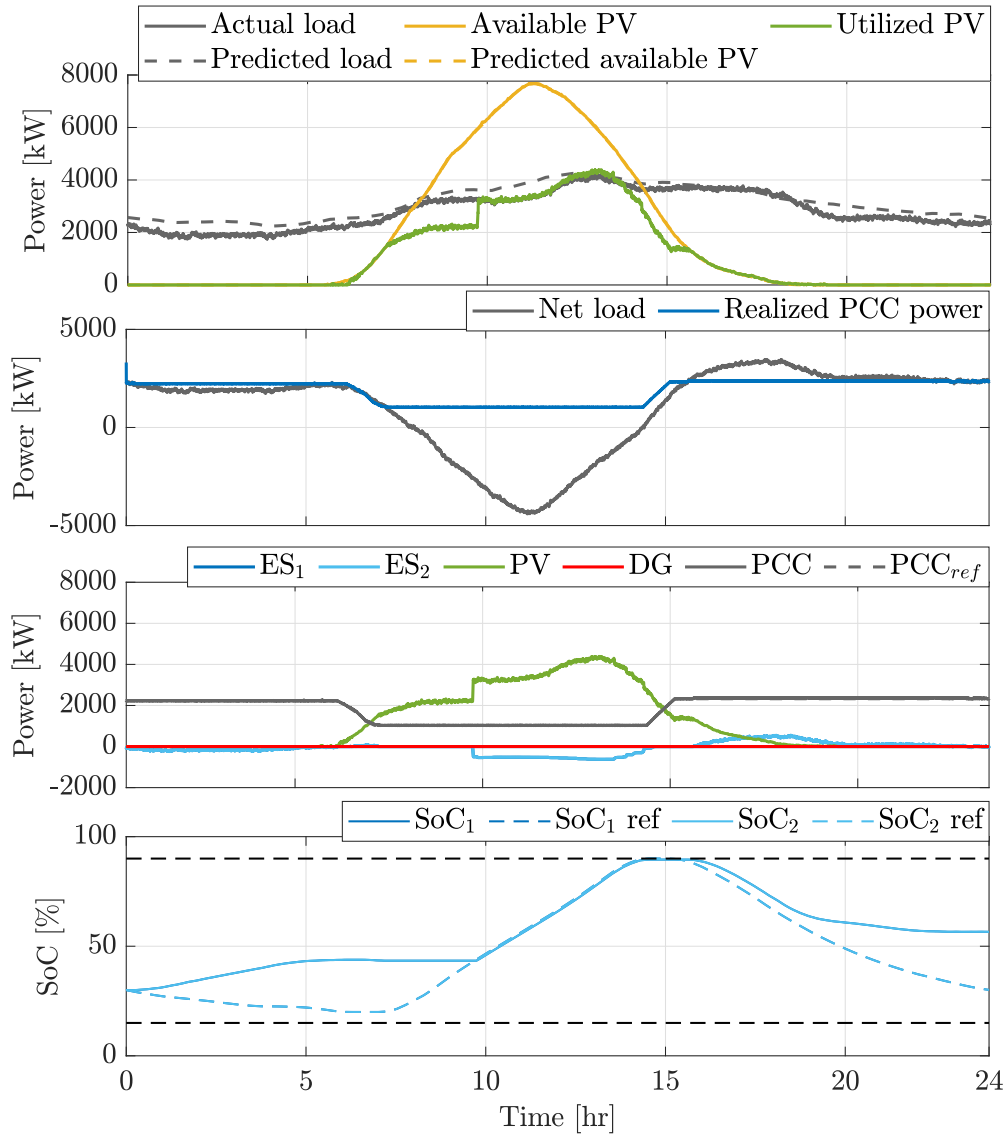
Figure 5.5. Scenario 3: Low PCC power variability and load overprediction
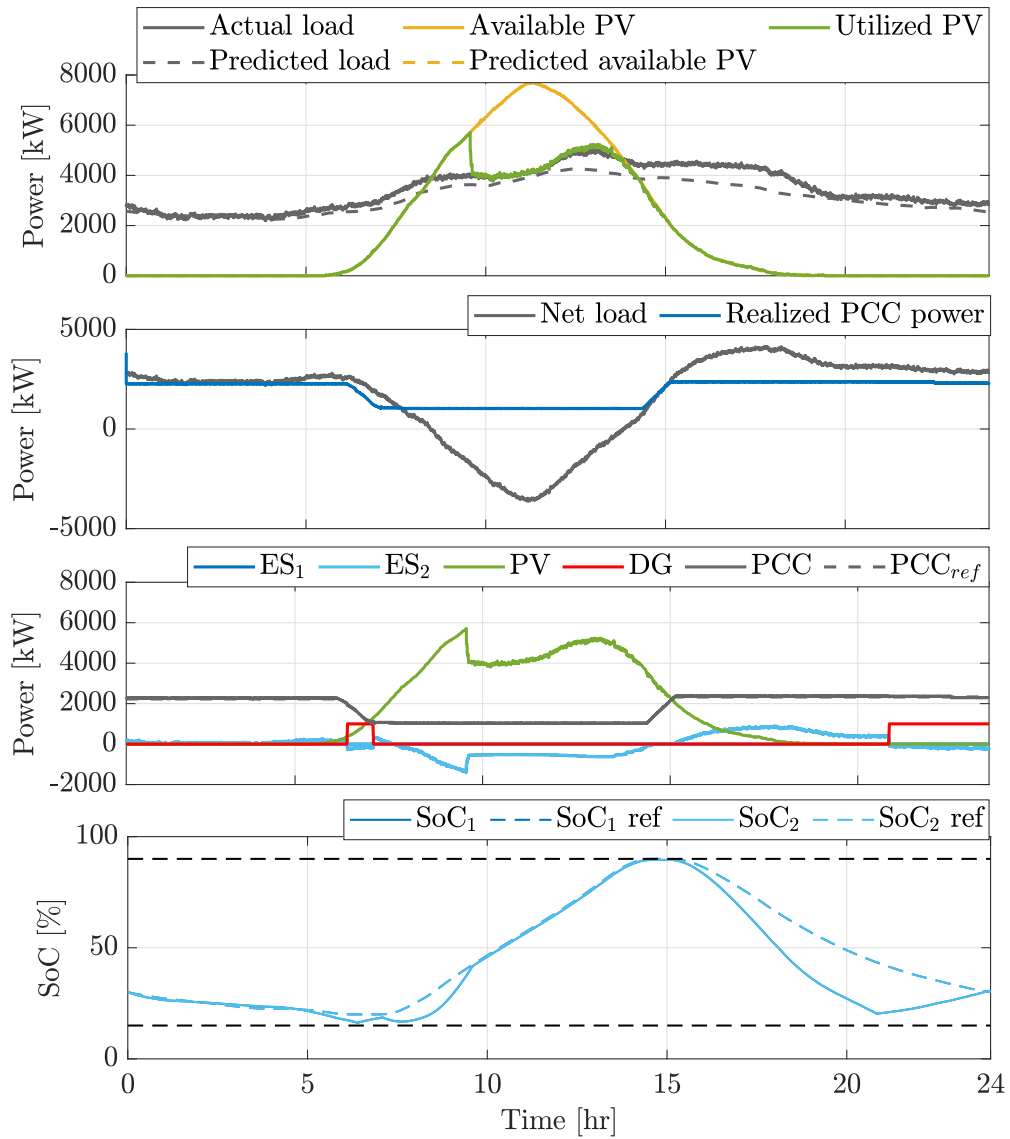
Figure 5.6. Scenario 4: Low PCC power variability and load underprediction

y) are computed and passed to the lower level controller (LLPC). The low level controller uses these references and in turn, solves the LLPC problem every second to compute th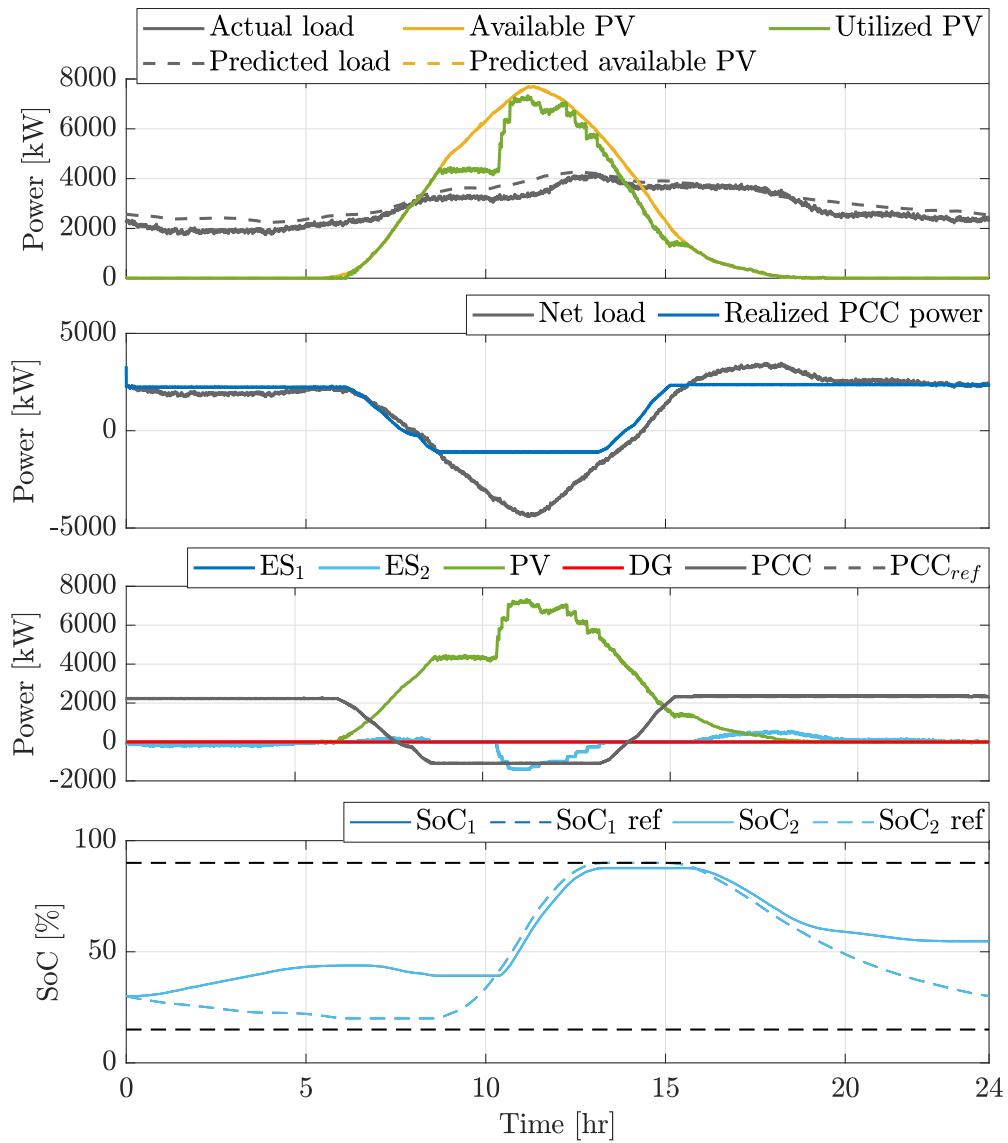e optimal dispatch commands to the DERs. Under ideal forecast assumption and without disturbances, the LLPC can ideally implement the references given by the HLPC and the DER dispatches will be precisely the same as those computed by the HLPC. However, due to errors in load and PV predictions, the LLPC utilizes additional degrees of freedom to achieve PCC power setpoint tracking by slight deviation from ES SoC references as well as by dispatch of the DG. The second plot in each scenario compares net load of the microgrid if all PV was directly used at the time of generation versus the PCC power profile realized under the proposed MPC control. The reduce variability and intermittency of the realized power profile is achieved by coordinated utilization of PV, energy storage, and diesel generation if needed. The third plot in each scenario indicates power dispatch of each DER at the end of the day resulted from hourly computation of the HLPC and every second computation of the LLPC. As seen in these plots, scenarios 1 and 2 demonstrate high PV utilization with relatively high PCC power variation throughout the day. However, the controller achieves the setpoint prescribed by the HLPC, smoothening power flow fluctuations and uncertainties due to PV intermittency and load variations. Scenarios 3 and 4, on the other hand, aim to achieve low variability in PCC power flow throughout the day and consequently achieve low PV utilization due to limited storage capacity. In scenarios 1 and 3 (load overprediction), real-time operation of LLPC does not mandate any diesel dispatch as the HLPC has accounted for more extreme load and PV conditions without diesel. Opposite circumstances in scenarios 2 and 4 require diesel dispatch at parts of the day to maintain balance and meet PCC and SoC tracking. The bottom plots in each scenario indicate corresponding SoC of ES systems under the computed dispatch. As observed in these plots, actual SoC profiles follow the optimal SoC computed by the HLPC closely and deviate only to account for unpredicted load

and PV deviations. In all scenarios, the resulting PCC power profile can closely track the profiles generated by the HLPC despite load and PV uncertainties and fluctuations.

5.6   Summary of discussed problem

A hierarchical predictive controller is proposed to control the operation of a large-scale PV microgrid with energy storage and auxiliary diesel generation. The controller aims to increase utilization of the available PV resources, reduce the variability of power flow between the microgrid and the main grid, while at the same time controlling power flow fluctuations at the point of connection. The controller is designed to utilize load and PV predictions on a receding time horizon and uses the flexibility of energy storage and diesel resources to compensate for prediction errors. A study of four different operational scenarios demonstrates successful operation of the proposed controller under different PV availability and load demand scenarios.

Acknowledgements

Chapter 6

Cooperative Energy Scheduling under Peak Demand Energy Plans

6.1   Introduction

For many small and medium-size commercial and industrial entities, electric utility charges involve two main components, one accounting for the entity's weighted hourly consumption (Time of Use or ToU) and the other for its peak demand during the entire billing interval (demand charge). ToU pricing imposes different unit prices at different times of the day to urge the users to shift their loads from certain peak hours to off-peak hours. On the other hand, peak demand charge urges the users to flatten their overall demand profile to realize smaller peak to average ratio.

Currently in California, peak demand charges account for up to 50% of some industrial users' monthly electricity costs [3]. Users' response to such pricing is dependent on their flexibility for time-shifting their loads as well as their energy storage capacity. While energy storage can be exploited by users to optimally schedule their consumption and reduce their costs, it can also benefit the grid by increasing its reliability under periods of high demand [64]. Optimal scheduling of energy storage is a major topic of interest for electricity users of different sizes. For some major contributions see [65, 66]. While each user with energy storage can optimize its storage schedule, joint

energy scheduling and optimization between multiple microgrids may further reduce their total cost. This can be roughly attributed to the fact that by joint scheduling, users who under-utilize their energy storage at some or all parts of the day can make it available to other users who need it at those times. The role of cooperative optimization in reducing intermittency and uncertainty has also fueled the interest in cooperative optimization methods [67]. Different works have studied cooperative management of loads and storage and joint optimization between multiple users [68, 69]. In [67], the authors consider the problem of cooperative energy management for two microgrids with ToU energy cost aiming to achieve total cost reduction as a result of cooperation. Shared ES management for a group of microgrids with profit coefficient sets is considered in [70]. The authors of [71] propose a stochastic formulation of the cooperative energy scheduling problem for a group of microgrids and consider ToU as well as operating costs of their local energy resources. The work of [72] proposes a model predictive framework for cooperative optimization of a network of interconnected microgrids and discusses the attained total cost saving for all users.

While the approaches proposed in the earlier works present feasible strategies for total cost saving by a group of users under cooperation, they do not discuss distribution of the obtained total savings between the participating users. It is desired to investigate mechanisms that make such exchange profitable for all participating parties so as to encourage participation. The work of [73] discusses cooperative power management between multiple microgrids with renewable generation and proposes a pareto-optimal solution using Nash bargaining that encourages microgrids to participate. In [74], the authors discuss fairness in optimal coordination of multiple users with quadratic energy cost. Also, the work [75] studies cooperative management in the wholesale electricity market and presents cost allocation solutions that have certain favorable properties. In [76], the authors have used a cooperative game approach to tackle direct energy trading

89

between DERs and energy consumers. In general, division of the attained cost saving between participating users in a fair and stable manner constitutes the major issue in the considered cooperative games [77].

In this work, we are interested in a specific yet prevailing case of cooperative energy scheduling; the case of multiple microgrids under ToU and demand charge energy plans. Cost distribution when the cost structure includes peak demand terms presents important stability implications that have not yet been addressed to the best knowledge of the authors. We will show that first, under such cost structure, joint scheduling will result in reduced total cost. Next, we will investigate how some cost distributions may destabilize the collaboration due to the existence of peak demand term in the cost function. An alternative algorithm is then proposed that can provably guarantee the benefit of all users from participation in the collaboration while maximizing some measure of fairness among them. Our main contribution lies in the consideration of demand charge in the cost structure which leads to non-submodularity of the cost function and therefore necessitates careful consideration of stability. We will show that for this problem, a stable distribution of the optimal cost between the users that is desirable from all users' standpoints will always exists and will provide an approach for computing such distribution.

6.2   Preliminaries and benchmark problem

Consider a distribution system with a single energy provider (utility) and a set of microgrids $\mathcal{N} = \{1, 2, ..., N\}$ where each microgrid $n \in \mathcal{N}$ is equipped with a smart meter and means of two-way data communications with the utility and other users. The terms *user* and *microgrid* are used interchangeably throughout the paper. Some users may additionally possess a battery energy storage (ES) system. The set $C = \{C_1, C_2, ..., C_N\}$ indicates the energy storage capacity of each user. We further take the set of time intervals $\mathcal{T} = \{1, 2, ..., T\}$ where each $t \in \mathcal{T}$ has length Δ_T to represent the energy

90

scheduling horizon. The energy demand vector for each user $n \in \mathcal{N}$ is defined as $d_n \triangleq \left[d_n^1, d_n^2, ..., d_n^T \right]$ while energy flow from the grid to user n is $x_n \triangleq \left[x_n^1, x_n^2, ..., x_n^T \right]$. The sum of energy supplied to each user from the main grid and from the user's ES during interval $t \in \mathcal{T}$ should equal d_n^t. The energy provided by the ES is denoted by e_n^t. Each user $n \in \mathcal{N}$ with storage capability can supply part or all of its demand according to

$$d_n^t = x_n^t + e_n^t \tag{6.1}$$

and its storage charge level c_n varies as

$$c_n^{t+1} = c_n^t - e_n^t \tag{6.2}$$

Such user can make dispatch decisions for storage charge/discharge (e_n^t) to optimize its electricity consumption subject to the following storage constraints

$$e_n^{min} \leq e_n^t \leq e_n^{max}$$
$$c_n^{min} \leq c_n^t \leq c_n^{max} \tag{6.3}$$
$$c_n^{t0} = c_n^{tend}$$

While this simplified model is adopted to only capture salient dynamics of the system and demonstrate the pivotal ideas of this work, the methods are mostly applicable under more complex microgrid models.

The energy consumers in this study are commercial and industrial users that are billed under both ToU and demand charge pricing plans. The total cost of energy for user n

91

under such rate plans can be computed as

$$f_n(x_n) = \sum_{t=1}^{T} p^t x_n^t + \alpha \max_{t \in \mathscr{T}} x_n^t \qquad (6.4)$$

where p^t is the ToU unit price at time t and α is the demand charge coefficient.

Optimization 1. The cost minimization problem for each individual user having ES can be formulated as

$$\underset{x_n}{\text{minimize }} f_n(x_n) \qquad (6.5)$$

$$\text{subject to } (1-3)$$

The optimal solution x_n^* to this problem will result in the optimal cost $f_n(x_n^*)$. The above problem has a convex objective function and affine constraints and therefore is a convex program [78]. If each user solves its energy optimization (*optimization 1*) individually without cooperation with other users, the total cost of all users would become

$$f_{non-coop} = \sum_{n=1}^{N} f_n(x_n^*) = \sum_{n=1}^{N} \left[\sum_{t=1}^{T} p^t x_n^{t\,*} + \alpha \max_{t \in \mathscr{T}} x_n^{t\,*} \right]$$

Next, we consider how a few users may cooperate to reduce this overall cost.

6.3 Cooperative optimization

6.3.1 Motivation

Medium and large-scale energy consumers have diverse demand patterns and often significantly high peak-to-average demand ratios. While demand charge is a major part of total energy cost for such consumers, substantial demand charges may be incurred due to uneven demand distribution and high peak-to-average ratio [3]. The addition of

storage for reducing peak demand could significantly reduce demand charge in such cases. Although individual microgrids can utilize their ES to optimize their demand as described in the previous section, joint storage utilization between multiple users in a distribution network can potentially bring additional benefits. This can be attributed to the benefits gained by shared storage utilization as well as the fact that sum of users peaks is always greater than or equal to the peak of the collective consumption of all users. We propose a method of joint optimization between multiple microgrids with identical cost structures, such that the group of collaborating microgrids, although physically remote, will purchase electricity from the main grid as a whole. This can be further conceptualized by considering an aggregator that manages interaction and cooperation of participants and represents them as a whole.

The main questions that we are after answering in this section are the following:

I. Does forming a cooperation between the microgrids under the described cost structure result in attaining a lower total cost?

II. How should the savings attained as a result of cooperation be distributed between the participants?

We devote the rest of this section to answering these questions.

6.3.2 Centralized cooperative optimization

Consider a group of microgrids some of which having energy storage and suppose that energy flow between the main grid and the group is measured at a virtual point of connection. Denoting the power flow at this point by x, the total cost incurred by such group of users is

$$f_{coop}(x) = \sum_{t=1}^{T} p^t x^t + \alpha \max_{t \in \mathcal{T}} x^t \tag{6.6}$$

93

Optimization 2. The cooperative optimization problem can be formulated as

$$\underset{x}{\text{minimize}}\ f_{coop}(x) \tag{6.7}$$

subject to the constraints

$$
\begin{aligned}
x^t &= \sum_{n=1}^{N} d_n^t - \sum_{n=1}^{N} e_n^t \\
c_n^{t+1} &= c_n^t - e_n^t \quad \forall n \in \mathcal{N} \\
e_n^{min} &\le e_n^t \le e_n^{max} \quad \forall n \in \mathcal{N} \\
c_n^{min} &\le c_n^t \le c_n^{max} \quad \forall n \in \mathcal{N}
\end{aligned}
\tag{6.8}
$$

The optimal cost resulting from this optimization is denoted by f_{coop}^*. Similar to *optimization 1*, this problem is a convex program and can be solved using standard techniques [78].

6.3.3 Cooperative game framework for user cooperation

We use concepts from cooperative games to study how different users may form coalitions to attain payoffs that would not be possible if they were to optimize their demand individually and how this increased payoff should be divided between them such that it satisfies some measures of fairness and stability. In this section, we introduce a few concepts from cooperative games including the notions of fairness and stability and will apply them to the cooperative energy optimization problem.

Consider the same set of users $\mathcal{N}$ as the previous section. Any nonempty subset $S \subseteq \mathcal{N}$ is called a coalition between the members of S. A coalitional cost game between the members of $\mathcal{N}$ is a pair $(\mathcal{N}, v)$ where $\mathcal{N}$ is the set of users and $v(S) : 2^{\mathcal{N}} \to \mathbb{R}^+$ is a set function representing the cost of each coalition $S \subseteq \mathcal{N}$. In a cost game, users prefer

less cost and therefore may form coalitions to reduce the total cost.

definitioncooperative game $(\mathcal{N}, v)$ is called an LP game if its set cost function can be expressed as $v(S) = \min_x u^T x$ subject to linear constraints on x.

We define the cost of each coalition S as $v(S) = f^*_{coop,S}$. Here $f^*_{coop,S}$ is the optimal cost resulting from the coalition of users of set S. The coalition $\mathcal{N}$, i.e. the coalition of all users in $\mathcal{N}$ is called the grand coalition. We also define $\psi \in \mathbb{R}^N$ as the vector of cost distribution between all users in the grand coalition with each user's cost being ψ_i.

definitiongame $(\mathcal{N}, v)$ is said to be *sub-additive* if given that $S \cap T = \phi$ it results that $v(S \cup T) \leq v(S) + v(T)$.

theoremhe above game $(\mathcal{N}, v)$ with $v(S) = f^*_{coop,S}$ is sub-additive.

Proof. Suppose S and T are two disjoint sets of users and $f^*_{coop,S}$ and $f^*_{coop,T}$ are their respective optimal costs. Now assume these two sets of users join to form the coalition $S \cup T$. If in the joint coalition, both sets of users S and T maintain their optimal schedules x^*_S and x^*_T from the optimal solution to *optimization 1* (this is possible because S and T are disjoint), then

$$
\begin{aligned}
f_{coop,S \cup T} &= \sum_{t=1}^{T} p^t (x_S^t + x_T^t) + \alpha \max_{t \in \mathscr{T}} (x_S^t + x_T^t) \\
&\leq \sum_{t=1}^{T} p^t x_S^t + \alpha \max_{t \in \mathscr{T}} x_S^t + \sum_{t=1}^{T} p^t x_T^t + \alpha \max_{t \in \mathscr{T}} x_T^t \\
&= f^*_{coop,S} + f^*_{coop,T}
\end{aligned}
$$

Therefore, for the above joint schedule, we will always have $f_{coop,S \cup T} \leq f^*_{coop,S} + f^*_{coop,T}$. Since we always have $f^*_{coop,S \cup T} \leq f_{coop,S \cup T}$, it results that $f^*_{coop,S \cup T} \leq f^*_{coop,S} + f^*_{coop,T}$ or $v(S \cup T) \leq v(S) + v(T)$. □

This property implies that the total saving increases as more users participate in

the game. It can also be intuitively verified that since the peak demand of the unified entity over a time horizon will always be equal or smaller than the sum of peak demands of all users, if all users maintain their optimal individual schedule without considering other users' schedules, the cost of the unified entity will be at worst equal to the sum of individual costs of all users. We have therefore found the answer to question I. While the sub-additivity property discusses the total saving of all participating users, it does not discuss the distribution of savings between the users. The next section will address the distribution of the total optimal cost between the users.

6.3.4   Distribution of saving from cooperative optimization

So far we have shown that the cost achieved as a result of cooperation between a group of users is at worst equal to the sum of costs of individual users if no cooperation took place. However, this does not necessarily lead to all users paying a lower cost than they did individually. In fact, whether or not users will be subject to a lower cost depends on the distribution of the total cost between the users. Two important concepts often considered while specifying cost distribution are stability and fairness. We will further characterize these two notions and study our cooperative game with regards to fairness and stability.

Fairness. A fair cost distribution $\psi \in \mathbb{R}^N$ divides the total cost of a cooperation based on different users' contributions in achieving that cost. The well-known characterization of fairness given be Shapley [79] that attributes certain desirable properties to a fair distribution is given as

theoremshapley1953value Given the coalitional game $(\mathcal{N}, v)$ with $v(S) = f^*_{coop,S}$, the unique cost distribution $\psi(\mathcal{N}, v)$ that divides the entire saving of the grand coalition

between the users and satisfies fairness axioms of [79] is given by

$$\psi_n(\mathcal{N}, v) = \frac{1}{|\mathcal{N}|!} \sum_{S \subseteq \mathcal{N} \setminus n} |S|! \, (|\mathcal{N}| - |S| - 1)! \big[v(S \cup n) - v(S)\big]$$

where $|\mathcal{N}|$ and $|S|$ are the cardinality of $\mathcal{N}$ and S respectively. The fairness axioms and proof can be found in [79]. The outcome of this theorem assigns portion ψ_n of the total saving to each user n, also known as the Shapley value of user n. The above computation involves determining the average marginal contribution of user n over all the different ways that the grand coalition can be formed from the zero coalition. Therefore one should solve *optimization 2* for all possible subsets of the grand coalition and then compute the marginal contribution of each user using the above relation.

Stability. Although the Shapley distribution guarantees fair and efficient distribution of the saving between the users in accordance with the given axioms, there is still no guarantee that such saving is binding for all users. In fact, we now aim to address the question of stability of the grand coalition: under the Shapley saving distribution given above and despite the fact that the game is sub-additive, could there be any incentive for a user or a group of users to refrain from joining the grand coalition and form smaller coalitions among themselves? To answer this question, we next introduce the concept of *core* in coalitional games.

definitioncost distribution vector $\psi \in \mathbb{R}^N$ is in the core of a coalitional game $(\mathcal{N}, v)$ if and only if

$$\sum_{n \in \mathcal{N}} \psi_n = v(\mathcal{N}) \text{ and } \sum_{s \in S} \psi_s \leq v(S), \forall S \subset \mathcal{N} \tag{6.9}$$

In other words, in order for a coalition to be stable, the sum of savings of any subset of users should be greater or equal to the saving that those users would have

obtained if that subset actually formed a sub-coalition. It is now reasonable to assume that rational users participating in a coalitional game would want to form the grand coalition only if the saving distribution vector is drawn from the core. We can henceforth relate the concept of core with the stability of a coalitional game. This concept is similar to the concept of Nash equilibrium in cooperative games. The difference here is that instead of investigating whether a single user can benefit by deviating from an action, we turn our attention to possible deviation of a group of users in order to form their own coalition. It can be shown [80] that the core of a cooperative game may be empty. If a game has an empty core, no saving distribution can possibly guarantee the stability of the grand coalition. In such case, a player or group of players may opt for smaller coalitions to increase their savings. The following theorem will examine non-emptiness of the core for the game considered in this work.

theoremhe core of the game $(\mathcal{N}, v)$ with $v(S) = f^*_{coop,S}$ is non-empty.

Proof. Since $v(S) = f^*_{coop,S} = \underset{x}{\text{minimize}} \ f_{coop,S}(x)$ can be expressed as a linear program with the linear cost functions of *optimization 2*, this game is an LP game. It can be proved [81] that an LP game has a nonempty core and therefore the core of the above game is non-empty. □

It can be shown that if the core of a coalitional game exists, it may not be unique [80]. For certain class of games known as submodular games, if the cost is distributed according to Shapley distribution, then the grand coalition will be stable.

definitiongame $(\mathcal{N}, v)$ is said to be *submodular* (concave) if $v(S \cup T) + v(S \cap T) \leq v(S) + v(T)$, $\forall S, T \subseteq \mathcal{N}$ or equivalently $v(S \cup \{i\}) - v(S) \geq v(T \cup \{i\}) - v(T), \forall S \subseteq T \subseteq \mathcal{N} \setminus \{i\}, \forall i \in \mathcal{N}$.

In the following, we will investigate the submodularity of the considered collaborative cost minimization game.

theoremhe game (N, v) with $v(S) = f^*_{coop,S}$ is not submodular.
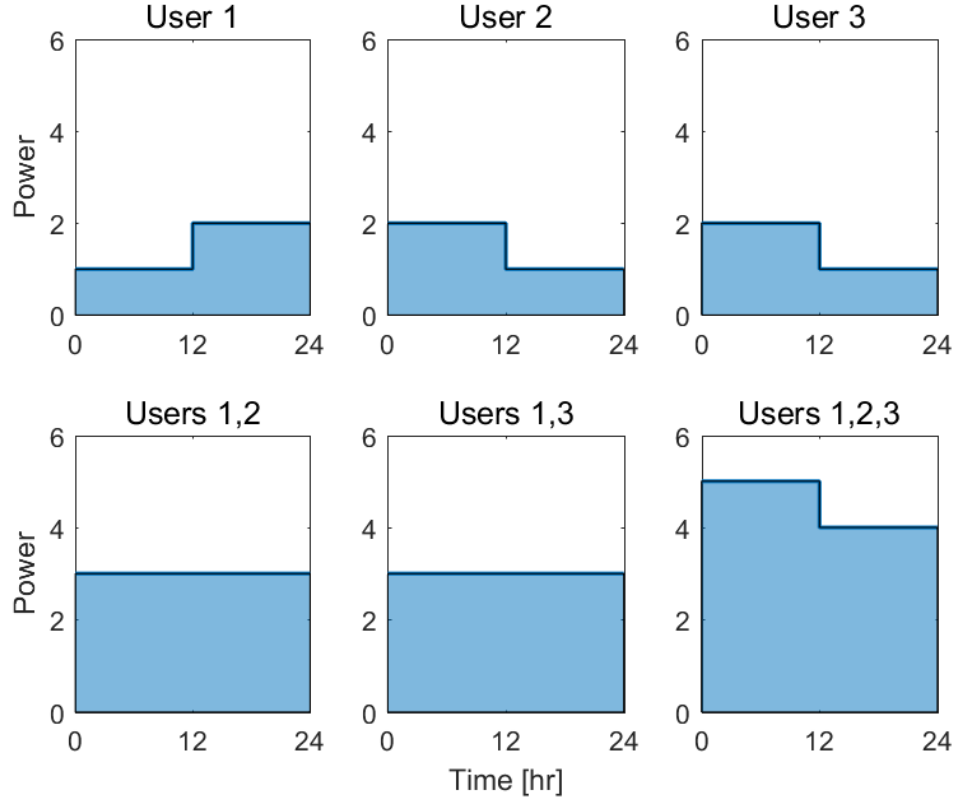
Figure 6.1. Users demand and consumption patterns without storage capacity. Top: Demand profiles for each of the users 1, 2, and 3. Bottom: Resulting demand profiles if coalitions form between different subsets of users.

Proof. We will show that this game violates the submodularity property by a simplified example of a three-user cooperative game. Assume that three users none of which have storage capacity participate in a cooperative power sharing game. Also for simplicity assume that $p(t) = 0$, $\forall t \in \mathscr{T}$, so only demand charge is applicable. Suppose the demand of each of the users follows the profiles of Fig. 6.1. Taking $S = \{1\}$ and $T = \{1, 2\}$ as two possible coalitions between the users and $i = 3$, we see that such coalitions satisfy

$S \subseteq T \subseteq \mathcal{N} \setminus \{i\}$. Now, it can be seen from Fig. 6.1 that

$$v(S) = 2 \,, v(S \cup \{i\}) = 3 \,, v(T) = 3 \,, v(T \cup \{i\}) = 5$$

$$v(S \cup \{i\}) - v(S) = 1 \not\geq 2 = v(T \cup \{i\}) - v(T)$$

Therefore the above game is not sub-modular according to definition .   □

It can further be shown that if the cost function contains onlly the ToU term, the game would satisfy the submodularity condition. The proof is eliminated due to space constraints. The lack of submodularity is therefore due to the existence of peak demand cost term. The lack of submodularity implies that the resulting Shapley value may fail to fall within the core of the game [81], as will be shown in the numerical case study of the next section. However, according to corollary , the core of the game is non-empty in both cases and therefore, one should be able to find another cost distribution that falls within the core. In fact, according to definition , all distributions ψ_n that satisfy the inequalities (6.9) constitute the core.

6.4   Fair and stable cost distribution algorithm

Non-emptiness and non-uniqueness of the core imply that multiple payoff distributions might exist that are within the core. In the ideal case, the Shapley distribution is chosen over other possible distributions due to its fairness properties. However, if Shapley distribution is not within the core (is not stable), we would want to have another notion of fairness that helps us pick one distribution among all stable distributions. To this end, we would define our notion of fairness as the difference between the highest and lowest percentage cost saving among all users for a given distribution vector. Using this fairness index, the stable and fair payoff distribution problem is formulated as

$$\underset{\psi}{\text{minimize}} \ \Delta$$

$$\text{subject to} \ \sum_{n \in \mathcal{N}} \psi_n = v(N)$$

$$\sum_{s \in S} \psi_s \leq v(S), \ \forall S \subset \mathcal{N} \qquad (6.10)$$

$$\Lambda_{min} \leq \frac{v(\{n\}) - \psi_n}{v(\{n\})} \leq \Lambda_{max}, \ \forall n \in \mathcal{N}$$

$$\Delta = \Lambda_{max} - \Lambda_{min}$$

In this LP, the first two constraints enforce stability while the next two constraints formulate a measure of fairness as the difference between maximum and minimum percentage cost saving among all users. The objective is then to minimize this difference subject to stability constraints. Since the game is proved to have a non-empty core, the solution of this LP will always exist and will fall within the core of the game. Based on this program, we formalize the following cooperative optimization and cost distribution algorithm between a group of users. It should be noted that since the resulting cost distribution will be drawn from the core, it is in the interest of all users regardless of their demand pattern and storage capacity to participate in this game.

Algorithm 2. Cooperative optimization and cost sharing

1: Collect load data for all users
2: Solve the cooperative optimization (*optimization 2*) with cost function (6.6) subject to the constraints (6.8)
3: Distribute the total cost between the users according to Shapley distribution
4: Check if the Shapley distribution falls within the core by checking conditions (6.9)
5: **If** Shapley distribution is within the core **then**
6:    Distribute the cost according to Shapley distribution
7: **else**
8:    Compute a fair and stable distribution by solving the linear program (6.10)
9: **End if**

By following this algorithm, a stable payoff distribution is computed so that all users will have an incentive to join and form the grand coalition. This cost distribution algorithm provides the answer to question II.

Remark. The complexity of checking condition (6.9) grows exponentially with $|\mathcal{N}|$. Therefore for very large number of participating microgrids, the Shapley computation steps and its stability checks may be skipped. The proposed optimization (6.10) can directly be used to obtain a stable distribution in such cases to ensure scalability of the cost distribution.

6.5   Case study

In this section we analyze two case studies and will assess the results of the proposed algorithms in each case.

Table 6.1. ToU unit prices (p^t)

Time	9am-12pm	12pm-6pm	6pm-9pm	9pm-9am
p^t	1.5	2	1.5	1

Case 1. Consider 3 users supplied within the same distribution feeder with load demand profiles shown in Fig. 6.2 left. The profiles shown in this figure are load predictions for three medium-size facilities. These users have storage capacities of respectively $500, 1000, 0$ kWh. Solving the convex optimization (*optimization 1*) individually for each user will result in the PCC power flow profiles of Fig. 6.2 right. Note that since user 3 has no storage it has to draw its entire load demand at each time from the main grid. The resulting energy cost for each user is shown in the first row of Table 6.2 . Next, solving the cooperative scheduling problem for these users in a centralized manner, the total cost of the system drops from 74603 to 73126. This

2 percent cost reduction indicates the effect of joint planning. *optimization 2* is also solved for all subsets of the Grand coalition to obtain the optimal cost of other possible sub-coalitions (see Table 6.2). Next, Shapley distribution is computed to obtain the share of each user in the total cost as shown in the 4th row of Table 6.3. To check whether this distribution is within the core of the game, the following set of inequalities are verified to hold

$$v(1) = 24997 \geq 24666 = \psi_1$$

$$v(2) = 23127 \geq 22494 = \psi_2$$

$$v(3) = 26480 \geq 25965 = \psi_3$$

$$v(12) = 47397 \geq 47161 = \psi_1 + \psi_2$$

$$v(13) = 50986 \geq 50632 = \psi_1 + \psi_3$$

$$v(23) = 48512 \geq 48460 = \psi_2 + \psi_3$$

$$v(123) = 73126 = 73126 = \psi_1 + \psi_2 + \psi_3$$

It can be concluded that according to definition , the Shapley distribution is within the core. Therefore, under such fair distribution all users will have a cost lower than their cost before cooperation and more importantly, the coalition is stable and no user is willing to drop out to form a smaller coalition. Therefore according to algorithm 1, this distribution is chosen over other possible distributions of the total cost.

    Case 2. Consider 3 users with load demand profiles shown in Fig.6.5 left and storage capacities of respectively $500, 300, 700kWh$. The load profiles represent predictions for two industrial and one commercial facilities. The same price specifications as the previous case apply. Solving the convex optimization *optimization 1* individually for each
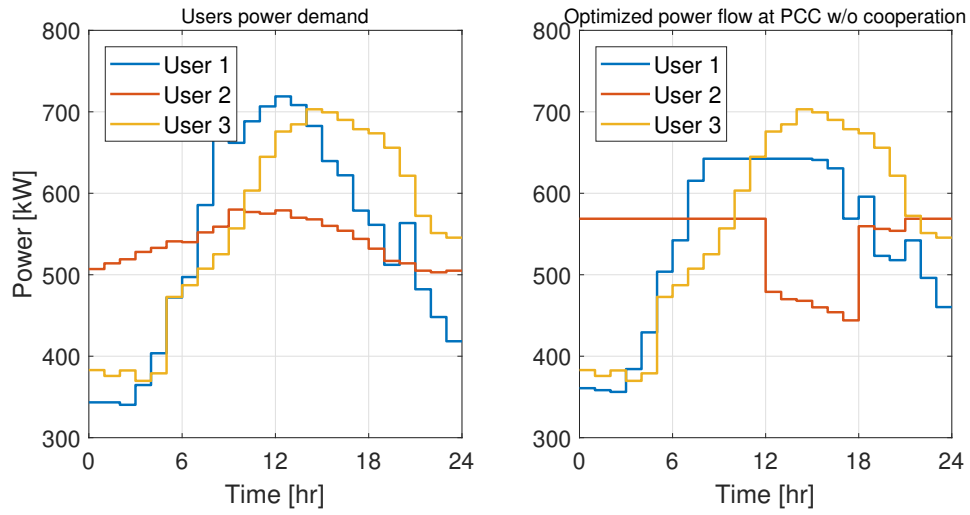
Figure 6.2. Left: Demand profiles for three industrial/commercial users in *case 1*. Right: Results of individual optimization (solution of *optimization 1*). User 3 has zero storage capacity
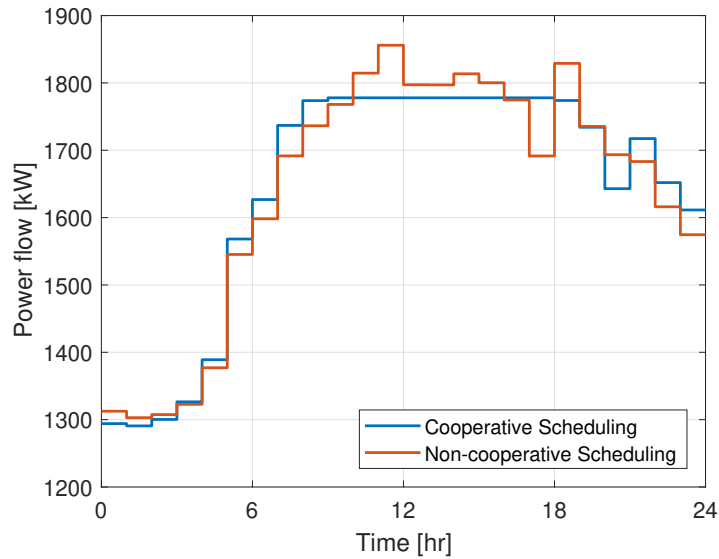
Figure 6.3. Result of cooperative optimization in *case 1* between all users (blue) vs. sum of all users' consumption under individual optimization (red). The flattened peak of the blue profile indicates the result of joint planning of all users for peak demand charge reduction

Figure 6.4. Cost of each user under individual optimization vs under different distributions of the coalitional optimization for example of *case 1*. Notice the reduction in cost if each user employs storage individually and also if users conduct cooperative planning. Also notice the slight variation in each user's cost distribution between Shapley distribution and the proposed fair distribution. Both these distributions fall within the core as indicated above

Table 6.2. Optimal cost of *optimization 2* under different possible sub-coalitions of the grand coalition in *case 1*

Coalition	{1}	{2}	{3}	
Cost	24997	23127	26480	
Coalition	{1,2}	{1,3}	{2,3}	{1,2,3}
Cost	47397	50986	48512	73126

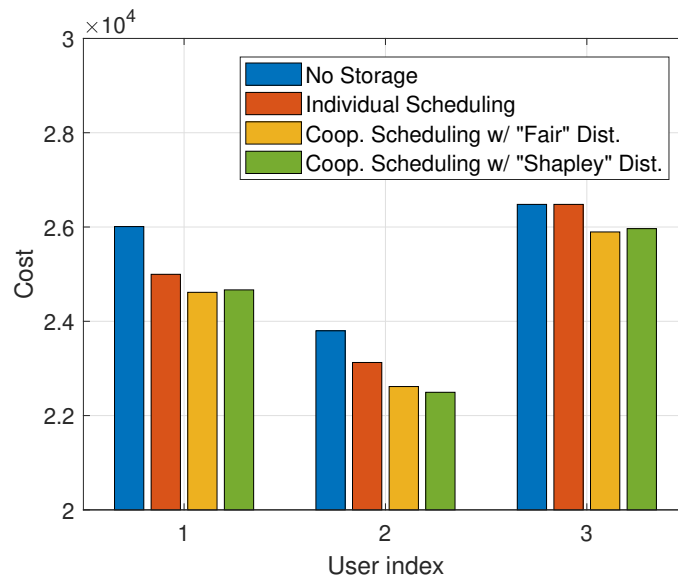**Table 6.3.** Cost of each user under individual optimization vs under different distributions of the coalitional optimization for example of *case 1*

Cost \ User	1	2	3	Total
Individual cost w/o storage	26009	23798	26480	76288
Individual Cost with storage	24997	23127	26480	74603
Cooperative cost with "Fair" distribution within the core	24615	22616	25895	73126
Cooperative cost with Shapley distribution	24666	22494	25965	73126

user will result in the PCC power flow profiles of Fig. 6.5 right. The resulting energy cost for each user is shown in the first row of Table 6.4. Next, solving the cooperative scheduling problem (*optimization 2*) for these users, the total cost of the system drops from 67432 to 66174 as a result of joint planning. The optimal cost of other possible sub-coalitions are also mentioned in Table 6.4. Next, Shapley values are computed to obtain the share of each user in the total cost as shown in the 4th row of Table 6.5. It is observed that the following inequality is violated

$$v(13) = 45851 \ngeq 45873 = \psi_1 + \psi_3$$

and therefore the Shapley distribution is not within the core of the game. Following algorithm 1, we then compute a fair cost distribution from the core by solving *optimization*

3. The resulting stable distribution is indicated in the 3rd row of Table 6.5 and also compared with other distributions in Fig. 6.7. Satisfaction of the following inequalities confirm the existence of this distribution within the core and therefore stability of the game.

$$v(1) = 25522 \geq 24881 = \psi_1$$

$$v(2) = 20399 \geq 20324 = \psi_2$$

$$v(3) = 21510 \geq 20970 = \psi_3$$

$$v(12) = 45806 \geq 45205 = \psi_1 + \psi_2$$

$$v(13) = 45851 \geq 45851 = \psi_1 + \psi_3$$

$$v(23) = 41587 \geq 41294 = \psi_2 + \psi_3$$

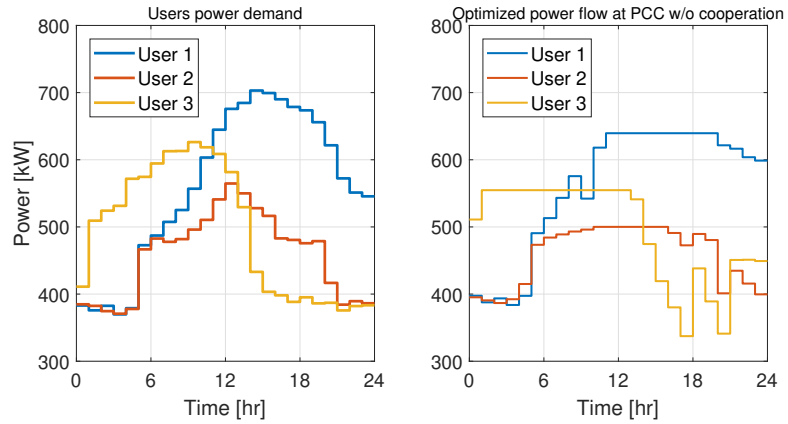$$v(123) = 66174 = 66174 = \psi_1 + \psi_2 + \psi_3$$

Figure 6.5. Left: Demand profiles for three industrial/commercial users in *case 2*. Right: Results of individual optimization (solution of *optimization 1*)
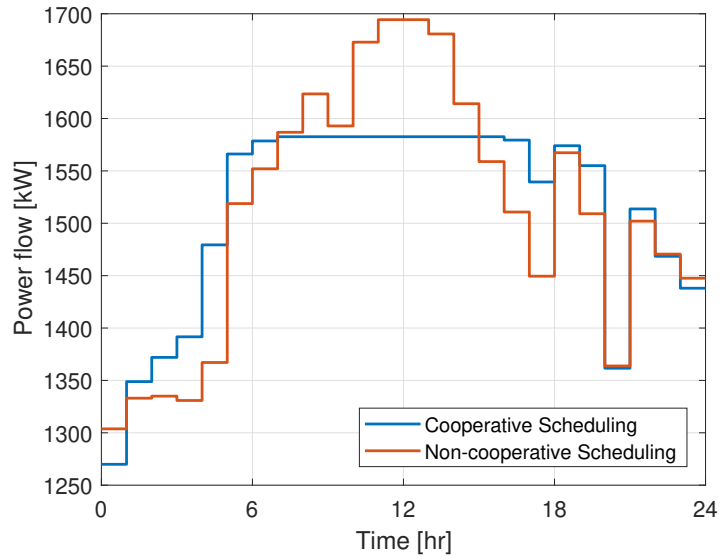
Figure 6.6. Result of cooperative optimization in *case 2* between all users (blue) vs. sum of all users' consumption under individual optimization (red). The flattened peak of the blue profile indicates the result of joint planning of all users for peak demand charge reduction

Table 6.4. Optimal cost of *optimization 2* under different possible sub-coalitions of the grand coalition in *case 2*

Coalition	{1}	{2}	{3}	
Cost	25522	20399	21510	
Coalition	{1,2}	{1,3}	{2,3}	{1,2,3}
Cost	45806	45851	41587	66174

Table 6.5. Cost of each user under individual optimization vs under different distributions of the coalitional optimization for example of *case 2*

Cost \ User	1	2	3	Total
Individual cost w/o storage	26480	21229	22348	70057
Individual cost with storage	25522	20399	21510	67432
Cooperative cost with "Fair" distribution within the core	24881	20324	20970	66174
Cooperative cost with Shapley distribution	24994	20301	20879	66174
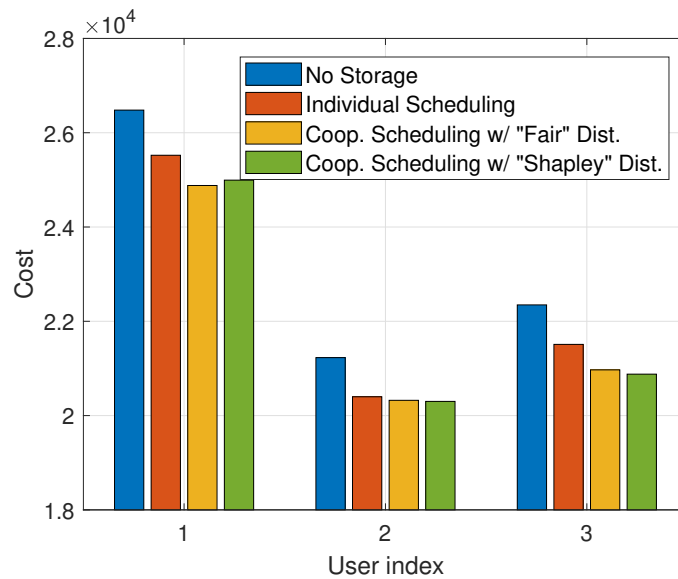
Figure 6.7. Cost of each user under individual optimization vs under different distributions of the coalitional optimization for example of *case 2*. Notice the reduction in cost if each user employs storage individually and also if users conduct cooperative planning. Despite the slight variation in each user's cost between Shapley distribution and the proposed fair distribution, distribution of the cost according to Shapley distribution does not result in a stable collaboration as shown above.

6.6   Summary of discussed problem

For a group of commercial and industrial microgrids participating in demand response programs, a cooperative energy planning algorithm is proposed that minimizes the total energy cost for the participating microgrids. To motivate participation among microgrids, it is intended to devise a cost allocation strategy that guarantees fair and stable cost distribution among microgrids. It is shown that such cost distribution will always exist and an algorithm is proposed that yields such stable and fair distribution.

Acknowledgements

Chapter 7

Concluding Remarks

This dissertation has proposed multiple techniques for optimal microgrid control, energy management, and scheduling in the presence of intermittent renewable resources, reserve non-renewable resources, and energy storage systems. The presented approaches consider microgrid optimization problems from the viewpoint of a single microgrid as well as multiple cooperating microgrids under a variety of energy cost structures and operating limitations imposed by resource constraints and the grid. Additionally, we present an approach of addressing both short-term scheduling and real-time power control in a unified model predictive control framework where the microgrid controller operates at two separate time scales. Techniques are proposed to relax the non-convex resource dispatch problem and enable solving the MPC at update rates comparable with renewable generation and demand variability time scales. To facilitate testing of different microgrid controllers with fast update rates, a remote hardware-in-the-loop microgrid testing setup is designed and utilized for testing the controllers proposed in this work. The proposed control and scheduling approaches are developed using data and models from real-world microgrids and some of the techniques are implemented in an actual microgrid in California with solar energy generation and an energy storage system.

Bibliography

[1] IEEE standard for the specification of microgrid controllers. Technical report, IEEE Std 2030.7-2017, 2018.

[2] Samuel Koebrich, Emily I Chen, Thomas Bowen, Sydney Forrester, and Tian Tian. 2017 renewable energy data book: Including data and trends for energy storage and electric vehicles. Technical report, National Renewable Energy Lab.(NREL), Golden, CO (United States), 2019.

[3] Jeremy Neubauer and Mike Simpson. Deployment of behind-the-meter energy storage for demand charge reduction. Technical report, National Renewable Energy Lab.(NREL), Golden, CO (United States), 2015.

[4] Lori Bird, Michael Milligan, and Debra Lew. Integrating variable renewable energy: Challenges and solutions. Technical report, National Renewable Energy Lab.(NREL), Golden, CO (United States), 2013.

[5] Paul Denholm, Matthew O'Connell, Gregory Brinkman, and Jennie Jorgenson. Overgeneration from solar energy in california. a field guide to the duck chart. Technical report, National Renewable Energy Lab.(NREL), Golden, CO (United States), 2015.

[6] Keith Casey, M Rothleder, D Le Vine, S Liu, X Wang, Y Zhang, JW Chang, JP Pfeifenberger, MG Aydin, CO Aydin, et al. Senate bill 350 study: The impacts of a regional iso-operated power market on california, 2016.

[7] California ISO. Impacts of renewable energy on grid operations. Technical report.

[8] Michael Milligan, Bethany Frew, Ella Zhou, and Douglas J. Arent. Advancing system flexibility for high penetration renewable integration. Technical report.

[9] Paul Denholm and Robert Margolis. Energy storage requirements for achieving 50% solar photovoltaic energy penetration in california. Technical report, National Renewable Energy Lab.(NREL), Golden, CO (United States), 2016.

[10] Renewables 2016 global status report. 2016.

[11] Daniel E Olivares, Ali Mehrizi-Sani, Amir H Etemadi, Claudio A Canizares, Reza Iravani, Mehrdad Kazerani, Amir H Hajimiragha, Oriol Gomis-Bellmunt, Maryam Saeedifard, Rodrigo Palma-Behnke, et al. Trends in microgrid control. *IEEE Transactions on smart grid*, 5(4):1905–1919, 2014.

[12] Raymond A. de Callafon, Abdulelah H. Habib, and Jan Kleissl. Scheduling of dynamic electric loads using energy storage and short term power forecasting. In *The IEEE Conference on Control Applications (CCA)*. http://ieeexplore.ieee.org/document/7588018/, 2016.

[13] Seon-Ju Ahn, Soon-Ryul Nam, Joon-Ho Choi, and Seung-Il Moon. Power scheduling of distributed generators for economic and stable operation of a microgrid. *IEEE Transactions on Smart Grid*, 4(1):398–405, 2013.

[14] Yu Zhang, Nikolaos Gatsis, and Georgios B Giannakis. Robust energy management for microgrids with high-penetration renewables. *IEEE Transactions on Sustainable Energy*, 4(4):944–953, 2013.

[15] Mohammad Shahidehpour and Mohammad Khodayar. Cutting campus energy costs with hierarchical control: The economical and reliable operation of a microgrid. *IEEE Electrification Magazine*, 1(1):40–56, 2013.

[16] Jaime De La Ree, Virgilio Centeno, James S Thorp, and Arun G Phadke. Synchronized phasor measurement applications in power systems. *IEEE Transactions on Smart Grid*, 1(1):20–27, 2010.

[17] Sai Akhil R Konakalla and Raymond de Callafon. Optimal filtering for grid event detection from real-time synchrophasor data. *Procedia Computer Science*, 80:931–940, 2016.

[18] Kjetil Uhlén, Luigi Vanfretti, MM De Oliveira, AB Leirbukt, Vemund Halmo Aarstrand, and Jan O Gjerde. Wide-area power oscillation damper implementation and testing in the norwegian transmission network. In *Power and Energy Society General Meeting, 2012 IEEE*, pages 1–7. IEEE, 2012.

[19] M. J. Khojasteh, M. Hedayatpour, and M. Franceschetti. Theory and implementation of event-triggered stabilization over digital channels. In *IEEE Conf. Decis. and Cont. (CDC)*, Nice, France, 2019.

[20] Mohammad Javad Khojasteh, Pavankumar Tallapragada, Jorge Cortés, and Massimo

Franceschetti. Time-triggering versus event-triggering control over communication channels. In *2017 IEEE 56th Annual Conference on Decision and Control (CDC)*, pages 5432–5437. IEEE, 2017.

[21] Mohammad Javad Khojasteh, Pavankumar Tallapragada, Jorge Cortés, and Massimo Franceschetti. The value of timing information in event-triggered control. *IEEE Transactions on Automatic Control*, 2019.

[22] Karl Schoder, Ziyuan Cai, Sindhuja Sundararajan, Ming Yu, Mike Sloderbeck, Isaac Leonard, and Michael Steurer. Real-time simulation of communications and power systems for testing distributed embedded controls. *IET Engineering & Technology Review*, 2016.

[23] RTDS Technologies Inc. Real time digital power system simulation. https://www.rtds.com/.

[24] Raymond A De Callafon, Babak Moaveni, Joel P Conte, Xianfei He, and Eric Udd. General realization algorithm for modal identification of linear dynamic systems. *Journal of engineering mechanics*, 134(9):712–722, 2008.

[25] Masih Haseli and Jorge Cortés. Approximating the koopman operator using noisy data: noise-resilient extended dynamic mode decomposition. In *2019 American Control Conference (ACC)*, pages 5499–5504. IEEE, 2019.

[26] Daniel N. Miller and Raymond A. de Callafon. Identification of linear time-invariant systems via constrained step-based realization. In *IFAC Proc. Volumes*, volume 45, pages 1155–1160, 2012.

[27] KE Martin, Gustavo Brunello, MG Adamiak, Galina Antonova, M Begovic, G Ben-mouyal, PD Bui, H Falk, V Gharpure, A Goldstein, et al. An overview of the IEEE standard C37.118.2 - synchrophasor data transfer for power systems. *IEEE Transactions on Smart Grid*, 5(4):1980–1984, 2014.

[28] Amir Valibeygi, Raymond A de Callafon, Mark Stanovich, Michael Sloderbeck Karl Schoder, James Langston Isaac Leonard, Sourindu Chatterjee, and Rick Meeker. Microgrid control using remote controller hardware-in-the-loop over the internet. In *2018 IEEE Power & Energy Society Innovative Smart Grid Technologies Conference (ISGT)*, pages 1–5. IEEE, 2018.

[29] Alexdandre Oudalov, Daniel Chartouni, Christian Ohler, and G_ Linhofer. Value analysis of battery energy storage applications in power systems. In *Power Systems Conf. and Expo., PSCE, 2006. IEEE PES*, pages 2206–2211. IEEE, 2006.

[30] Aliasghar Baziar and Abdollah Kavousi-Fard. Considering uncertainty in the optimal energy management of renewable micro-grids including storage devices. *Renewable Energy*, 59:158–166, 2013.

[31] Hongyu Wu, Mohammad Shahidehpour, Zuyi Li, and Wei Tian. Chance-constrained day-ahead scheduling in stochastic power system operation. *IEEE Transactions on Power Systems*, 29(4):1583–1591, 2014.

[32] Pawel Malysz, Shahin Sirouspour, and Ali Emadi. An optimal energy storage control strategy for grid-connected microgrids. *IEEE Transactions on Smart Grid*, 5(4):1785–1796, 2014.

[33] Alessandra Parisio, Evangelos Rikos, and Luigi Glielmo. A model predictive control approach to microgrid operation optimization. *IEEE Transactions on Control Systems Technology*, 22(5):1813–1827, 2014.

[34] Alex Park and Petros Lappas. Evaluating demand charge reduction for commercial-scale solar pv coupled with battery storage. *Renewable Energy*, 108:523–532, 2017.

[35] R Hanna, J Kleissl, A Nottrott, and M Ferry. Energy dispatch schedule optimization for demand charge reduction using a photovoltaic-battery storage system with solar forecasting. *Solar Energy*, 103:269–287, 2014.

[36] Anna-Lena Klingler and Lukas Teichtmann. Impacts of a forecast-based operation strategy for grid-connected pv storage systems on profitability and the energy system. *Solar Energy*, 158:861–868, 2017.

[37] Farshid Shariatzadeh, Paras Mandal, and Anurag K Srivastava. Demand response for sustainable energy systems: A review, application and implementation strategy. *Renewable and Sustainable Energy Reviews*, 45:343–350, 2015.

[38] Sina Parhizi and Amin Khodaei. Market-based microgrid optimal scheduling. In *Smart Grid Communications (SmartGridComm), 2015 IEEE International Conference on*, pages 55–60. IEEE, 2015.

[39] Abdulelah H Habib, Jan Kleissl, and Raymond A de Callafon. Model predictive load scheduling using solar power forecasting. In *American Control Conference (ACC), 2016*, pages 3200–3205. IEEE, 2016.

[40] Amin Khodaei, Shay Bahramirad, and Mohammad Shahidehpour. Microgrid planning under uncertainty. *IEEE Transactions on Power Systems*, 30(5):2417–

2425, 2015.

[41] Ioannis Sarantis, Farid Alavi, and Bart De Schutter. Optimal power scheduling of fuel-cell-car-based microgrids. In *Decision and Control (CDC), 2017 IEEE 56th Annual Conference on*, pages 5062–5067. IEEE, 2017.

[42] Pedram Samadi, Hamed Mohsenian-Rad, Vincent WS Wong, and Robert Schober. Tackling the load uncertainty challenges for energy consumption scheduling in smart grid. *IEEE Transactions on Smart Grid*, 4(2):1007–1016, 2013.

[43] Alessandra Parisio and Luigi Glielmo. Stochastic model predictive control for economic/environmental operation management of microgrids. In *Control Conference (ECC), 2013 European*, pages 2014–2019. IEEE, 2013.

[44] Zukui Li, Ran Ding, and Christodoulos A Floudas. A comparative theoretical and computational study on robust counterpart optimization: I. robust linear optimization and robust mixed integer linear optimization. *Industrial & engineering chemistry research*, 50(18):10567–10603, 2011.

[45] Zhi Wu, Wei Gu, Rui Wang, X Yuan, and W Liu. Economic optimal schedule of chp microgrid system using chance constrained programming and particle swarm optimization. In *Power and Energy Society General Meeting, 2011 IEEE*, pages 1–11. IEEE, 2011.

[46] Abraham Charnes and William W Cooper. Chance-constrained programming. *Management science*, 6(1):73–79, 1959.

[47] Xin Jin, Kyri Baker, Steven Isley, and Dane Christensen. User-preference-driven model predictive control of residential building loads and battery storage for demand response. In *American Control Conference (ACC), 2017*, pages 4147–4152. IEEE, 2017.

[48] Ionela Prodan and Enrico Zio. A model predictive control framework for reliable microgrid energy management. *International Journal of Electrical Power & Energy Systems*, 61:399–409, 2014.

[49] Yan Zhang, Rui Wang, Tao Zhang, Yajie Liu, and Bo Guo. Model predictive control-based operation management for a residential microgrid with considering forecast uncertainties and demand response strategies. *IET Generation, Transmission & Distribution*, 10(10):2367–2378, 2016.

[50] Amir Valibeygi, Abdulelah H Habib, and Raymond A de Callafon. Robust power

scheduling for microgrids with uncertainty in renewable energy generation. In *2019 IEEE Power & Energy Society Innovative Smart Grid Technologies Conference (ISGT)*, pages 1–5. IEEE, 2019.

[51] Hamid Shaker, Hamidreza Zareipour, and David Wood. Impacts of large-scale wind and solar power integration on california s net electrical load. *Renewable and Sustainable Energy Reviews*, 58:761–774, 2016.

[52] Roohallah Khatami, Masood Parvania, Yu Christine Chen, Swaroop Guggilam, and Sairaj Dhople. Dynamics-aware continuous-time economic dispatch: A solution for optimal frequency regulation.

[53] Paul Denholm and Robert Margolis. Energy storage requirements for achieving 50% solar photovoltaic energy penetration in california. Technical report, National Renewable Energy Lab.(NREL), Golden, CO (United States), 2016.

[54] Rodrigo Palma-Behnke, Carlos Benavides, Fernando Lanas, Bernardo Severino, Lorenzo Reyes, Jacqueline Llanos, and Doris Sáez. A microgrid energy management system based on the rolling horizon strategy. *IEEE Transactions on smart grid*, 4(2):996–1006, 2013.

[55] Le Xie and Marija D Ilic. Model predictive economic/environmental dispatch of power systems with intermittent resources. In *2009 IEEE Power & Energy Society General Meeting*, pages 1–6. IEEE, 2009.

[56] Samir M Dawoud, Xiangning Lin, and Merfat I Okba. Hybrid renewable microgrid optimization techniques: A review. *Renewable and Sustainable Energy Reviews*, 82:2039–2052, 2018.

[57] Fabian Kennel, Daniel Görges, and Steven Liu. Energy management for smart grids with electric vehicles based on hierarchical mpc. *IEEE Transactions on industrial informatics*, 9(3):1528–1537, 2012.

[58] Julia Sachs and Oliver Sawodny. A two-stage model predictive control strategy for economic diesel-pv-battery island microgrid operation in rural areas. *IEEE Transactions on Sustainable Energy*, 7(3):903–913, 2016.

[59] Stefano Raimondi Cominesi, Marcello Farina, Luca Giulioni, Bruno Picasso, and Riccardo Scattolini. A two-layer stochastic model predictive control scheme for microgrids. *IEEE Transactions on Control Systems Technology*, 26(1):1–13, 2017.

[60] Miguel A Velasquez, Julian Barreiro-Gomez, Nicanor Quijano, Angela I Cadena,

and Mohammad Shahidehpour. Intra-hour microgrid economic dispatch based on model predictive control. *IEEE Transactions on Smart Grid*, 2019.

[61] Javier Contreras, Rosario Espinola, Francisco J Nogales, and Antonio J Conejo. Arima models to predict next-day electricity prices. *IEEE transactions on power systems*, 18(3):1014–1020, 2003.

[62] Jan Kleissl. *Solar energy forecasting and resource assessment*. Academic Press, 2013.

[63] Sophie Pelland, Jan Remund, Jan Kleissl, Takashi Oozeki, and Karel De Brabandere. Photovoltaic and solar forecasting: state of the art. *IEA PVPS, Task*, 14:1–36, 2013.

[64] Paul Denholm and Robert Margolis. The potential for energy storage to provide peaking capacity in california under increased penetration of solar photovoltaics. Technical report, National Renewable Energy Lab.(NREL), Golden, CO (United States), 2018.

[65] Lijun Chen, Na Li, Libin Jiang, and Steven H Low. Optimal demand response: Problem formulation and deterministic case. In *Control and optimization methods for electric smart grids*, pages 63–85. Springer, 2012.

[66] K Mani Chandy, Steven H Low, Ufuk Topcu, and Huan Xu. A simple optimal power flow model with energy storage. In *Decision and Control (CDC), 2010 49th IEEE Conference on*, pages 1051–1057. IEEE, 2010.

[67] K Rahbar, C C Chai, and R Zhang. Energy cooperation optimization in microgrids with renewable energy integration. *IEEE Transactions on Smart Grid*, 2016.

[68] Amir-Hamed Mohsenian-Rad, Vincent WS Wong, Juri Jatskevich, Robert Schober, and Alberto Leon-Garcia. Autonomous demand-side management based on game-theoretic energy consumption scheduling for the future smart grid. *IEEE transactions on Smart Grid*, 1(3):320–331, 2010.

[69] Wicak Ananduta, José María Maestre, Carlos Ocampo-Martinez, and Hideaki Ishii. Resilient distributed energy management for systems of interconnected microgrids. In *2018 IEEE Conference on Decision and Control (CDC)*, pages 3159–3164. IEEE, 2018.

[70] Katayoun Rahbar, Mohammad R Vedady Moghadam, Sanjib Kumar Panda, and Thomas Reindl. Shared energy storage management for renewable energy integration in smart grid. In *2016 IEEE Power & Energy Society Innovative Smart Grid*

Technologies Conference (ISGT), pages 1–5. IEEE, 2016.

[71] Duong Tung Nguyen and Long Bao Le. Optimal energy management for cooperative microgrids with renewable energy resources. In *Smart Grid Communications (SmartGridComm), 2013 IEEE International Conference on*, pages 678–683. IEEE, 2013.

[72] Ahmed Ouammi, Hanane Dagdougui, Louis Dessaint, and Roberto Sacile. Coordinated model predictive-based power flows control in a cooperative network of smart microgrids. *IEEE Transactions on Smart grid*, 6(5):2233–2244, 2015.

[73] Kaveh Dehghanpour and Hashem Nehrir. An agent-based hierarchical bargaining framework for power management of multiple cooperative microgrids. *IEEE Transactions on Smart Grid*, 2017.

[74] Zahra Baharlouei, Massoud Hashemi, Hamed Narimani, and Hamed Mohsenian-Rad. Achieving optimality and fairness in autonomous demand response: Benchmarks and billing mechanisms. *IEEE Transactions on Smart Grid*, 4(2):968–975, 2013.

[75] Hieu Nguyen and Long Le. Bi-objective based cost allocation for cooperative demand-side resource aggregators. *IEEE Transactions on Smart Grid*, 2017.

[76] Woongsup Lee, Lin Xiang, Robert Schober, and Vincent WS Wong. Direct electricity trading in smart grid: A coalitional game analysis. *IEEE Journal on Selected Areas in Communications*, 32(7):1398–1411, 2014.

[77] Walid Saad, Zhu Han, H Vincent Poor, and Tamer Basar. Game-theoretic methods for the smart grid: An overview of microgrid systems, demand-side management, and smart grid communications. *IEEE Signal Processing Magazine*, 29(5):86–105, 2012.

[78] Stephen Boyd and Lieven Vandenberghe. *Convex Optimization*. Cambridge university press, 2004.

[79] Lloyd S Shapley. A value for n-person games. *Contributions to the Theory of Games*, 2(28):307–317, 1953.

[80] Martin J Osborne and Ariel Rubinstein. *A Course in Game Theory*. MIT press, 1994.

[81] Imma Curiel. *Cooperative game theory and applications: cooperative games*

arising from combinatorial optimization problems, volume 16. Springer Science & Business Media, 2013.

[82] Amir Valibeygi and Raymond A de Callafon. Cooperative energy scheduling for microgrids under peak demand energy plans. *arXiv preprint arXiv:2001.11983*, 2020.